

11. SITE 742¹

Shipboard Scientific Party²

HOLE 742A

Date occupied: 29 January 1988
Date departed: 2 February 1988
Time on hole: 3 days, 17 hr
Position: 67°32.98'S, 75°24.27'E
Bottom felt (rig floor; m, drill-pipe measurement): 426.2
Distance between rig floor and sea level (m): 10.5
Water depth (drill-pipe measurement from sea level, m): 415.7
Total depth (rig floor; m): 742.2
Penetration (m): 316.0
Number of cores (including cores with no recovery): 34
Total length of cored section (m): 316.0
Total core recovered (m): 168.73
Core recovery (%): 53
Oldest sediment cored:
Depth sub-bottom (m): 316.0
Nature: silty claystone, sand-silt-claystone, and diamictite
Earliest age: ?Eocene-Oligocene
Latest age: Quaternary
Measured velocity (km/s): 2.087

Principal results: Site 742 is situated on the middle part of the shelf in Prydz Bay, eastern Antarctica (67°32.98'S, 75°24.27'E, 415.7 m water depth). The site is part of a profile across the shelf consisting of Sites 739 through 743. The main objective at Site 742 was to characterize and date the sediment section lying stratigraphically between the marine Paleogene glacial sequence recovered at Site 739 (seaward) and the nonmarine sequence cored at Site 741 (landward). We hoped that both the onset of glacial conditions in Prydz Bay could be dated and the preglacial environment of the area would be determined.

A seismic survey was run to optimize recovery of the stratigraphic sequence lying between those recovered at Sites 739 and 741. Site 742 was chosen on the seaward side of a small buried rise, about 29 km southeast of Site 739. Drilling began on 30 January 1988, with the rotary core barrel (RCB) and continued in one hole to 316.0 m below seafloor (mbsf), where operations were suspended because of safety considerations. Though total gas quantities were low, the low ratio of methane to ethane and the detection of propane indicated the possibility of hydrocarbon migration from greater depths. The inference of faults in the area from the study of seismic profiles provided a possible pathway for migration. Coring was terminated above the calculated lower boundary of the gas-hydrate stability zone, and after logging, the hole was filled with cement.

The lithologies found are principally of massive diamictite, separable into different units based on degrees of compaction, stratification, directional fabric, and special mineral components. Near the base (304–316 mbsf), thin units of laminated silty claystone, sorted sandstone, and carbonaceous siltstone are interstratified with diamictite and appear to signify nonmarine conditions of deposition.

The coal, plant, and (Cretaceous–Oligocene) spore-pollen detritus appears to be mainly reworked from below. The overlying diamictites (173–304 mbsf) are characterized by minor calcareous layers containing detrital micrite; they contain Eocene–Oligocene fossils. A significant stratigraphic break may occur at 173 mbsf, correlated with a change to firm, more gravelly diamictites (134–173 mbsf). Stratified diamictites, a thin diatomite, and intraclast breccia are located in a thin unit between 115 and 134 mbsf that is marine and dated as late early Pliocene to early late Pliocene. Thick (5.4–115 mbsf), firm, and homogeneous diamictite of Pliocene–Quaternary age follows. It contains several poorly recovered levels that are apparently concentrations of boulders. A thin, uncompacted, upper Quaternary unit of diatomaceous glacial sediment occurs at the top.

Taken with the results of Sites 739 and 741, Site 742 demonstrates that the onset of glaciation in Prydz Bay coincided closely with the onset of marine conditions there. Glaciation began at least by the earliest Oligocene and possibly by the middle to late Eocene. Sedimentation rates appear to have been high during this interval. Thus, the thick glacial sediments at Sites 742 and 739, which underlie the lower Oligocene diatomaceous sediments in Hole 739C (170–310 mbsf) based on seismic stratigraphy and superposition, need not be much older than the diatomaceous sediments.

BACKGROUND AND OBJECTIVES

Site 742 lies on the shelf of eastern Antarctica in eastern Prydz Bay (67°33'S, 75°24.3'E, in 415.7 m of water). The site is on the eastern part of the rather broad Four Ladies Bank. The site is one in a transect of drilling sites (739–743) across the shelf along the seismic line PB-21 of Stagg (1985) and is about 29 km southeast of Site 739.

The general background for the site is described in the "Background and Objectives" sections of the "Site 739" and "Site 740" chapters (this volume). The main objective at Site 742 was to characterize and date the sediment section lying stratigraphically between the marine Paleogene glacial sequence recovered at Site 739 (seaward) and the nonmarine sequence cored at Site 741 (landward). This sediment section is expected to record both the onset of glacial conditions in Prydz Bay and the preglacial environment of the area.

When Site 739 was cored to 486.8 mbsf, the shipboard party discovered that the surface of the preglacial material occurred somewhat deeper than this level. Based on the occurrence of Cretaceous nonmarine sediments at Site 741, an examination of seismic line PB-21 of Stagg (1985), and the site survey data from Site 739 (see "Site Geophysics" section, "Site 739" chapter), we hypothesized that a reflector (EE) at about 1177 mbsf probably marked the preglacial surface or, alternatively, was a horizon stratigraphically below that surface. This level was traced southeast with some difficulty. The drilling place was selected at a position where horizon EE was within the maximal permitted drilling depth and as close to Site 739 as possible, in order to enhance the possibility of finding datable marine deposits in the glacial and preglacial sequences. The site was selected seaward of a small buried ridge, which possibly could represent a paleocliff with marine deposits seaward. The presumed preglacial sequence is covered with 300–450 m of sediments, which may correlate with the glacial sediments cored at Site 739, and partly represents deeper stratigraphic levels. The seafloor at Site 742

¹ Barron, J., Larsen, B., et al., 1989. *Proc. ODP, Init. Repts.*, 119: College Station, TX (Ocean Drilling Program).

² Shipboard Scientific Party is as given in the list of Participants preceding the contents.

seems to be hard and uneven on a meter scale, probably as a result of ice scouring.

The primary objectives of coring at Site 742 were (1) to sample and date the base of the glacial sequence in order to determine the onset of glaciation and explain the preglacial conditions in the area, (2) to study the glacial sediments as an example of a more proximal glacially-influenced shelf succession than at Site 739 and as a contribution to an overall model of a shelf dominated by glacial processes, and (3) to study the glacial stratigraphy, especially in relation to the early history of the glaciation in eastern Antarctica.

SITE GEOPHYSICS

Site Survey

Ocean Drilling Program (ODP) survey line 119-07 was recorded between Sites 741 and 742 using the standard geophysical gear (see "Explanatory Notes" chapter, this volume) and Global Positioning System (GPS) and Transit satellite navigation (Fig. 1). Seas were rough during the transit and site survey, but only a few icebergs and growlers were encountered. The Australian Bureau of Mineral Resources seismic line PB-21 crossed the same area; however, resolution of reflection horizons in line PB-21 was inadequate to trace the sedimentary sequences beneath the central parts of the Prydz Bay shelf to the new drill site. ODP line 119-07 was recorded with a smaller source and shorter pulse width than line PB-21, resulting in higher frequency and greater resolution. The new seismic section provided a more reliable correlation between Sites 741 and 742. During the transit, sonobuoy 7 was recorded near an alternate drilling site on the central shelf (see "Underway Geophysics" chapter, this volume).

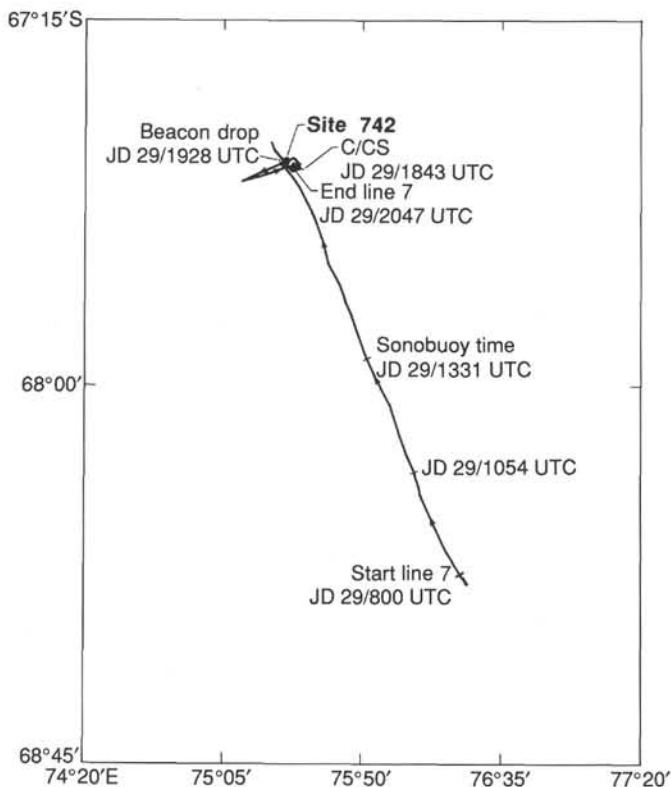


Figure 1. Index map of seismic lines recorded during surveys for Site 742.

The location for Site 742, on the seaward side of a small buried rise, was selected along the transit line. The ship returned to the site on a reciprocal course, and the beacon was dropped (shotpoint 4089). GPS navigation was available up to a few minutes before the beacon was dropped. The ship then proceeded to a point about 2 km southwest of Site 742 where a crossline was recorded. Satellite fixes later indicated that the crossline passed about 0.25–0.5 km northwest of Site 742. Sonobuoy 8 was deployed across the crossline about 1 km from Site 742 and recorded to an offset of about 9 km. The seismic gear was recovered, and the ship returned to the beacon to begin drilling. The seismic results are discussed in the "Seismic Stratigraphy" section (this chapter).

Sonobuoy Data

Sonobuoy 8 was used during the site survey to study the velocity structure of the sedimentary section underlying Site 742 and to determine the depth of strong reflectors believed to be continuous from Sites 739 to 742.

The sonobuoy was deployed successfully and gave good results in the rough sea conditions (Fig. 2). Seismic arrivals, although weak, were adequate for determining wide-angle reflection and refraction velocities, especially after amplifier gains were increased about 10 min after starting the sonobuoy station. Unfortunately, the sonobuoy could not be replayed aboard ship to more clearly resolve the wide-angle reflections near the start of the sonobuoy. At this location, as at others in Prydz Bay, the direct-wave arrival was not strong. This was surprising because, unlike at the other Prydz Bay sites, the rough seas at Site 742 had mixed the upper water column, giving a uniform velocity along the direct path between the water guns and sonobuoy hydrophone. The cause of the weak arrivals is attributed to poor sonobuoy response.

Six wide-angle reflections were traced on the sonobuoy record (Table 1 and Fig. 3). Because of the weak signals near the start of the sonobuoy and the numerous multiple reflections from the seafloor, only three of the wide-angle reflections could be traced back to the vertical-incidence seismic record. The other three reflections were recorded clearly only at ship-to-sonobuoy offsets greater than 1.5 km and were projected back to vertical incidence using distance-squared vs. time-squared plots. The reflection with the greatest horizontal offset (FF) has the greatest potential error because direct-wave arrivals for this reflector had to be projected to far ranges based on comparison with the seafloor reflection.

The wide-angle reflections provided good estimates of rms velocities, plotting as nearly straight lines on a time-squared vs. distance-squared graph. Minor corrections (-65 m/s) were added to rms and refraction velocities to correct for a questionable direct-wave arrival (see sonobuoy error discussion, "Underway Geophysics" chapter).

Continuous and curved refraction arrivals were recorded for the interval from the seafloor to about 400 m depth within the sedimentary section. The curved arrivals were approximated using three straight lines to determine velocities. The computed rms, interval, and refraction velocities are given in Table 1.

Refraction arrivals from deeper horizons could not be seen although wide-angle reflections exist at the deeper levels (Fig. 3). The curved first-break refraction arrivals indicate that velocity gradients exist. Some "shingling" (e.g., time offset of first-break refractions) occurs, indicating that thin low-velocity layers are present. The abrupt attenuation of refraction amplitudes at about 3 km offset may also result from thin low-velocity horizons or thinning beds. These observations are consistent with the measurement of variable velocities in the upper 270 mbsf where downhole logging was done (see "Logging" section, this chapter).

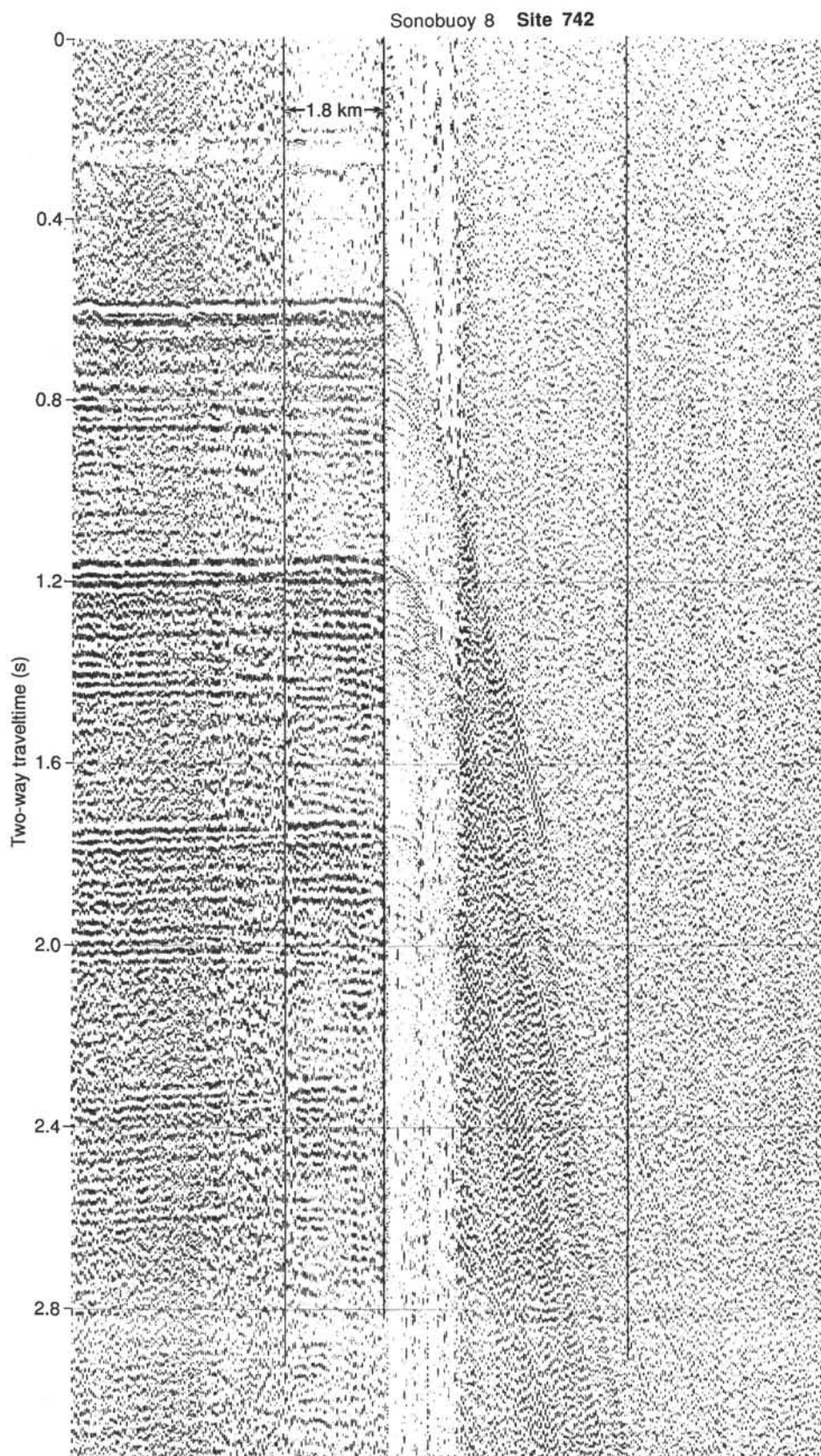


Figure 2. Vertical-incidence seismic and sonobuoy seismic record for sonobuoy 8. Site 742 lies about 1 km from where the sonobuoy was deployed. See Figure 1 for location.

Table 1. Preliminary results for sonobuoy 8 at Site 742.

Horizon ^a	Vrms (km/s)	Vint ^b (km/s)	Ti ^b (s)	Zi (km)	Vrfr (km/s)	To (s)
AA	1.450	2.16	0.55	0.416	2.19	0.424
BB	1.684	2.20	0.77	0.654	2.29	0.484
CC	1.767	3.00	0.90	0.796	2.51	0.540
DD	2.025	2.74	^c 1.08	1.066	nr	
EE	2.229	—	^c 1.45	1.604	nr	

Vrms = rms velocity for horizon; Vint = interval velocity computed using Vrms, Ti, and Dix equation (e.g., between horizon AA and BB is 2.16 km/s); Ti = vertical incidence reflection time (two-way) to horizon; Zi = total depth from sea level to horizon (water depth = 416 m); Vrfr = refraction velocities cannot be directly associated with a specific horizon, rather they comprise a gradient from near seafloor into the upper part of the section; To = intercept time for refractor associated with horizon; nr = no refractor observed.

^a Letters of horizons do not correlate between drill sites and do not correspond to prior stratigraphic analyses.

^b Velocities and times used for computing depths Zi.

^c These vertical reflection times are derived from analysis of a distance-squared vs. time-squared plot.

Sonobuoy interval velocities of 2.16–2.74 km/s characterize the upper 1188 m of the sedimentary section (Table 1 and Fig. 4). These values are similar to those at Site 739, which lies in the prograding glacial sediments beneath the outer shelf. The interval and refraction velocities for the uppermost parts of the sedimentary section (AA–CC, the glacial diamicton) are 2.16–2.51 km/s, which are high values for shallow depths because of glacial compaction of the sediment.

Velocities increase at horizon CC (380 mbsf) to 3.0 km/s. An apparent velocity inversion (to 2.74 km/s), however, occurs at greater depths. The inversion may result from the uncorrected effects of layer dip in parts of the sedimentary section below the first seafloor multiple reflection. Alternatively, the velocity inversion may be real. A similar velocity inversion was observed at Site 739 between two reflection horizons (DD and EE, “Site Geophysics” section, “Site 739” chapter) that have the same acoustic character as those at Site 742. At both sites, the curved, first-break refraction arrivals are strongly attenuated at large offsets. The sudden attenuation may indicate low-velocity rocks that lie within an acoustically well-layered unit that is continuous between the sites. Some of the lower-velocity rocks could be unconsolidated sands and gravels similar to those presumed at shallower depths at Site 739 (see “Logging” section, “Site 739” chapter). Low velocities at Site 742 could also be caused, in part, by interbedded sands and gravels.

In summary, the sedimentary section at Site 742 is characterized by indurated sediment with high refraction and interval velocities directly below the seafloor. These high velocities, which are similar to those obtained from laboratory measurements (see “Physical Properties” section, this chapter), are characteristic of heavily glaciated areas. For depths up to about 380 mbsf, only a small increase was seen in interval velocity (to 2.20 km/s) and is probably due to the combined effect of thin, interbedded, high- and low-velocity strata. A velocity inversion may occur beneath the strong regional reflector (DD) in the seismic profiles. If real, the inversion may be caused by interbedded unconsolidated sand and gravel layers like those interpreted at Site 739.

OPERATIONS

Sites 741 to 742

After departing on a southeasterly course and streaming seismic gear, the vessel turned and crossed Site 741. The track then continued northwest toward the new site (742) about 89 km to the northwest at profiling speed. Weather conditions deteriorated during the transit, with heavy snow showers reducing visibility and winds gusting to 35 kt. The beacon was launched on the first pass over the site. After continuing about 0.8 km past the site, the ship made a wide, looping turn and recrossed the drill site from the northeast. The geophysical gear was then recovered, and the ship returned to the site.

Site 742–Outer Prydz Bay

The new site lies along the same reference profile as Sites 739–741, about 29 km southeast of Site 739. As the thrusters and hydrophones were lowered in rough seas, the wind occasionally reached 40 kt. About 1 hr was required for the automatic station-keeping system to get a sufficient fix on the beacon to take station. An additional hour was spent in determining whether the ship could hold position within acceptable limits for spudding in only 415.7 m of water. Although yellow 2% alarms were common, few “red” alarms signalling excursions of 3% of water depth or more occurred, and weather conditions were improving slowly. The pipe trip was begun with vessel heave occasionally reaching 2.5 m.

Positioning was marginal when the pipe had been run to place the RCB core bit just above the seafloor. As the first core was to be a mud-line punch core without rotation or circulation, it was taken and retrieved without deploying the top drive. That provided additional time to “watch” the station-keeping system with the bit out of the hole before picking up the top drive and coring ahead. With only an occasional brief yellow warning, conditions finally were judged to be safe to continue the coring operation.

The now-familiar hard glacial sediment was again encountered, this time at a depth of about 24 mbsf. After 9 hr and a difficult 38 m of hole, the approach of a large iceberg threatened to force abandonment of the hole. The iceberg, which was considered to be too large for towing, was projected to pass within 0.8 km of the site. The risk to the bit and bottom-hole assembly involved in redrilling warranted the deployment of a free-fall funnel (minicone) to insure their safety. During the 2 hr required to rig and drop the minicone, the *Maersk Master* circled the iceberg with her floating tow rope in an effort to at least deflect it from its course. Before the towing operation could begin, however, the iceberg changed direction on its own and passed safely.

RCB coring then continued in the glacial diamictite with surprisingly good hole conditions, but with extremely poor core recovery (Table 2). Normal recovery was usually only a few cobbles, which apparently were rolling under the bit and also jamming the core catchers. At about 150 mbsf, the drill entered a more normally compacted glacial unit with fewer/smaller hard rocks. Core recovery and rate of penetration both increased dramatically from that point.

Constant monitoring of cores for gas produced only sporadic traces. The vacutainer samples were analyzed within minutes of recovery of the cores. Although total gas quantities were low, the low ratio of methane to ethane and the presence of propane indicated the possibility of hydrocarbon migration from greater depths. The inference of several faults in the area (from study of the seismic profiles) provided a possible pathway for migration. On the basis of that information, coring was terminated above the calculated lower boundary of the gas hydrate stability zone. Total depth was 316 mbsf.

A wiper trip was then made to condition the hole for logging before releasing the mechanical bit release and flushing the hole with drilling mud. Although no hole stability problems had been experienced during the coring program, 19 m of fill was found in the hole upon completion of the short trip.

The logging sheaves were rigged, and a successful seismic stratigraphic combination log was recorded from fill at 30 m above total depth up to the end of the drill string. The geochem-

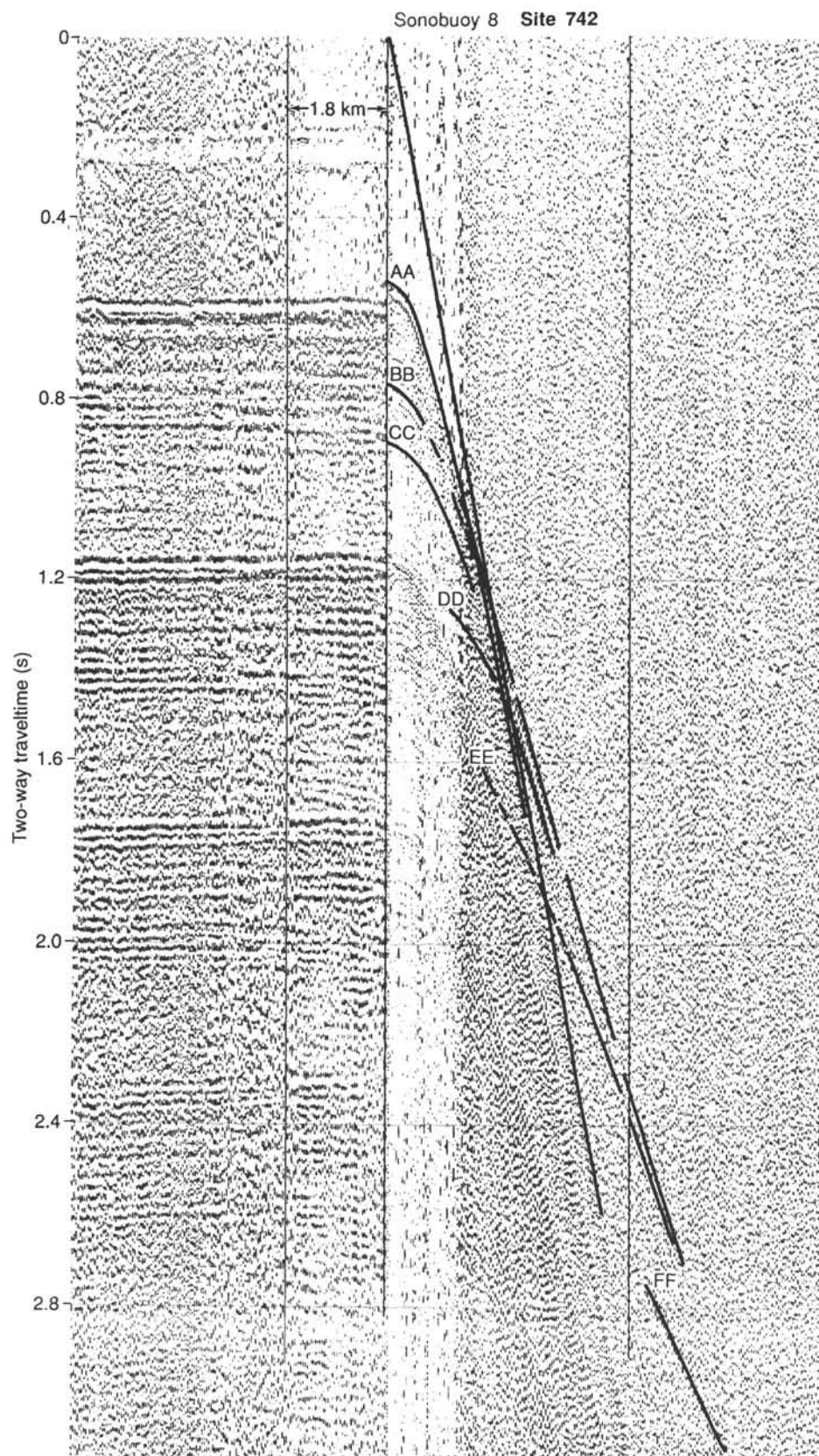


Figure 3. Vertical-incident seismic and sonobuoy seismic record for Site 742 showing wide-angle reflection and refraction interpretations. Letters denote layers given in Table 1. See Figure 1 for location.

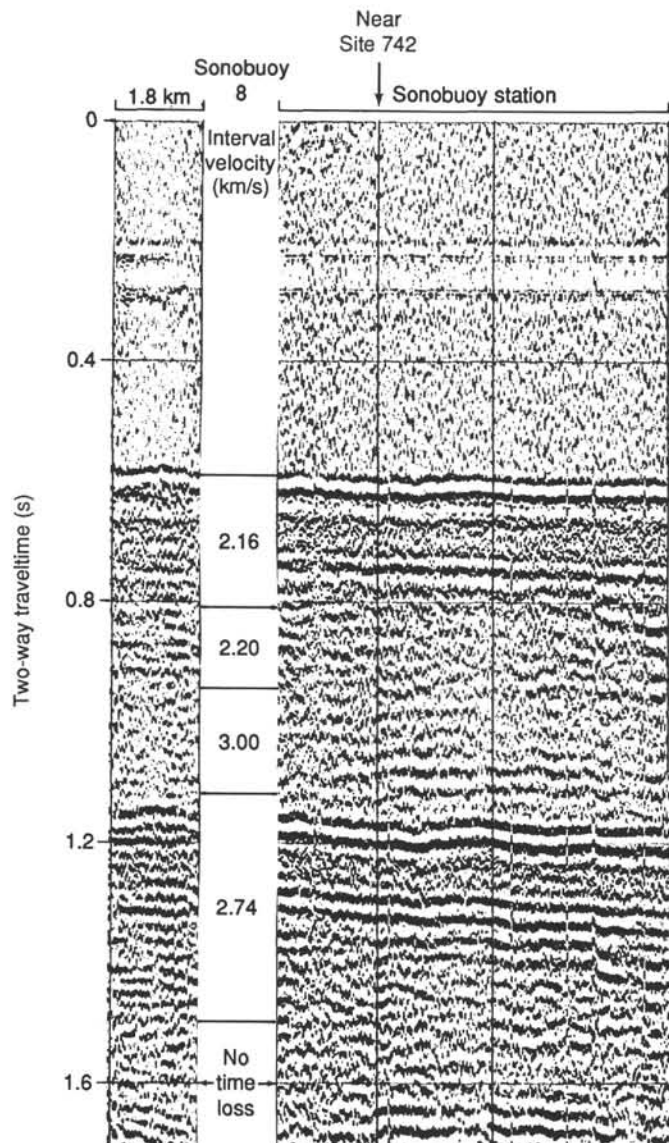


Figure 4. Vertical-incident seismic profile near Site 742 showing interval velocities computed from wide-angle reflections in sonobuoy 8.

istry combination log was attempted next, but the run had to be aborted because of downhole tool problems. The final log run, lithodensity-porosity, was successful, but the hole had filled to 258 mbsf.

In accordance with *JOIDES* Pollution Prevention and Safety Panel requirements, the hole was then plugged with cement and abandoned. The drill string was recovered, and the vessel was underway at 0730 hr, 2 February.

LITHOSTRATIGRAPHY AND SEDIMENTOLOGY

Site 742, located in 415.7 m water depth, achieved relatively deep penetration of the Prydz Bay glacially-dominated, continental margin sequence at a more proximal location than Site 739. Owing to sparse dating control from fossils and the sometimes poor core recovery, the lithostratigraphy proved difficult to interpret. Dilution of the fossil contents by glacial debris, the possibility of several episodes of significant erosion, evidence of extensive reworking of microfossils, and termination of the hole very soon after entering nonmarine facies posed additional problems for interpretation.

Table 2. Coring summary, Site 742.

Core no.	Date (1988)	Time	Depth (mbsf)	Length		Recovery (%)
				cored (m)	recovery (m)	
119-742A-						
1R	Jan. 30	0840	0.0-4.5	4.5	4.45	98.9
2R	30	1150	4.5-14.1	9.6	1.07	11.1
3R	30	1415	14.1-23.7	9.6	1.37	14.3
4R	30	1715	23.7-33.4	9.7	0.86	8.9
5R	30	2100	33.4-37.9	4.5	0.12	2.7
6R	30	2255	37.9-45.9	8.0	0.40	5.0
7R	31	0000	45.9-55.5	9.6	0.23	2.4
8R	31	0150	55.5-65.1	9.6	4.31	44.9
9R	31	0320	65.1-74.7	9.6	0.61	6.4
10R	31	0455	74.7-84.4	9.7	3.72	38.3
11R	31	0605	84.4-94.1	9.7	3.46	35.7
12R	31	0705	94.1-103.7	9.6	0.25	2.6
13R	31	0750	103.7-113.3	9.6	0.90	9.4
14R	31	0835	113.3-123.0	9.7	3.91	40.3
15R	31	0920	123.0-132.7	9.7	5.88	60.6
16R	31	1035	132.7-142.3	9.6	3.51	36.5
17R	31	1250	142.3-152.0	9.7	9.46	97.5
18R	31	1450	152.0-161.7	9.7	9.08	93.6
19R	31	1645	161.7-171.3	9.6	9.43	98.2
20R	31	1750	171.3-181.0	9.7	3.67	37.8
21R	31	1855	181.0-190.7	9.7	3.79	39.1
22R	31	2000	190.7-200.3	9.6	9.34	97.3
23R	31	2115	200.3-209.9	9.6	9.12	95.0
24R	31	2230	209.9-219.6	9.7	5.80	59.8
25R	31	2320	219.6-229.2	9.6	0.00	0.0
26R	Feb. 1	0055	229.2-238.8	9.6	7.25	75.5
27R	1	0155	238.8-248.5	9.7	9.80	101.0
28R	1	0305	248.5-258.1	9.6	9.85	102.0
29R	1	0405	258.1-267.8	9.7	8.98	92.6
30R	1	0525	267.8-277.4	9.6	8.92	92.9
31R	1	0635	277.4-287.1	9.7	5.82	60.0
32R	1	0755	287.1-296.7	9.6	6.04	62.9
33R	1	0920	296.7-306.3	9.6	8.46	88.1
34R	1	1105	306.3-316.0	9.7	8.87	91.4
				316.0	168.73	53.4

Although diamictite and diamicton compose the bulk of recovery, five lithologic divisions were recognized, based on some significant minor lithologies (e.g., diatomite, sorted sands) or on differences in the diamictites (e.g., bedding, calcareous content; Table 3, Figs. 5 and 6). Unit I (Quaternary, 0-5.4 mbsf) embraces the soft uppermost units of pebbly diamicton and diatomaceous silt-clay. Unit II lithologies (5.4-115.2 mbsf) are of compacted massive diamictite, with an apparently high content of pebbles and boulders at some levels that correlated with intervals of exceptionally low recovery. Unit III (115.2-134.4 mbsf) is a thin, comparatively well-stratified unit of (?early) Pliocene age, containing diverse lithologies—diamictite, diatomite, and sandy and bouldery intervals. Lithologically layered diamictites (Unit IV, 134.4-172.5 mbsf) lie below and pass down into the diamictites of Unit V (172.5-304.3 mbsf) with a minor calcareous component. That component shows similarity with the lowest subunit (IVB) at Site 739, especially in that both units contain Oligocene and Eocene fossils. Below this level at Site 742, Unit VI is a diamictite interstratified with laminated claystones or with texturally sorted sandstones and carbonaceous siltstones. These levels are apparently of nonmarine origin. Spore pollen and dinoflagellate remains in Unit VI appear to be reworked, and serve only to define the age as somewhat younger than ?Eocene/Cretaceous.

Procedures for the analysis of these sediments involved smear slide examinations (Fig. 5), mesoscopic textural and grain fabric analyses, X-ray diffraction (XRD), X-ray fluorescence (XRF), and carbonate/carbon chemical analyses as well as close visual logging of bedding relations, deformation features, physical properties, and colors. The descriptive terms used are described

Table 3. Lithologic units, Hole 742A.

Lithologic unit	Age	Recovery range	Depth (mbsf)	Thickness (m)	Lithology
IA	late Quaternary	1R-1, 0-7 cm	0-0.07	0.1	Diatomaceous sand-silt
IB		1R-1, 7 cm, to 2R-1, 90 cm	0.07-5.4	5.3	Massive pebbly diamicton (up to 15% gravel)
II	Quaternary-late Pliocene	2R-1, 90 cm, to 14R-2, ?49 cm	5.4-115.2	109.8	Homogeneous massive diamicton with pebbles and boulders (up to 15% gravel)
IIIA		14R-2, 42? cm, to 15R-4, 20 cm	115.2-127.7	12.5	Stratified diamicton (average 5% gravel)
IIIB	(?early) Pliocene	15R-4, 20-80 cm	127.7-128.3	0.6	Diatomite with minor silt and clay
IIIC		15R-4, 80 cm, to 16R-1, 96 cm	128.3-133.7	5.4	Stratified diamicton, sandstone, and siltstone
IIID		16R-1, 96 cm, to 16R-2, 17 cm	133.7-134.4	0.7	Boulders and pebbles probably in diamicton
IV		16R-2, 17 cm, to 20R-1, 131 cm	134.4-172.5	38.1	Diamicton with diffuse layering (1%-7% gravel)
V	?Oligocene-Eocene	20R-1, 131 cm, to 33R-6, 9 cm	172.5-304.3	131.8	Pale diamicton with minor carbonate-rich layers (1%-5% gravel)
VIA		33R-6, 9 cm, to 34R-1, 120 cm	304.3-307.5	3.2	Interbedded sand-silt-claystones (with minor gravel) and silty claystones
VIB		34R-1, 120 cm, to 34R-5, 95 cm	307.5-313.3	5.8	Pale massive diamicton (1%-5% gravel)
VIC	?early Eocene-Oligocene	34R-5, 95 cm, to 34R-CC	313.3-316.0	2.7	Carbonaceous, well-sorted sand and siltstone with interbedded diamicton

in the "Explanatory Notes" chapter. In smear slides, the feldspar contents were usually underestimated compared with thin-section estimations, due to the difficulty of discriminating unaltered, untwinned feldspar from quartz. The two minerals should only be considered in combination in the smear slide data.

Drilling Disturbance

Site 742 was drilled using the RCB. Soupy disturbance due to the rotary drilling took place near the mud line (Subunit IA), and moderate disturbance of the soft diamicton occurred in Subunit IB. For some cores (119-742A-5R to 119-742A-7R and 119-742A-12R), the recovery consisted of clasts isolated from their matrix (presumably diamicton), probably because of grinding and washing out during prolonged drilling of the harder metamorphic pebbles/cobbles and boulders. Unit II posed the greatest problems for recovery. Sediments recovered in Unit V (Cores 119-742A-20R to 119-742A-25R) commonly have dark, 1-5-mm-thick bowed bands (convex), which appear to be due to incipient shearing of the core under rotary stress. Scattered throughout the core are drilling breccias, consisting of fragmented pieces of firm sediment embedded within a drilling paste. This type of breccia can be difficult to distinguish from normal diamicton. Cores 119-742A-15R and 119-742A-19R were coated with drill mud, as a result of incomplete flushing of the hole after mud treatments and/or a malfunction in the release valve at the top of the core barrel.

Lithologic Units

Unit I

Section 119-742A-1R-1, 0-90 cm; depth, 0-5.4 mbsf.
Age: Quaternary.

Unit I comprises the soft sediments overlying the firm diamictons. It consists of two subunits, an upper diatomaceous sand-silt and a soft diamicton.

Subunit IA

Section 119-742A-1R-1, 0-7 cm; depth, 0-0.07 mbsf.
Age: late Quaternary.

Subunit IA consists of a homogeneous, olive (5Y 5/3) diatomaceous sand-silt. The homogeneity of this subunit may be due

to a combination of the liquid state of sediment and drilling disturbance; soupy disruption was observed. The sand and the silt fractions each attain about 45%, the remaining 10% being clay fraction. Quartz and feldspar are the dominant clastic constituents, accounting for 50% of the sediment. The diatom content is about 20%. Clay minerals, opaque minerals, garnet, mica, and pyroxene are present in minor amounts.

Subunit IB

Sections 119-742A-1R-1, 7 cm, through 119-742A-2R-1, 90 cm; depth, 0.07-5.4 mbsf.

Age: (in the upper part) ?late Pliocene-Quaternary.

Subunit IB is characterized by massive, poorly sorted, soft diamicton. It is greenish gray (5G 4/1) to dark gray (5Y 4/1). No sedimentary structures were detected. Grain-size distributions fluctuate slightly. Excluding the gravel content, smear slide analyses indicate clayey silt or sand-silt-clay textures with 10%-40% sand, 40%-60% silt, and 20%-30% clay fraction. The main components of the sediment are quartz and feldspar (about 60% combined) and clay minerals (about 15%-20%). Opaque phases, garnet, pyroxene, amphibole, and spinel also occur in minor quantities. Throughout the subunit, diatom abundances are about 5%; sporadic radiolarians are present.

The estimated gravel content is 5%-10%. Most clasts are < 1 cm in diameter, with the maximum size 4 cm. The larger ones are mainly subrounded. Observed types include different classes of gneiss, granite, quartz rock, and weathered sandstone. The clasts are randomly distributed throughout the subunit and seem to have no preferred orientation.

The lower boundary with Unit II is sharp but irregular and apparently deformed.

Unit II

Sections 119-742A-2R-1, 90 cm, through 119-742A-14R-2, ?49 cm; depth, 5.4-115.2 mbsf.

Age: (at top) late Pliocene-Quaternary.

Unit II is a homogeneous, poorly sorted, and firm diamicton with high gravel content (up to 15% in recovered intervals). Its color is very dark gray (5Y 3/1 and 2.5G 3/0) to black (5Y 2.5/1). No sedimentary structures were observed, and it is compacted, but still friable. Excluding the gravel content, smear slide analy-

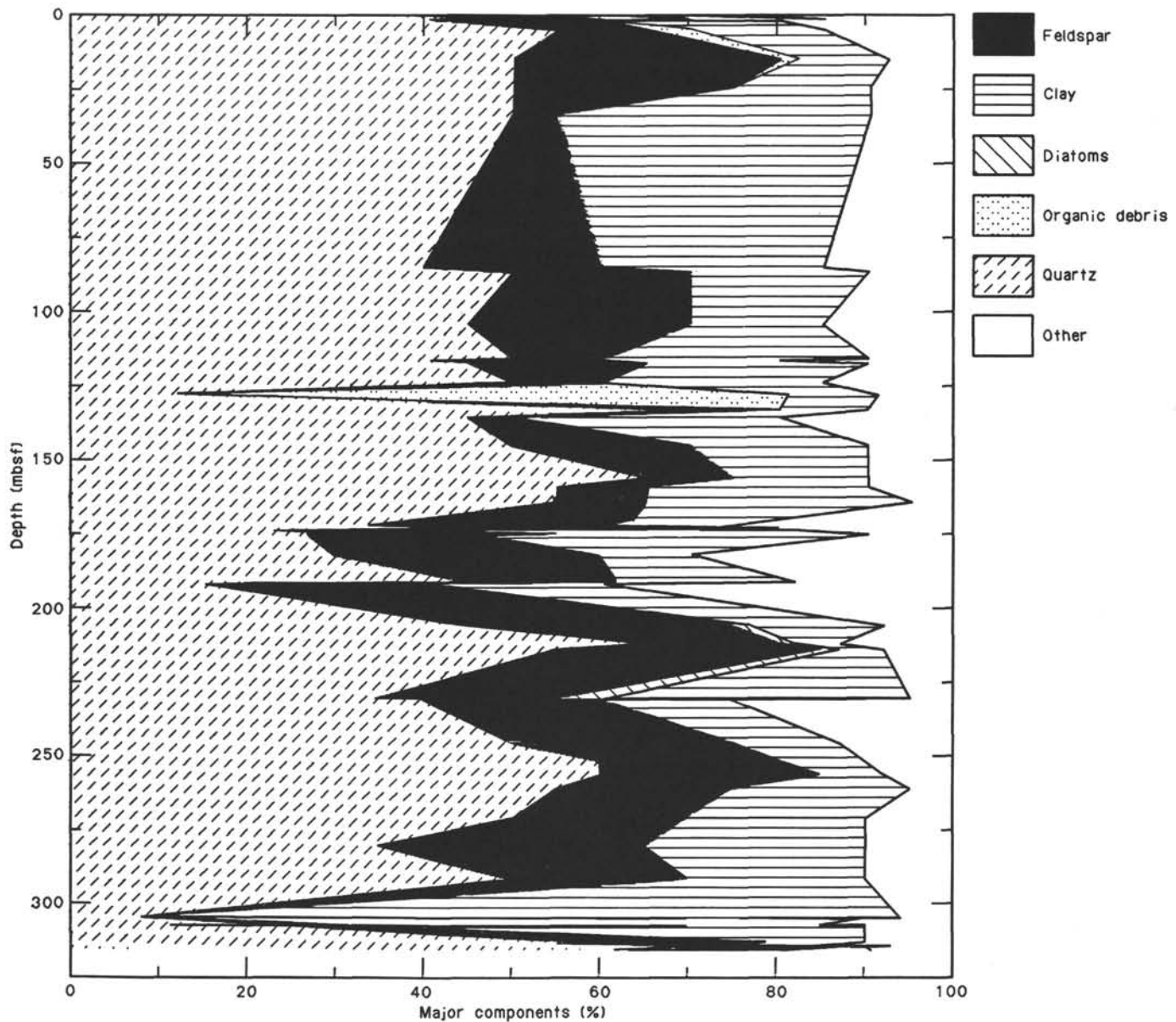


Figure 5. Percentage major components from smear slide examinations at Site 742. The substantial gap in data between 30 and 80 mbsf mostly corresponds to poor recovery.

ses indicate that most of the sediment can be described as sand-silt-clay (20%–35% sand, 35%–60% silt, and 15%–45% clay), with mostly quartz-feldspar (55%–80%), clay (10%–35%), mica (1%–3%), pyroxene-amphibole (2%–4%), and opaque minerals (5%).

A quantification of the overall gravel content is not possible because of the poor recovery in this unit. Typically, only loose clasts with very minor amounts of disturbed diamictite matrix were recovered. Estimated values of the percent gravel actually held within the recovered diamictite seem to be lowest in Cores 119-742A-5R, 119-742A-8R, and 119-742A-9R (33–38 and 56–75 mbsf). The recovered boulder fragments and smaller clasts consist of metamorphic rocks (gneiss, granulite, and amphibolite). In Core 119-742A-11R (85–88 mbsf), black coaly shale and some coal fragments are present. Clast roundness analysis showed that most of the small gravel recovered *in situ* is subangular to subrounded (about 10%–20% angular, 35%–45% sub-

angular, 35%–50% subrounded, and only 5%–10% rounded). However, the larger clasts tend to be better rounded than the smaller ones.

Grain fabrics at these levels in the underlying Unit III show that preferred orientations are typical of the bulk of this unit. Near the base of the unit, however, is a random fabric.

Unit III

Sections 119-742A-14R-2, 42 cm, to 119-742A-16R-2, 17 cm; depth, 115.2–134.4 mbsf.
Age: ?early Pliocene.

Unit III is a lithologically variable unit typified mainly by its stratification. It is comprised of stratified diamictite (Subunits IIIA and IIIC), a diatomite bed (Subunit IIIB), and a thin, bouldery interval (Subunit IIID). Whether Subunit IIID lies more naturally with Unit III or IV is unclear.

Subunit IIIA

Sections 119-742A-14R-2, 42 cm, through 119-742A-15R-4, 20 cm; depth, 115.2–127.7 mbsf.
Age: unknown.

The predominant lithology in this subunit is a compacted but friable diamictite (Fig. 7), weakly to moderately stratified on a centimeter to decimeter scale, and varying from black (5Y 2.5/1) to dark gray (10Y 3/1 and 2.5G 2.5/0). Although the stratification is generally diffuse, some sharp contacts occur, a few of which are deformed. The gravel content varies from 1% to 10%, but averages 5%. Rapid changes in sand and the finer size classes occur between diffuse, more gravelly and clayey horizons (the latter form thin intervals in Core 119-742A-15R). Grain-size estimates from smear slides indicate 30%–50% sand, 30%–40% silt, and 20%–30% clay. Compositionally, the sediment consists of 60%–65% quartz and feldspar combined, 20%–25% clay, and 3%–10% opaques and minor carbonate, amphibole, mica, garnet, and accessory minerals. Clasts in the unit include granitoid rocks (with quartz, feldspar, magnetite, and amphibole), mafic (biotite-amphibole) gneisses, quartz rocks, carbonate-cemented sandstones, and coal. The clasts are mainly of pebble size and have roundness statistics of about 62% subangular and 38% subrounded.

Several beds (e.g., Sections 119-742A-15R-2, 111–115 cm, and 119-742A-15R-4, 0–20 cm) contain rip-up intraclasts of the diatomaceous siltstone-claystone and diatomite (Subunit IIIB) that lie directly beneath. In the prime example (Section 119-742A-15R-4; Fig. 8) the intraclasts are ragged, up to 1 cm in size, and compose 10%–80% of a bed that otherwise consists of poorly sorted coarse sandstone with rare granules and pebbles. Coarse-tail grading appears to have taken place. The lower contact is sharp and deformed by loading (Fig. 8).

In places the stratification of Subunit IIIA is inclined to the horizontal. This and other deformation structures suggest that slumping occurred (Section 119-742A-15R-3). The deformation did not affect the underlying Subunit IIIB.

Clayey siltstone horizons occur in Section 119-742A-14R-2, 93–99 cm, and form bands with diffuse boundaries in Section 119-742A-14R-3, 42–26 cm. They are dark greenish gray (5BG 4/1) to dark bluish gray (5B 4/1). The uppermost horizon contains a pyrite-enriched layer 2–7 mm thick and a deformational structure interpreted as a result of slumping. Smear slide estimates of grain size indicate 5% sand, 60% silt, and 35% clay, and compositionally the sediment consists of 60% quartz and feldspar, 30% clay, 5% opaques, 4% amphibole, and 1% mica.

Subunit IIIB

Sections 119-742A-14R-4, 20 cm, through 119-742A-14R-4, 80 cm; depth, 127.7–128.3 mbsf.
Age: late early to early late Pliocene.

This distinctive subunit of diatomite is greenish gray (5G 5/1) to gray (unnamed, 10Y 5/1). It is a well-consolidated sediment, although crumbly in part. A weak planar stratification is developed, and quartz grains and intraclasts of less diatom-rich siltstone are disseminated throughout (Fig. 8). The amount of intermixed terrigenous sediment increases toward the base. A smear slide grain-size estimate indicates 5% sand, 75% silt, and 20% clay. Compositionally, it contains 70% diatoms, 11% quartz and feldspar, 10% clay, 5% opaque minerals, and 4% amphibole.

Subunit IIIC

Sections 119-742A-14R-4, 80 cm, through 119-742A-16R-1, 96 cm; depth, 128.3–133.7 mbsf.
Age: unknown.

Subunit IIIC consists mainly of black (5Y 2.5/1), weakly stratified diamictite, with a strongly fluctuating sand and gravel

(1%–50%) content, a bed (Section 119-742A-15R-4, 80–97 cm) of poorly sorted dark gray (2.5Y 4/0) sandstone, and a dark gray (5Y 4/1) clayey siltstone with <<1% gravel (Section 119-742A-16R-1, 17–43 cm). The siltstone has a loaded (or alternatively scoured) top and an irregular, transitional base. In terms of sedimentary structures, the lithologies are similar to Subunit IIIA.

Subunit IIID

Sections 119-742A-16R-1, 96 cm, through 119-742A-16R-2, 17 cm; depth, 133.7–134.4 mbsf.
Age: unknown.

Subunit IIID is marked by drilling recovery from one large boulder and several individual cobbles. Because no matrix is associated, we do not know whether the unit has affinity with Subunit IIIC above or Unit IV below. The boulder measured 62 cm downcore, but was certainly much taller *in situ* before losses of thickness at the drilling-induced breaks. All clasts are of gneiss or granite.

Unit IV

Sections 119-742A-16R-2, 17 cm, through 119-742A-20R-1, 131 cm; depth, 134.4–172.5 mbsf.
Age: unknown.

Dark, compact but friable, diamictite characterizes Unit IV. Colors are very dark gray (5Y 3/1) to black (5Y 2.5/1) and rather uniform throughout. Smear slide compositional data show 50%–75% quartz and feldspar, 1%–2% pyroxene/amphibole, 1%–2% micas, 3%–20% opaques, and 10%–30% clay. Grain sizes are estimated as 10%–30% sand, 30%–70% silt, and 20%–40% clay fraction. Gravel contents are in the range 1%–7%, and increase up through the unit (Fig. 6). Gravel roundness statistics are 5%–15% rounded, 34%–36% subrounded, 35%–42% subangular, and 9%–18% angular. Comparatively large clasts (2–14 cm) are common in the upper part of the unit, but uncommon toward the base. The larger clasts show a much higher degree of rounding (0% angular, 30% subangular, 40% subrounded, and 30% rounded) than the granules. Clast compositions include gneiss, granite, quartz rocks, quartz and feldspar (granule sizes), carbonate-cemented sandstones, and coal.

The unit is not featureless, but has clear evidence of diffuse layering on a scale of >0.5 m. Below 148 mbsf (Section 119-742A-17R-5), it is marked by subtle variations in gravel content, large clast (>2 cm) abundance, color changes, and horizontal fabrics (Section 119-742A-20R-1, 30–31 cm; wispy in Section 119-742A-20R-1, 125–127 cm). Thin layers, with minor carbonate content (detrital micrite up to 10%), occur in Sections 119-742A-18R-2, 55–75 cm, 119-742A-18R-6, 95–112 cm, and 119-742A-19R-3, 72–87 cm.

The contact with Unit V is sharp and may be a disconformity. It is accompanied by color changes in the lower parts of Unit IV, which may indicate incorporations of material from the underlying unit.

Two grain fabrics in the unit showed random orientations near the top (Core 119-742A-16R), but preferred orientations in the middle (Core 119-742A-17R).

Unit V

Sections 119-742A-20R-1, 131 cm, through 119-742A-33R-6, 9 cm; depth, 172.5–304.3 mbsf.
Age: ?Eocene/Oligocene.

Unit V is a dark to pale gray (5Y 3/1, 5Y 4/1, and 10GY 4/1) or dark olive gray (5Y 3/2) homogeneous diamictite. Both the upper and lower boundaries are sharp and well defined in the recovered core. The main distinguishing features relative to the other diamictites at this site are the paler color tone, lower gravel content, and the presence of micritic carbonate and car-

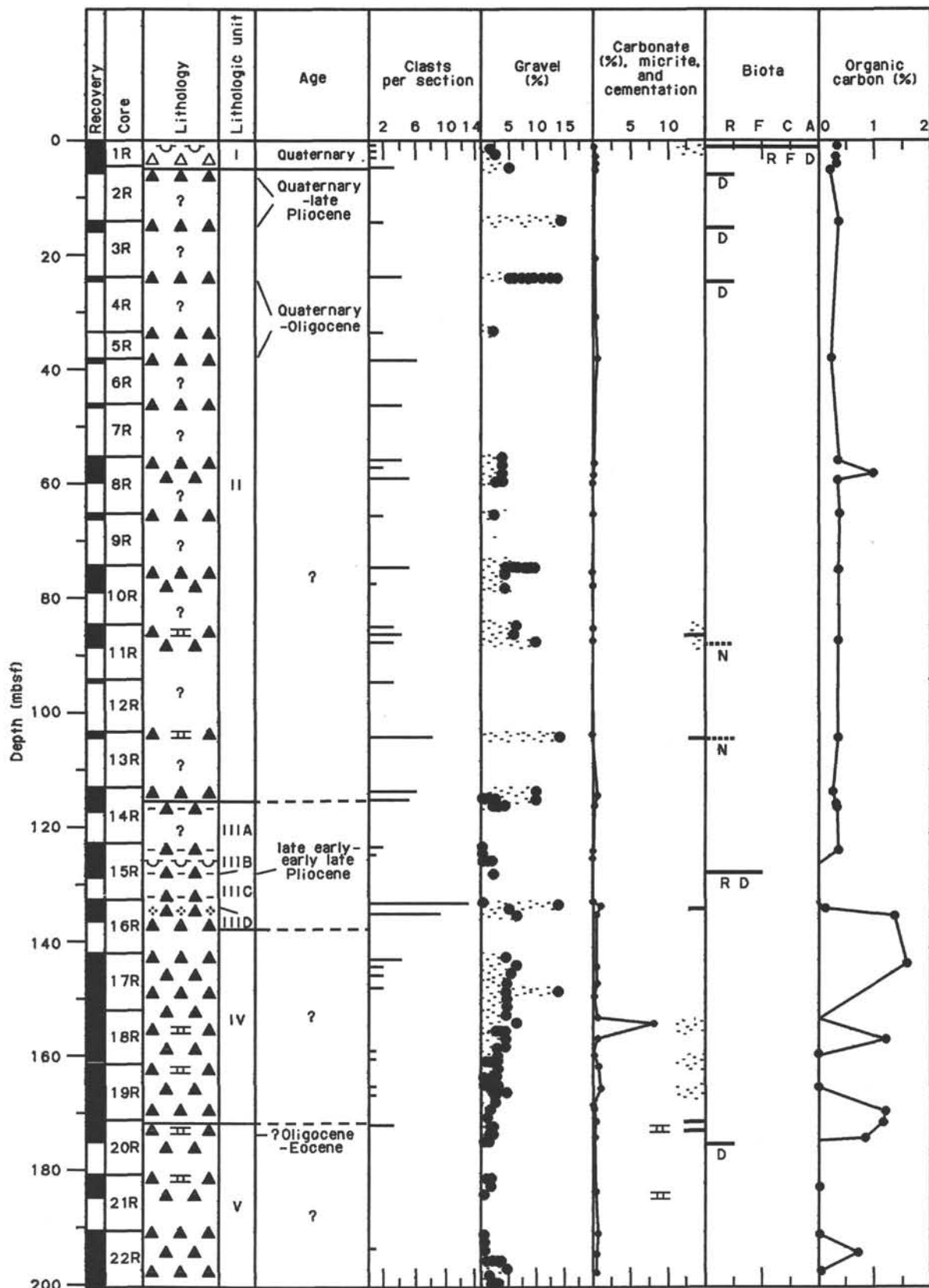
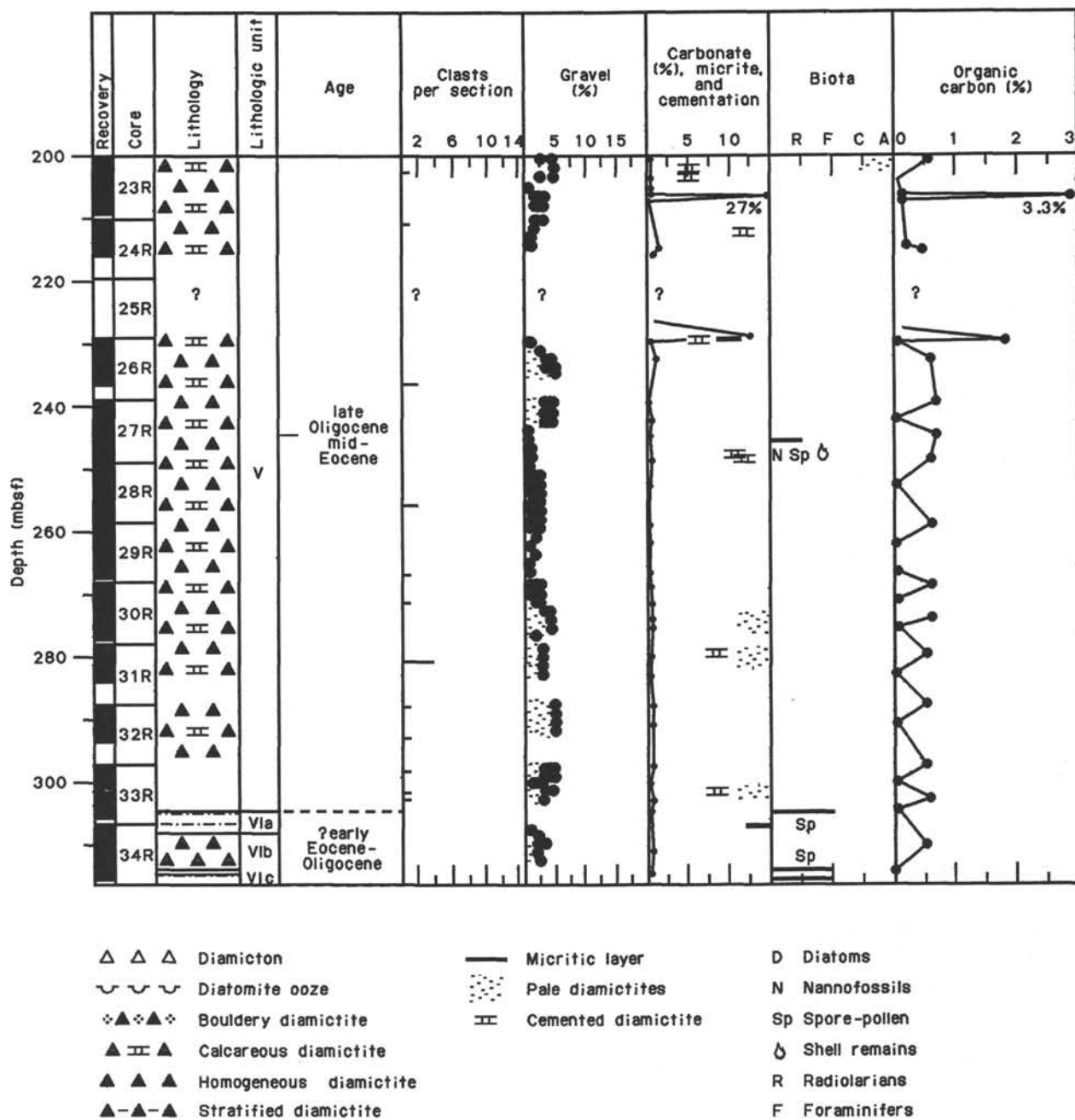


Figure 6. Lithostratigraphic summary of Site 742.



Note: Where recovery is <100%, a discrepancy in the depth of a horizon may appear between the downhole log record and the recovery log. This error is ±0.5 the loss of recovery.

Figure 6 (continued).

bonate-cemented layers (5–40 cm thick) and rare benthic shell remains.

The diamictite is compact and friable. Lithologically, it consists of poorly sorted silty clay, clayey silt, and sand-silt-clay, containing 1%–5% gravel composed of granule-sized and minor pebble-sized clasts up to 3 cm in length. The granules are composed predominantly of quartz, but the pebbles show a more variable composition and include granite, amphibolite, diamictite, and various types of gneiss. Analysis of the gravel shows that most clasts are fresh and subrounded to subangular (up to 82% combined), but with a strong angular component

(up to 33%). Clast and grain orientations appear to be random. The amount of sand observed in the smear slides varies from 0% to 60%. Pale-colored, sand-rich, and darker colored sand-poor pockets and lenses are common. A small-scale (19-cm thick) coarsening-upward sequence consisting of a gravel-free silty clay grading up into coarser noncalcareous gravelly diamictite occurs in Section 119-742A-20R-1, 131–150 cm. The top of this minor sequence defines the upper boundary of Unit IV.

One of the most distinctive features is the presence throughout the unit of carbonate-rich zones (Sections 119-742A-23R-2, 119-742A-23R-4, 119-742A-27R-CC, 119-742A-29R-2, 119-742A-

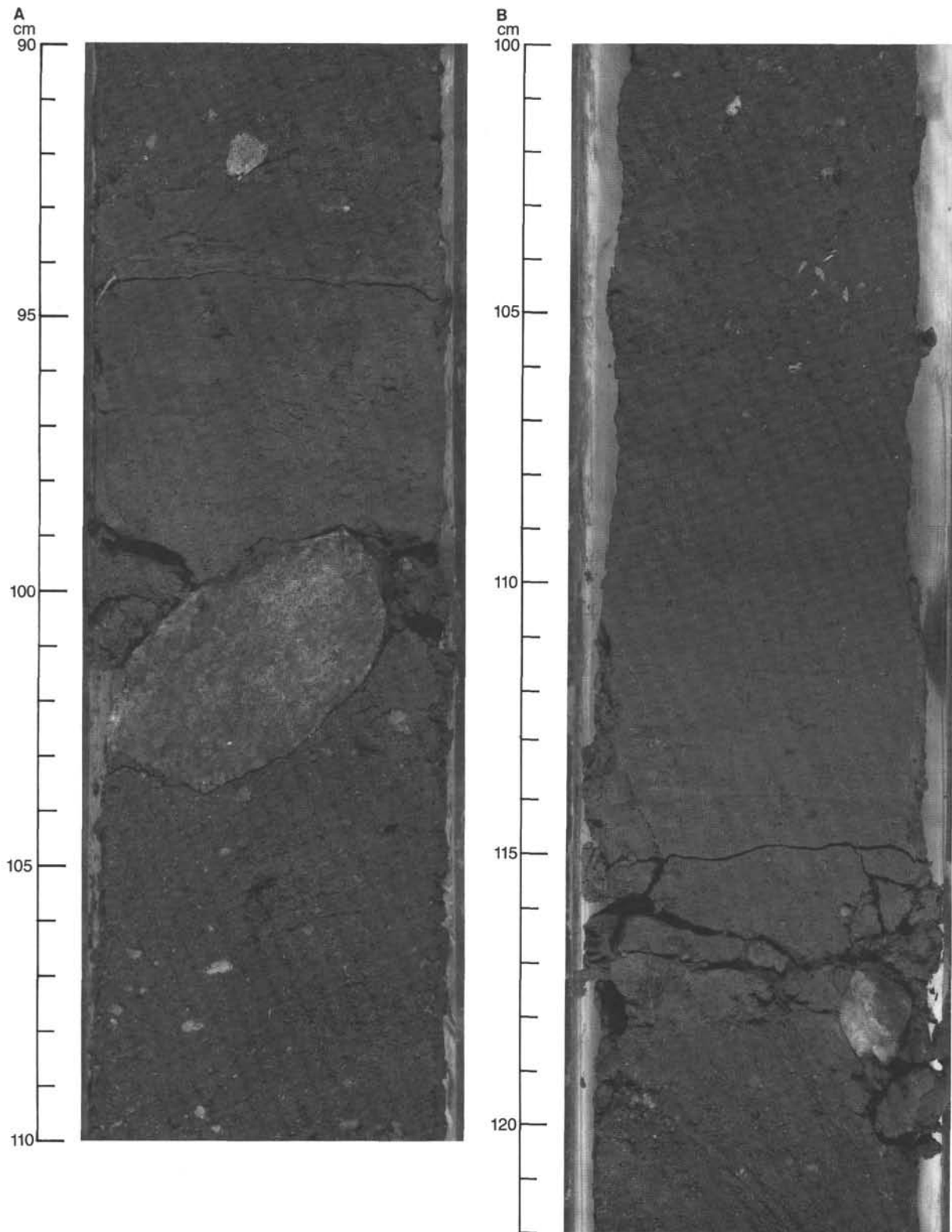


Figure 7. Stratified diamictite in lithologic Subunit IIIA. **A.** Interlayered gravel- and clast-rich diamictite and sand-silt-clay (Section 119-742A-14R-2, 90–110 cm). **B.** Interval with layers of gravelly diamictite, laminated sand-silt-clay, and intraclast-rich sandy gravel (Section 119-742A-15R-2, 100–122 cm).

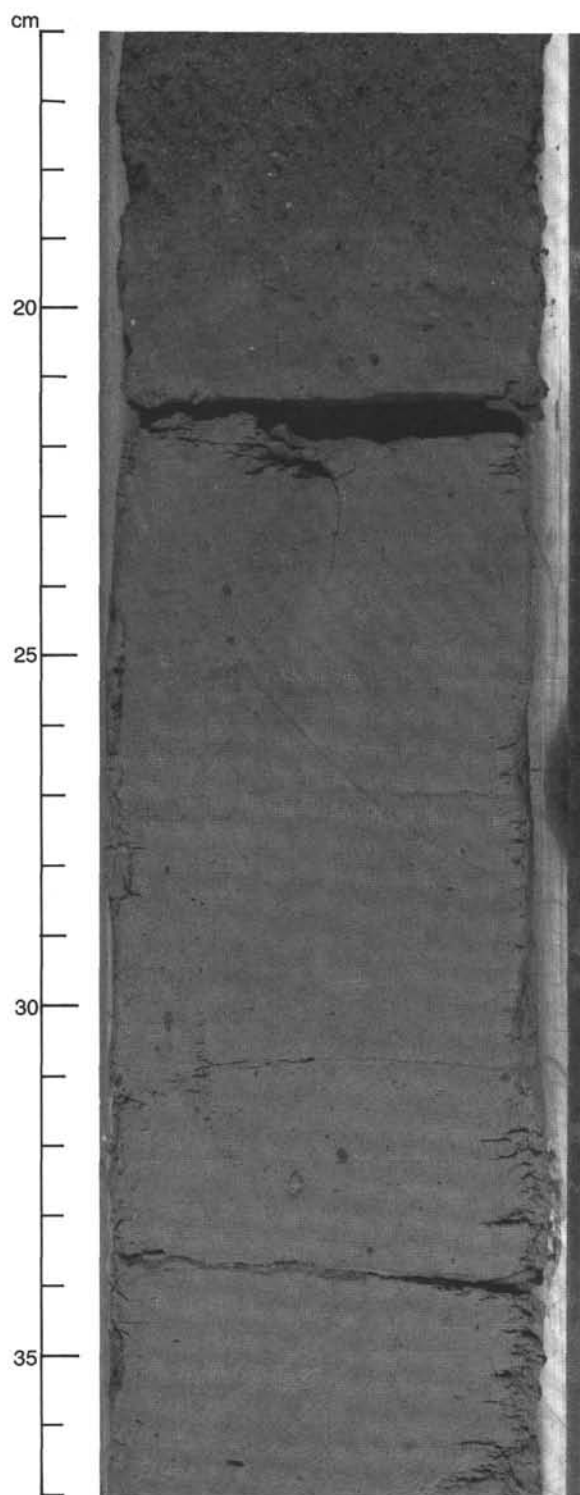


Figure 8. Top of the diatomite lithologic Subunit III B, showing scattered coarse quartz sand (ice-rafted detritus?), small intraclasts (at top), and minor deformations of bedding at the upper boundary (Section 119-742A-14R-4, 16–37 cm).

30R-2, 119-742A-30R-6, 119-742A-31R-2, and 119-742A-32R-3). Smear slide examination of carbonate-rich samples shows that they contain up to 30% micrite. Broken shell fragments are present sporadically in the lower part of the subunit. Fine silt-

clay segregated from under one such remain (Section 119-742A-27R-5, 20 cm) yielded rare specimens of ?late Oligocene/middle Eocene nannofossils and abundant spore-pollen (see “Biostratigraphy” section, this chapter).

Green to greenish black (10GY 5/1) layers a few millimeters thick also occur sporadically. The greenish coloration is thought to be due to the presence of clay minerals or glauconite. Pyrite is abundant locally and was found disseminated throughout Section 119-742-23R-1.

Two grain-orientation measurements showed random or only weak directional patterns.

Unit VI

Sections 119-742A-33R-6, 9 cm, through 119-742A-34R-CC; depth, 304.3–316.0 mbsf.

Age: ?early Eocene/Oligocene.

In this unit, diverse depositional and post-depositional processes have given rise to three distinctive lithologic subunits: VIA—interbedded silty claystones and sand-silt-clay comparable in character to the normal diamictite lithology, IVB—pale, homogeneous diamictite, and IVC—interlayered sorted sandstones, carbonaceous siltstones, and diamictite.

Subunit VIA

Sections 119-742A-33R-6, 9 cm, through 119-742A-34R-1, 120 cm; depth, 304.3–307.5 mbsf.

Age: unknown.

A close (1–3 cm) interbedding of dark gray (2.5Y 4/1) silty claystones and gray (10YR 5/1) poorly sorted sand-silt-claystones typifies this 3.1-m-thick subunit (Fig. 9). For the present, we see no evidence that the banding is rhythmical. Most of the bed junctions are vague, and, although a few of the bed bases of the silty-claystones are sharp (and irregular over sand grains and granules), no erosion appears at any of these bed bases. Sand, silt, and a few gravel clasts are scattered throughout both the principal lithologies as individual grains or in ill-defined layers. No examples of graded or cross bedding were found. A proportion of the grains stand upright, and in some cases they protrude up from the sandy layers into the claystones without attendant scour or mud draping. No burrows or rootlet structures appear evident. Outsized angular/subangular gravel grains occur both in isolation and associated with the sandy trains and centimeter-thick units of sand. Many are clearly dropstones. Although no evidence of erosion was obtained, rip-up intraclasts of the silty claystone were deposited at several levels (e.g., Section 119-742A-34R-2, 21 cm). These intraclasts have well-rounded shapes, range from 0.5 to 2 cm in size, and occur within both the silty claystone and coarse sand-silt-clay layers.

The coarser lithologies (sand-silt-clay) closely resemble the more gravel-free variety of diamictites in the surrounding subunits. Grain-size distributions, judged from smear slide examinations, are 60% sand, 30% silt, and 10% clay, but the slides do not fully sample the coarser examples. The predominant grain compositions are 70%–78% quartz and feldspar (combined), 5%–7% opaque minerals, 3%–5% organic debris, 2% mica, and 10%–15% clay.

The silty claystone lithologies have a comparable mineralogy, but texturally contain 0%–5% sand, 75% silt, and 20% clay. Mineral constituents are 9%–70% quartz and feldspar, 3%–85% clay, 3%–5% mica, 2%–20% opaques, and 3%–5% organic carbon. No cementation is evident in the core samples or in the smear slides. The overall softness (see “Physical Properties” section) implies a lack of lithification.

Fossil remains in Subunit VIA include principally the organic (plant) debris of the sand-silt fraction (see “Biostratigraphy” section, this chapter), but also some white, segmented

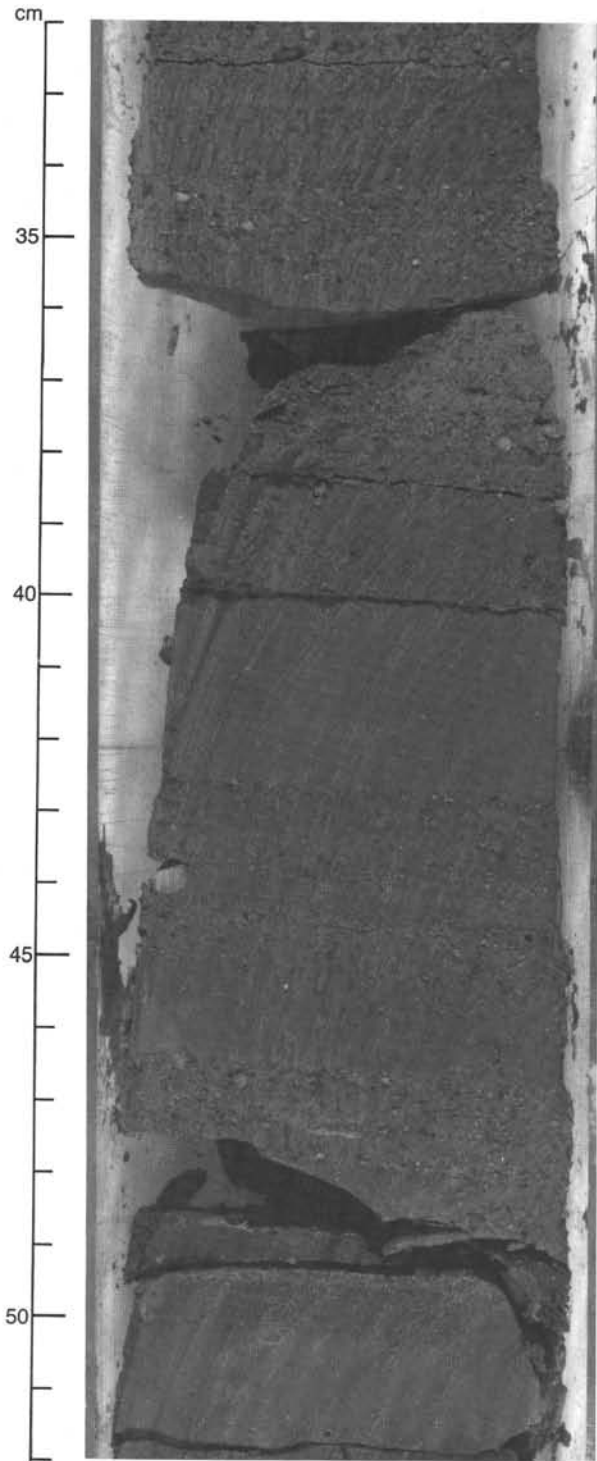


Figure 9. Portion of lithologic Subunit VIA, consisting of interbedded silty claystones and sand-silt-claystones, with scattered dropstone gravels (Section 119-742A-34R-1, 32–52 cm).

casts infilled with authigenic clay noted on some bedding planes (Section 119-742-33R-6, 20 cm). These latter resemble arthropod remains.

Subunit VIB

Sections 119-742A-34R-1, 120 cm, through 119-742A-34R-5, 95 cm; depth, 307.5–313.3 mbsf.
Age: unknown.

A 5.8-m-thick diamictite intervenes between Subunits VIA and VIC. It is similar to the diamictite and the coarse sand-silt-clay parts of those subunits. Colors are gray (5Y 3/1 to 5Y 5/1), and the textures are 70% sand, 20% silt, and 10% clay in smear slides. Compositionally, the constituents are 80% quartz-feldspar, 10% clay, and 5% opaques. From visual observations, gravel constitutes only 1%–5%, and consists mostly of metamorphic lithologies, quartz and feldspar grains, and coal. The gravel attains sizes of up to 1.2 cm and the clasts are subrounded to subangular. No preferred orientation or imbrication fabrics have been noted for the gravel clasts. The subunit is homogeneous, except for vague, dark, lamination-like structures near the base (Section 119-742A, 34R-5, 46–95 cm; see core photographs). They bear very close resemblance to “flow nose structures” found in debris flows (e.g., Eyles and Miall, 1984).

Subunit VIC

Sections 119-742A-34R-5, 95 cm, through 119-742A-34R-CC; depth, 313.3–316.0 mbsf.
Age: ?early Eocene/Oligocene.

The principal features of Subunit VIC are (1) an interlayering between sorted white sandstones, black carbonaceous siltstones, and gray diamictite (sand-silt-clay) and (2) marked soft-sediment deformation (Fig. 10). The subunit is also notable as the most carbonaceous of any in the glacial sequences at Sites 739, 742, and 743 and for its relatively high abundance of mica flakes (as is plainly visible in the core).

The overall mineralogy of the sorted sands is quite comparable to that of the sand component of the diamictites through Unit V, but texturally they are 70%–90% sand, 10%–20% silt, and 0%–10% clay (smear slide data). Colors are white to off-white (10Y 7/1). The sand components are not rounded and coarse-particle and heavy mineral lag layers are not present. The grain compositions (from smear slide data) are approximately 80%–87% quartz and feldspar combined, 5% opaques, 0%–3% organic debris (lignite), 0%–3% garnet, and 0%–10% clay. The composition may be described as immature.

The associated siltstones are much richer in organic debris (5%–10%) and mica (0%–3%) than the sorted sands and the associated nonsorted sand-silt-clays and show color tones from black (2.5Y 3/1) to dark gray (N 4/1). Boundaries to both the sorted sands and sand-silt-clay beds are abrupt, and the lower parts of the clayey siltstones are often particularly rich in organic detritus (e.g., Section 119-742A-34R-6, 123–125 cm). Mostly, however, the siltstones are internally homogeneous and show no graded bedding or lamination. Sand-silt-clay proportions are 1%, 50%, and 49%, respectively (smear slide data); no gravel is present. Compositionally, the siltstones contain about 44% quartz and feldspar, 25% opaque minerals (including some coal), 10% particles identifiable as organic debris, 3% mica, and 15% clay.

The nonsorted sand-silt-clay horizons resemble the Unit VI diamictites, except that no gravel is detected and the lithologies are better sorted. They form 1- to 30-cm-thick units and have textural parameters of 50%–70% sand, 20%–35% silt, 10%–15% clay (all three from smear slides), and 2%–3% gravel (visually from the core, Fig. 11). The color tones are gray (5Y 4/1 to 5Y 5/1). Unlike the nonsorted sand-silt-clay lithologies of the Unit VI diamictites, layering is present as laminae of better-sorted sand or higher carbonaceous content. A higher proportion than usual of the gravel and coarse sand is composed of black-brown (5YR 3/1) lignite clasts. They have a rounded to subrounded form and were clearly emplaced as clasts (pebbles) rather than wood. Mineralogical constituents are 65%–78% quartz and feldspar, 5%–7% opaques (including some coal), 3%–5% organic debris, 5% mica, and 10%–15% clay.

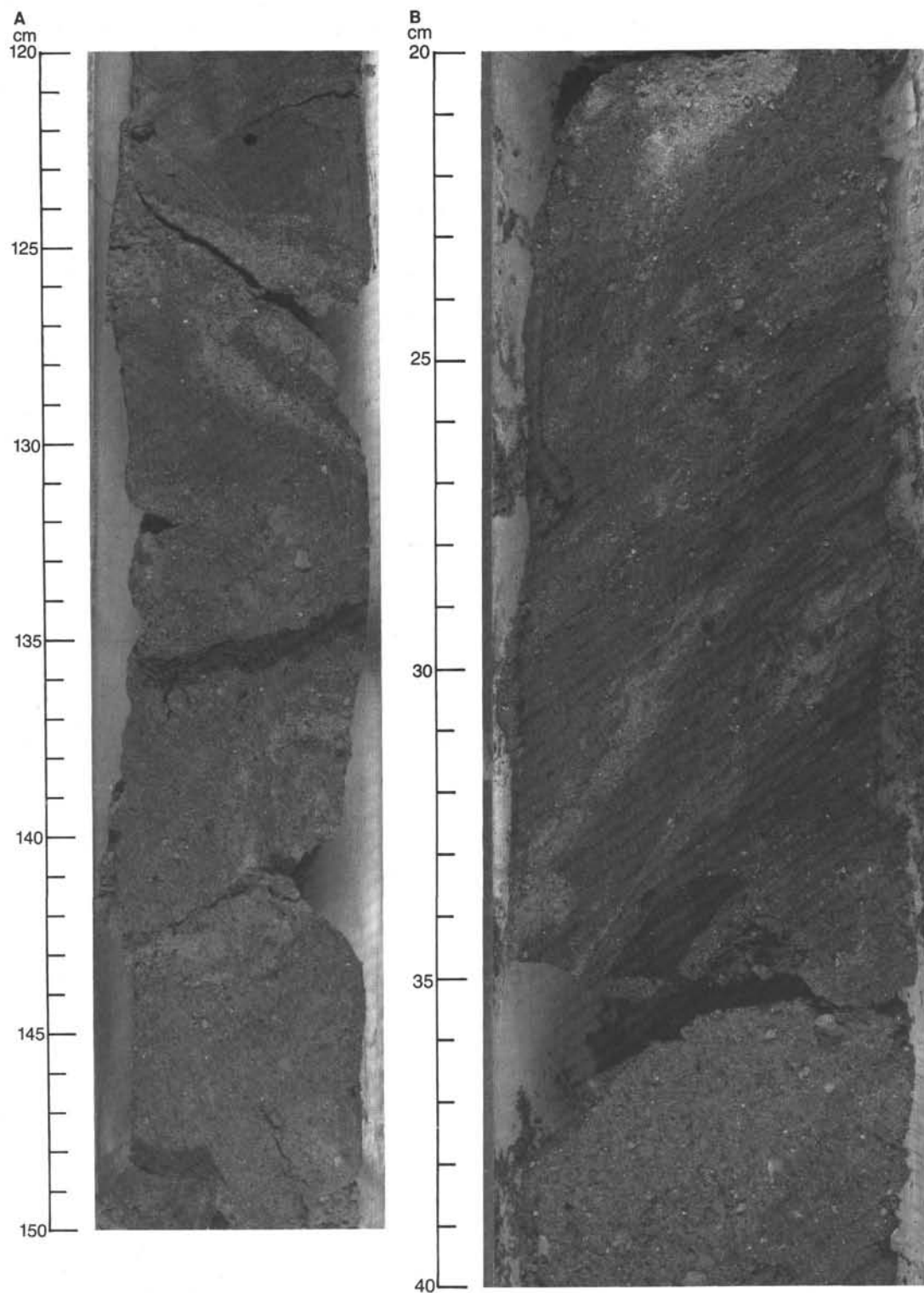


Figure 10. The deformed nature of lithologic Subunit VIC and the interlayering of sorted sandstone, carbonaceous siltstone, and diamictite sand-silt-clay. **A.** Section 119-742A-34R-5, 120–150 cm. **B.** Section 119-742A-34R-6, 20–40 cm.

The subunit has suffered extensive soft-sediment deformation. The upper boundary of the subunit truncates the deformational structure, but is itself a drilling rupture of the core, and the exact relation between Subunits VIB and VIC cannot be known. However, at its base, Subunit VIB shows structures indicative of debris-flow movement or emplacement for this 5.8-

m-thick massive diamictite. Deformation within Subunit VIC consists of recumbent fold hinges (Fig. 10A), diapiric sorted-sand segregations (Section 119-742A-34R-6, 117 cm), horizontal as well as subvertical inclinations on the warped bedding, and, mostly, a soft-sediment (plastic) character of deformation. Brittle dislocation of some sandy layers is seen (Fig. 10B), but this is

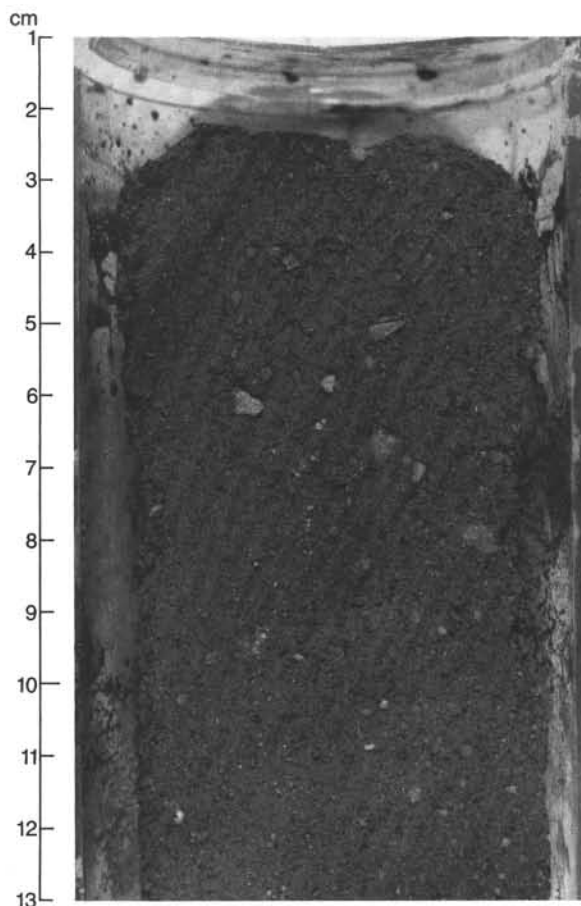


Figure 11. Diamictite, the lowest sediment in lithologic Subunit VIC of Hole 742A (Section 119-742A-34R-CC, 1–13 cm).

a common feature of sand layers in soft deformations. Both vertical and horizontal dislocations occur, in keeping with the highly disorganized geometry of deformation.

Drilling at Site 742 concluded with Section 119-742A-34R-CC, in diamictite (Fig. 11). The stratigraphic extent of Subunit VIC (the sorted sands and carbonaceous siltstones) is, therefore, undetermined.

Interpretation

Facies Analysis

Subunit IA is a marine sediment with glacial influences, deposited in conditions close to those of the present day (i.e., distal glaciomarine—terminology of Barrett et al., in press). Deep-shelf diatom accumulation is augmented with ice-rafted debris.

In the case of Subunit IB, biogenic components were overwhelmed by glacially-derived clastic sediments in a proximal glaciomarine setting. Potentially, this may result when permanent ice covers the sea surface and blocks pelagic (diatom) productivity and also when clastic supply is vastly increased. Subunit IB would appear to relate to a stage in the retreat of the last full-scale Quaternary glaciation (late Wisconsinan). Grounding icebergs may have played a role in mixing the biogenic and clastic facies and perhaps in deforming the Unit I/Unit II boundary (see also “Drilling Disturbance,” this section).

The top 15 m of Unit II also contains minor biogenic evidence of glaciomarine deposition, but the bulk of the unit lacks fossil material. Its anomalously compacted state (see “Physical

Properties” and “Logging” sections, this chapter) suggests that ice-loading occurred on its upper surface at some time since the late Pliocene. The Unit I/Unit II boundary is probably strongly erosional. Depositional conditions for Unit II were probably diverse. The recovered sediments indicate deposition as lodgement till, as indicated by preferred orientation fabrics, probable interbedded bouldery and sandy unrecovered intervals (see “Logging” section), and the massive character of the diamictite. The nonrecovered intervals may hide a complex advance-retreat sequence. Random grain fabrics and a massive character at the base indicate waterlain till deposition. A homogeneous appearance in waterlain tills would result from extremely rapid accumulation of the debris, and/or constancy through time of the grounding-line position, preventing climate changes from being reflected in the record. Closer inspection of the clast directional fabrics, downhole logging results, and diatom taphonomy is required to provide more information on these problems of facies.

Marine conditions of glacial-related deposition are proposed for the upper lower to lower upper Pliocene Unit III, which is weakly stratified and includes an 80-cm-thick diatomite. The stratification and clastic/biogenic variations indicate facies sensitivity to climatic fluctuations in proximal and distal glaciomarine environments. Size grading and rip-up intraclasts are associated with soft-sediment deformations, and some of the sediments at least owe emplacement to mass-flow (slumping) processes. The observed deformation structures in Subunits IIIA and IIIC have not affected Subunit IIIB. This suggests discrete events, related to instability of a waterlain till or proximal glaciomarine sediment on a slope. The formation appears to be anomalously compacted (see “Physical Properties” and “Logging” sections), implying that the upper boundary may be strongly erosional and that ice loading probably occurred after late early to early late Pliocene time. Minor ice rafting continued during deposition of the diatomite (Subunit IIIB).

The origin of the Subunit IIID concentration of cobbles and a large boulder cannot be determined from the core. It may represent a water- or current-washed lag deposit at the top of the massive diamictite of Unit IV, fabrics from the upper part of which suggests a waterlain origin.

Unit IV diamictites are weakly stratified on a scale of <0.5 m, as expressed in color tones, gravel abundances, micritic carbonate content, and physical properties (see “Physical Properties” and “Logging” sections). The coarseness, as indicated by gravel content, declines toward the base. Another special feature of Unit IV is its raised organic carbon (plant and palynomorph) content (Fig. 6), thought to be due to incorporation of lignitic materials from older formations such as Unit IV of Site 741. Along with the preceding features, the random or weak grain-orientation fabrics in the unit suggest waterlain till to proximal glaciomarine deposition. However, no marine fossils were found.

The massive, homogenous character and random grain-orientation fabrics of the majority of Unit V indicate that it was deposited as a waterlain till or proximal glaciomarine sediment (terminology of Barrett et al., in press). A possible grounded-ice influence is indicated by a preferred orientation of grains in Core 119-742-17R, although no other difference is obvious in the sediment. Rare occurrences of calcareous nannofossils and possible bivalve shells are further indications of marine conditions. These are the lowest known remains of marine biota in the core. Well-sorted micritic carbonate occurs as detrital material at many levels. Its origin is unclear, although one hypothesis is that it originates from calcretes like those found in Unit III at Site 740 (see “Summary and Conclusions” section, “Site 740” chapter). Cementation at some levels has apparently resulted from the presence of carbonate. Unit V has raised, but not high, levels of detrital organic carbon.

Unit VI contains thin facies that may be interpreted as terrestrial. Subunit VIA shows laminated silty claystone deposition under conditions of no biopelagic (e.g., diatom) supply and no bottom currents of any type. Lacustrine deposition is the most plausible origin, with the coarse scattered and layered debris originating through ice rafting. Several metamorphic/igneous clasts in the unit are obviously dropstones. Intraclasts of the same silty claystone have also been emplaced, although in the absence of water flow at the seafloor.

Stratigraphically below lies a thin sequence of diamictites with low gravel contents (Subunit VIB), followed by folded, relatively sorted, well-bedded sands and carbonaceous siltstones interbedded with the same type of surrounding diamictite at the base of the hole (Subunit VIC). The sorted sands and carbonaceous siltstones may be fluvial/lacustrine deposits; no conglomerates or heavy-mineral lag laminae are associated as would be expected in fluvial channel sediments, and relatively still-water (lacustrine) deposition is again favored. The sands appear to have been locally derived from glacial sediments, matching exactly in mineral content with the associated diamictites and showing no significant rounding of grains. Lignite in Subunit VIC was emplaced as pebbles and granules rather than as wood, and, so far as is known, the organic carbon present (including palynomorphs) represents materials reworked from older horizons. Subunit VIC is obviously deformed (folded); significant aspects of this have already been described.

At present, two plausible explanations exist:

1. Subunit VIC is a natural depositional unit, conformable with the rest of Unit VI, that deformed by loading from the rapid emplacement of Subunit VIB as a mass flow. In support of the latter are structures in the base of Subunit VIB that are indicative of mass flows of sand (Eyles and Miall, 1984). Furthermore, structural fabrics in Subunit VIC indicate folding rather than shearing as the deformational mode.

2. The Subunit VIC sorted sands and carbonaceous siltstones were deformed as material rafted at the base of moving ice, represent bodily incorporation of beds from another formation (e.g., Unit III, Site 741), and are interlayered with diamictite by glaciotectionic folding and shearing.

General Interpretation

Correlations between all the drilled sites at Prydz Bay are a necessary precursor to interpretations of the glacial history of Prydz Bay. Figure 12 illustrates the probable correlations of units drilled along the Prydz Bay transect, based on paleontology, lithology, seismic stratigraphy, and downhole logging (see "Lithostratigraphy and Sedimentology," "Biostratigraphy," "Logging," and "Seismic Stratigraphy" sections of the chapters for Sites 739-743) and dependent on the preliminary examination of Leg 119 data.

No datable facies or fossil assemblage appears within the Eocene-Pliocene section, which occurs in both of the deep-penetration Holes 739C and 742A, indicating that multiple erosion episodes linked to glacial advances may have removed many ice-retreat and glaciomarine (interglacial) facies. The glacial history is mainly preserved in diamictite facies.

BIOSTRATIGRAPHY

The series of different diamictite units recovered at Site 742 is lacking good biostratigraphic control because of the paucity of calcareous and siliceous microfossils. Sequences that contain sufficient fossils for age determination are of Pliocene to Quaternary and Eocene to Oligocene age.

The best biostratigraphic control for the Pliocene to Quaternary sediments is provided by diatoms and sporadic radiolarians. Foraminifers are present only in the mud-line sample. Up-

per Quaternary sediments are represented in the first core and are related to the diatom *Thalassiosira lentiginosa* Zone. Radiolarians in this core are diagnostic of the *Antarctissa denticulata* interval of Pleistocene age. The sequence down to Core 119-742A-3R contains poorly preserved diatoms and indicates a late Pliocene to Quaternary age. Core 119-742A-15R yields a diverse, moderately preserved diatom assemblage, which indicates an age between the late early Pliocene to early late Pliocene. This is supported by the presence of a radiolarian assemblage that suggests an early Pliocene age.

A calcareous nannofossil assemblage of middle to early Eocene age occurs in Cores 119-742A-11R and 119-742A-13R and is regarded as being reworked. The sequence between Cores 119-742A-15R and 119-742A-27R provides no biostratigraphic control, with the exception of Core 119-742A-20R, which contains rare fragments of Oligocene diatoms.

Eocene to Oligocene sediments are identified in Core 119-742A-27R based on the presence of the calcareous nannofossil species *Reticulofenestra daviesi*. This age is supported by palynomorphs found in Core 119-742A-34R. Pollen and spores indicate an age no older than Late Cretaceous, but a certain degree of reworking may have occurred. The presence of dinoflagellate cysts indicates an early Eocene to Oligocene age for the last core (Sample 119-742A-34R-6, 60 cm).

Calcareous Nannofossils

All core-catcher samples from Site 742 were examined, and only two were found to contain calcareous nannofossils. Sample 119-742A-11R-CC yields rare *Chiasmolithus altus*, *Chiasmolithus expansus*, *Coccolithus pelagicus*, *Cyclicargolithus floridanus*, *Reticulofenestra reticulata*, *Reticulofenestra samodurovi*, *Reticulofenestra umbilica*, and *Sphenolithus moriformis*. Sample 119-742A-13R-CC contains rare *Reticulofenestra reticulata*. The species in these two samples are diagnostic of the middle to upper Eocene and are probably reworked, as the diatom data suggest a Pliocene age for this interval. In addition, Sample 119-742A-27R-5, 13 cm (246 mbsf), from next to a pelecypod shell yields rare, but well-preserved, *Reticulofenestra daviesi*, which ranges from middle Eocene to late Oligocene.

Foraminifers

Foraminifers at Site 742 are present in the mud-line sample, but all core-catcher samples examined below this were found to be barren. The surface assemblage contains abundant benthic foraminifers, showing a high species diversity. The number of living specimens forms approximately 30%-40% of the total population. Planktonic foraminifers are only represented by *Neogloboquadrina pachyderma*. The preservation of planktonic specimens is moderate; whereas, calcareous benthic specimens are well preserved. Agglutinated species dominate the assemblage. Common species include *Miliammina arenacea*, *Cribrostomoides jeffreysi*, *Textularia earlandi*, *Textularia* sp., *Reophax* spp., and tubular species related to the family of Astrorhizidae. The calcareous component is formed by *Nonionella* sp., *Angulogerina earlandi*, *Globocassidulina subglobosa*, *Eponides tumidulus*, *Pullenia simplex*, *Astrononion gallowayi*, and other rare species. The species composition of the surface assemblage resembles that of Holes 741 and 739.

Diatoms

Diatoms are present in samples examined from Cores 119-742A-1R through 119-742A-4R, 119-742A-6R, 119-742A-15R, and 119-742A-20R. Diatom preservation and abundance vary from sample to sample, ranging from poor to moderate and rare to common, respectively. The diatom assemblage consists of species characteristic of the Southern Ocean and is somewhat similar to that observed at Site 739. Although zonal indicators

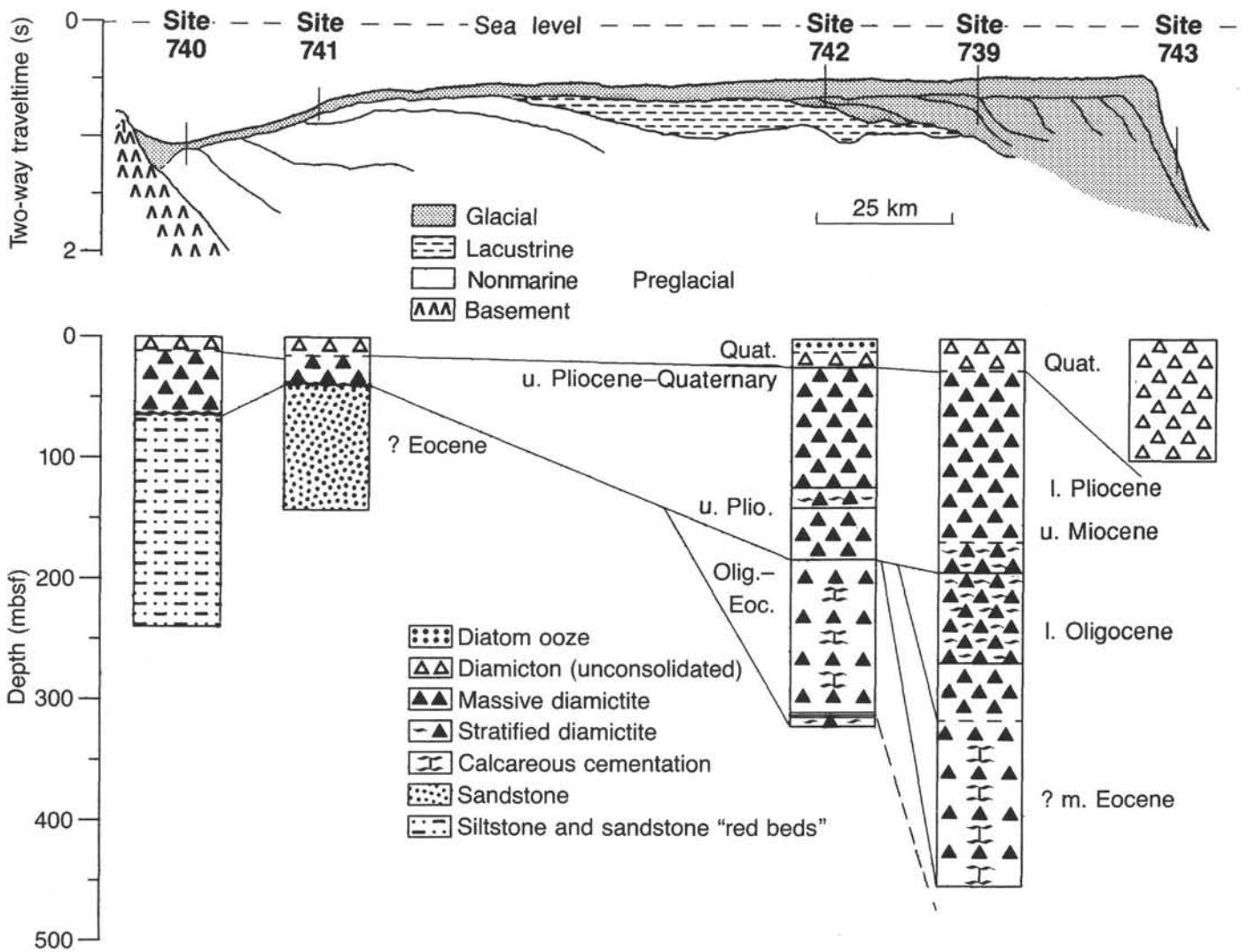


Figure 12. Representation of the sediment facies recovered from Prydz Bay during Leg 119, based on the collected seismic and stratigraphic data.

are sparse, secondary indicators provide tentative age estimates. The occurrence of *Thalassiosira lentiginosa*, *Nitzschia kerguelensis*, and *Thalassiosira gravida* in Sample 119-742A-1R-CC allows placement of this sample in the late Quaternary *Thalassiosira lentiginosa* Zone.

Cores 119-742A-2R and 119-742A-3R contain poorly preserved, rare to few diatoms. The occurrence of *Nitzschia kerguelensis*, *T. lentiginosa*, *Thalassiosira gracilis*, and *Nitzschia angulata* suggests a late Pliocene to Quaternary age for these cores. The occurrence of rare specimens of *Thalassiothrix longissima* in core-catcher Samples 119-742A-4R and 119-742A-6R provides an Oligocene to Quaternary age for these samples.

Samples 119-742A-15R-4, 30 cm, and 119-742A-15R-4, 50 cm, contain common diatoms having moderate preservation. The assemblage observed includes common *Rouxia antarctica*, *N. angulata*, *Nitzschia kerguelensis*, *Thalassiosira oliverana*, *Actinocyclus ingens*, *T. gracilis*, *Coscinodiscus kolbei*, *Cosmidiscus insignis*, *T. lentiginosa*, and rare specimens of *Nitzschia interfrigidaria* and *Nitzschia praeinterfrigidaria*. This assemblage indicates a late early Pliocene to early late Pliocene age for these samples.

Rare fragments of *Pyxilla* sp. and *Stephanopyxis* sp. occur in Sample 119-742A-20R-2, 54 cm. The occurrence of *Pyxilla*

indicates an Oligocene to Eocene age, assuming that the fragments observed are *in situ*.

Radiolarians

Radiolarians were found only in Samples 119-742A-1R-CC and 119-742A-15R-4, 38–40 cm. In the upper sample, rare and moderately preserved *Antarctissa denticulata* and *Spongotrochus glacialis*, diagnostic of the *Antarctissa denticulata* interval (Pleistocene), were found. In Sample 119-742A-15R-4, 38–40 cm, 10 species were recognized. No zone can be proposed, but the abundance of *Antarctissa ewingi*, *Antarctissa antedenticulata*, and *Saccospyris preantarctica* indicate an early Pliocene age. This sample is tentatively correlated to the *A. ewingi* interval, which spans the Pliocene. Some specimens of *Helotholus praevevema* were found in the same sample, but all specimens are broken and could be reworked.

Palynomorphs

Core 119-742A-34R contains a number of organic-rich levels, as evidenced by the presence of macroscopic wood material and coal fragments. Three smear slides (119-742A-34R-5, 130–132 cm, 119-742A-34R-6, 60 cm, and 119-742A-34R-6, 116 cm) were examined for their palynomorph content. Each sample con-

tains a small number of moderately well-preserved spores and pollen. In addition, Sample 119-742A-34R-6, 60 cm, contained three poorly-preserved dinoflagellate cyst species.

Sample 119-742A-34R-5, 130–132 cm, contains four palynomorph taxa, *Monosulcites* sp., *Microachrydites antarcticus*, *Neoraistrickia* sp., and *Cyathidites minor*. While all of these forms are relatively long-ranging (Mesozoic–Cenozoic), the presence of *Monosulcites* sp. and *Neoraistrickia* sp. indicates at least an Early Cretaceous age for this assemblage (Kotova, 1983).

Sample 119-742A-34R-6, 60 cm, contained four varieties of spores and pollen (*Monosulcites* sp., *M. antarcticus*, *Cyathidites australis*, and *C. minor*), which indicate an age no older than Late Cretaceous (Kotova, 1983). However, this sample also contains three dinoflagellate cyst species, *Odontochitina costata*, *Deflandrea phosphoritica*, and *Lentinia* sp. The latter two forms are regarded as indicative of an early Eocene–Oligocene age (Williams and Bujak, 1985; B. Tocher, pers. comm., 1988), while *O. costata* ranges from the late Albian to the Campanian. Therefore, at least some reworking is present at this level, although the possibility that the entire assemblage is reworked cannot be ignored.

Sample 119-742A-34R-6, 116 cm, contains only the following spores and pollen: *Callialasporites* sp., *Cicatricosporites* sp., *M. antarcticus*, *Cicatricosporites carlyensis*, and *Monosulcites* sp. Once again, most of these forms are relatively long-ranging, but the presence of *C. carlyensis* indicates a Late Cretaceous age (McLachlan and Pieterse, 1978) for this assemblage.

The occurrence of a variety of age assessments for these assemblages indicates that a strong degree of reworking is present in these sediments. Probably only the Eocene–Oligocene dinoflagellate cysts are in place, although this cannot be determined for certain at this time.

All of the spores and pollen were golden yellow to orange-brown in color, indicating that they are thermally mature (oil and gas phase).

PALEOMAGNETICS

Paleomagnetic studies were conducted on 221 discrete oriented samples from Hole 742A. The natural remanent magnetization (NRM) of each sample was measured on a spinner magnetometer. The samples were very strongly magnetized (generally ranging from 10 to 200 mA/m). Figure 13 is a stratigraphic plot of sample inclinations and NRM intensities. Several sampling hiatuses in the hole are marked by hatched patterns in the figure. Despite these gaps, the majority of the samples from this hole are characterized by normal polarity (negative inclinations within the Southern Hemisphere). Several brief intervals of reversed polarity (positive inclinations within the Southern Hemisphere) have been identified in this sequence and appear to correlate with the polarity pattern (shown in Fig. 13) produced by measurement of the demagnetized archive halves of the sediment cores on the shipboard cryogenic magnetometer. Ten reversed polarity zones were identified in the hole (Fig. 13). Numbers 2 and 3 are identified as separate zones in the demagnetized results but were not separated in the discrete sample data. The deepest reversed unit, number 10, was not identified in the discrete sample data set but can be clearly seen in the half-core cryogenic magnetometer data set.

The magnetic inclinations recorded by the cryogenic magnetometer display two different distributions (Fig. 14). In the upper portion of the hole, from 0 to 135 mbsf, the inclinations are scattered. This type of distribution is commonly associated with a weak overprint of secondary magnetization, commonly of the opposite polarity. Such a low coercivity component was identified in the alternating field (AF) demagnetization experiments described in the following. Within Hole 742A at depths greater than 135 mbsf, the inclinations are characterized by a more nor-

mal Gaussian distribution. The mean inclination between 175 and 180 mbsf is approximately 80°. Between 180 and 310 mbsf the inclinations become conspicuously shallower. This pattern of shallowing inclinations downhole is also seen in the NRM discrete sample measurements made on the spinner magnetometer. The shallowing inclination downward in the hole is interpreted as a decrease in the paleolatitude of the site with increasing time before the present day, reflecting the plate tectonic motions of this site.

Alternating field demagnetization studies were carried out on a set of 20 representative samples. The peak demagnetization field ranged from 10 to 50 mT. The mean destructive field for these samples was 9.8 mT. The orthogonal plots (Fig. 14) indicate that the samples are characterized by either a single component, which decays toward the origin of the plot (indicating stable magnetization in fields up to 40 mT), or they display two components of magnetization. Where two components are present, the secondary component was easily removed in fields of < 10 mT. In these cases the primary component of magnetization decayed toward the origin of the diagram (indicating stable magnetization in fields < 40 mT). At fields > 40 mT, these samples appear to display erratic magnetic directions. This observation is consistent with the acquisition of a laboratory-induced anhysteretic remanent magnetization (ARM). Based on the laboratory demagnetization studies below 40 mT, the samples from Hole 742A record stable magnetization.

Only very limited age assignments are available for Hole 742A. Diatoms and radiolarians at 115 mbsf have been assigned an age of early Pliocene (see “Biostratigraphy” section). Calcareous nannofossils and diatoms at 172 mbsf have been assigned ages of middle Eocene to Oligocene. No other age constraints are available. No unique and definitive correlations between the reversal sequence found at this site can be made with reference to geomagnetic time scales. Therefore, no age assignments have been suggested for this sedimentary sequence.

SEDIMENTATION RATES

Site 742 recovered 316 m of diamictite. Sporadic occurrences of microfossils within this sequence and the lack of index species do not permit an accurate calculation of sedimentation rates.

A late Quaternary age is assigned to the upper 4.5 mbsf and indicates a maximum age of 0.62 Ma. The next interval down to 132.7 mbsf (Core 119-742A-15R) is dated as Pliocene to early Quaternary and is younger than 4.2 Ma.

With the exception of rare Eocene to Oligocene diatoms between 171 and 181 mbsf, the sequence between 132.7 and 238.8 mbsf provides no biostratigraphic control. The sequence below 238.8 mbsf was assigned to an Eocene/Oligocene age based on calcareous nannofossils in Core 119-742A-27R (248.5 mbsf) and palynomorphs at the base of the hole (316 mbsf).

INORGANIC GEOCHEMISTRY

A single hole was cored in 415.7 m of water at Site 742 on the continental shelf of eastern Antarctica in Prydz Bay. Eleven whole-round minicores 5–10 cm in length were sampled between 3 and 303 mbsf for interstitial-water chemical studies. All of the sediment samples consist of glaciomarine diamictites and diamictites and range in age from Eocene to Quaternary (for a more complete lithologic description see “Lithostratigraphy and Sedimentology” section, this chapter). The samples contain 0.3%–1.4% organic carbon and 0%–0.7% calcium carbonate (see “Organic Geochemistry” section, this chapter).

Results

Site 742 interstitial-water samples were analyzed for pH, alkalinity, salinity, chloride, sulfate, magnesium, calcium, phos-

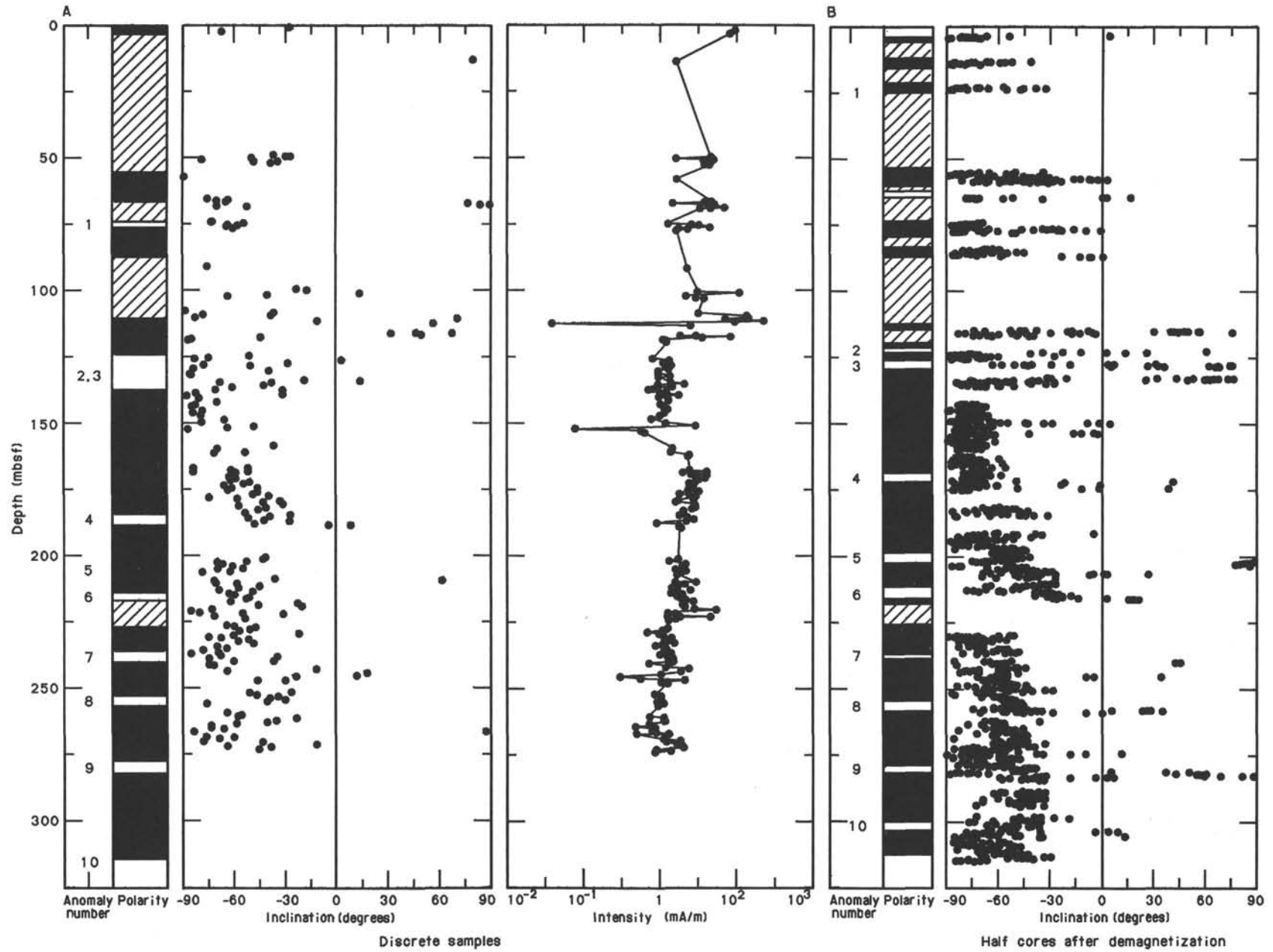


Figure 13. **A.** Stratigraphic plots from Site 742 of polarity event (anomaly) numbers, polarity, NRM sample inclinations, and intensity for discrete samples measured on a spinner magnetometer. The hatched patterns on the column indicate zones of poor or no recovery. **B.** Stratigraphic plot of event numbers, polarity, and inclinations for Site 742 half-core measurements of inclination, measured on a cryogenic magnetometer. In general, the two sequences show very good agreement in polarity.

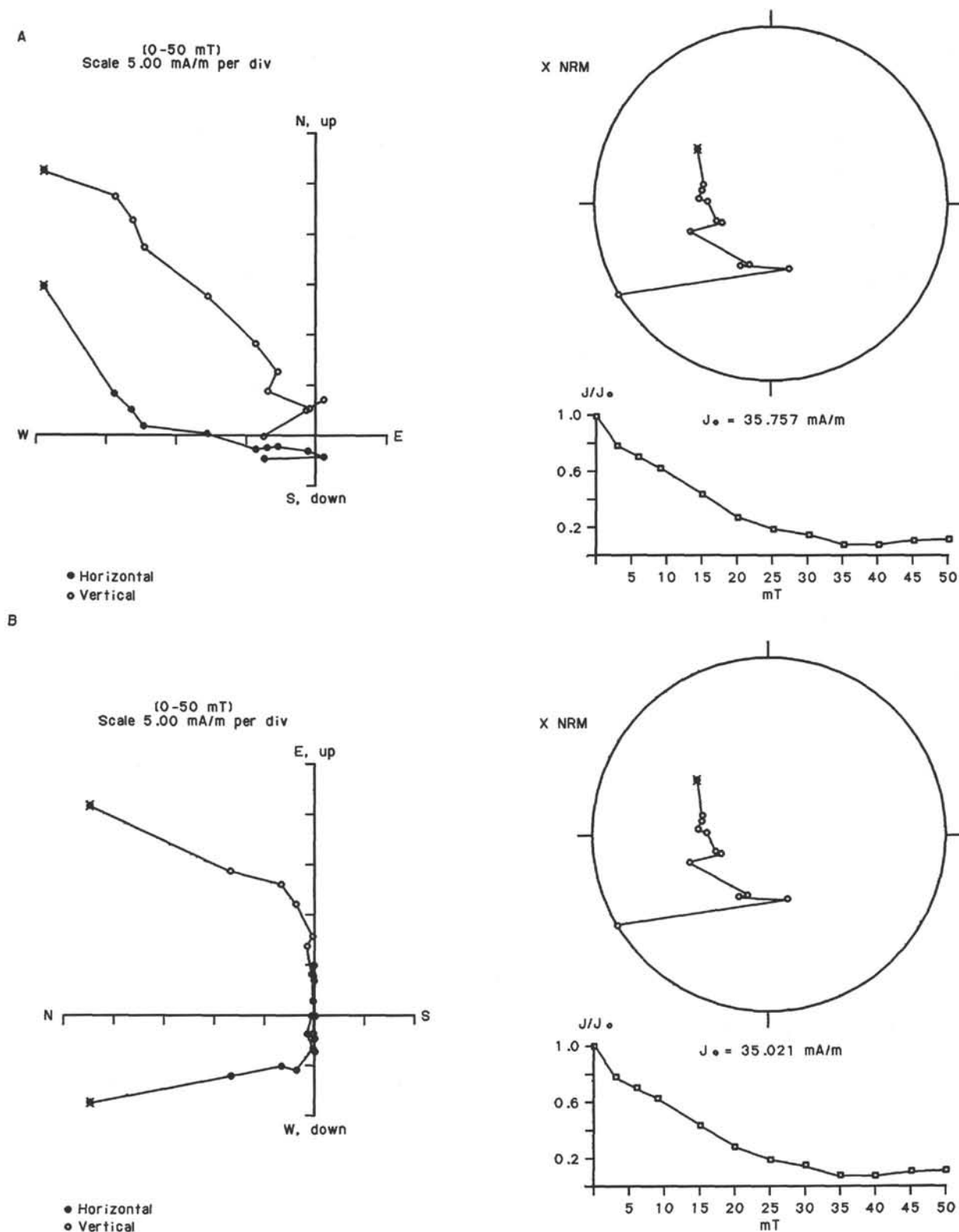


Figure 14. Orthogonal plots, equal area stereographic projections, and demagnetization curves are shown for two representative samples of AF demagnetization experiments. The shipboard demagnetization experiments were conducted using three-axis demagnetization without the benefit of a tumbler system. The absence of a tumbler is likely to result in the acquisition of ARM, particularly at high alternating-field levels. **A.** Sample 119-742A-34R-3, 38–40 cm, displays a gradual decay of magnetization, with increasing alternating fields up to 40 mT. At fields > 40 mT, a spurious moment of magnetization is acquired (note increasing intensity in demagnetization curve) that appears to be a laboratory-induced ARM. **B.** Sample 119-742A-26R-1, 26–28 cm, displays a gradual loss of intensity in fields up to 25 mT. A low coercivity component of magnetization was removed at fields between 0 and 6 mT. Between 6 and 25 mT a higher coercivity primary component of magnetization can be identified. Between 25 and 50 mT, a spurious moment of magnetization, again believed to be ARM, can be identified.

phate, ammonium, and silica using the methods outlined in the "Explanatory Notes" chapter. Charge-balance calculations were performed on each of the interstitial-water samples to check for gross irregularities in the data. Sodium and potassium were calculated by multiplying the ratio of each cation to chloride for average seawater, using the values given by Stumm and Morgan (1981), by the chloride concentration of each sample. All of the samples have charge imbalances <2%, indicating that drilling contamination is minimal and that the waters have a seawater origin. All of the data obtained at Site 741 are shown in Table 4.

Salinity and Chloride

Salinity decreases with increasing depth, and chloride concentrations are quite variable in the interstitial-water samples from Site 742 (Fig. 15). The mean chloride concentration for the set of samples is 550 mmol/L, with a standard deviation of 8 mmol/L. Approximately one-third of this variation can be attributed to analytical errors. A minimum in the chloride concentration vs. depth profile between 116 and 245 mbsf and may be explained by contamination of the samples with the surface seawater that is pumped into the hole during rotary coring or by the decomposition of gas hydrates. Steadily decreasing sulfate concentrations in this zone (see the following) indicate that no sample contamination occurred. Several cores within this interval contained small amounts of hydrocarbon gases, but no direct evidence of gas hydrates was found (see "Organic Geochemistry" section). The steady decrease in salinity with increasing depth indicates that low-salinity interstitial waters (i.e., ground water) may exist at greater depths. This possibility is supported by the presence of terrestrial sediments at the bottom of Hole 742A (see "Lithostratigraphy and Sedimentology" section).

Magnesium and Calcium

Dissolved magnesium and calcium are well correlated ($r = -0.938$) in the uppermost 174 mbsf at Site 742, but this relationship deteriorates with increasing depth (Figs. 15 and 16). The regression line in Figure 16 passes through data points representing samples from 3 to 174 mbsf and has a slope of -0.89 . Magnesium concentrations in the interstitial waters generally decrease with increasing depth, but this trend is reversed in a maximum that occurs between 116 and 206 mbsf. Dissolved calcium concentrations increase to a distinct maximum at 87 mbsf (25.5 mmol/L) and then decrease with increasing depth (14.4 mmol/L, 303 mbsf). The good correlation between calcium and magnesium concentrations in the uppermost 174 mbsf implies conservative behavior, but the calcium maximum at 87 mbsf requires a calcium source within the sediments near this depth. The excess calcium may be produced during the alteration of unstable detrital phases. An alkalinity minimum exists in the

same interval as the calcium maximum, which implies that solid carbonate phases are precipitating within this zone. Below 174 mbsf, dissolved calcium concentrations remain nearly constant (14.6 mmol/L, s.d. = 0.3 mmol/L, $n = 4$), and the sediments are described as calcareous (see "Lithostratigraphy and Sedimentology" section), supporting the possibility of active carbonate recrystallization or cementation above this level.

Silica

The concentration of silica in the Site 742 interstitial-water samples decreases about 89% with increasing depth from 3 to 303 mbsf (Fig. 15). Samples in the uppermost 15 mbsf are significantly enriched in silica (mean = 683 $\mu\text{mol/L}$) relative to seawater as a result of the dissolution of biogenic silica in the sediments. Most of the observed decrease in silica concentrations occurs between 15 (672 $\mu\text{mol/L}$) and 58 mbsf (192 $\mu\text{mol/L}$). A large increase in dissolved silica near 116 mbsf (304 $\mu\text{mol/L}$) is probably related to the dissolution of biogenic silica in the diatomite bed noted at 127.7–128.3 mbsf (see "Lithostratigraphy and Sedimentology" section). The overall decrease in silica concentrations with increasing depth indicates that silicate-poor and possibly low-salinity interstitial waters exist below 303 mbsf. Some of the decrease in silica concentrations may also be due to the formation of authigenic silicates. The abrupt concentration decrease below 15 mbsf reflects a change in the diffusion coefficient of silica as a result of the sharp decrease in porosity near 5 mbsf (see "Physical Properties" section). This barrier to downward diffusion should cause much of the dissolved silica generated near the sediment/water interface to diffuse upward into the overlying water column.

pH, Alkalinity, and Sulfate

The pH values increase whereas alkalinity and sulfate concentrations decrease with increasing depth in the interstitial waters at Site 742 (Fig. 15). Most of the pH increase occurs between 15 mbsf (7.6) and 58 mbsf (8.1). Below 58 mbsf, pH values are relatively stable (mean = 8.2, s.d. = 0.1, $n = 9$). Alkalinity values are approximately twice as high as that of average seawater (2.3 mmol/L; Stumm and Morgan, 1981) at 3 mbsf (4.74 mmol/L) and decrease to a minimum at 87 mbsf (1.32 mmol/L). Below 116 mbsf, alkalinities approach and stabilize near average seawater values (2.24 mmol/L, s.d. = 0.21 mmol/L, $n = 5$). Interstitial-water sulfate concentrations are similar to that of seawater above 87 mbsf, but steadily decrease with increasing depth below this level. The good negative correlation between ammonium and sulfate concentrations ($r = -0.875$) in this set of samples indicates that most of the sulfate depletion is due to microbial sulfate reduction. The failure of alkalinity values to increase in response to bisulfide production indicates that some of the alkalinity is being precipitated, possibly

Table 4. Interstitial-water geochemical data at Site 742.

Core, section, interval (cm)	Depth (mbsf)	Volume (mL)	pH	Alkalinity	Salinity (g/kg)	Magnesium (mmol/L)	Calcium (mmol/L)	Chloride (mmol/L)	Sulfate (mmol/L)	Phosphate ($\mu\text{mol/L}$)	Ammonium (mmol/L)	Silica ($\mu\text{mol/L}$)	$\text{Mg}^{2+}/\text{Ca}^{2+}$
119-742A-													
1R-2, 145-150	2.95	16	7.5	4.74	35.5	51.0	10.7	551	28.9	19	0.14	694	4.8
3R-1, 129-134	15.39	11	7.6	3.98	35.7	50.4	12.9	550	29.5	5	0.18	672	3.9
8R-2, 140-150	58.40	7	8.1	2.16	36.0	39.9	23.6	561	27.8	2	0.08	192	1.7
11R-2, 140-150	87.30	12	8.1	1.32	35.5	36.8	25.5	558	23.4	1	0.09	167	1.4
14R-2, 140-150	116.20	17	8.2	1.60	34.8	36.8	23.8	558	21.2	1	0.14	304	1.5
17R-5, 140-150	149.70	7	8.4	2.16	34.2	39.2	19.1	545	20.1	0	0.26	129	2.0
20R-2, 140-150	174.20	5	—	—	34.2	41.6	17.1	540	17.8	0	0.28	171	2.4
23R-4, 140-150	206.20	8	8.0	2.22	33.8	36.1	15.0	536	13.4	0	0.50	80	2.4
27R-4, 140-150	244.70	8	8.1	2.22	33.5	33.0	14.6	555	10.7	—	0.64	86	2.3
30R-4, 135-145	273.65	8	8.1	2.58	33.0	32.8	14.5	546	10.1	0	—	122	2.3
33R-4, 140-150	302.60	7	8.3	2.00	32.8	28.9	14.4	550	6.8	—	—	78	2.0

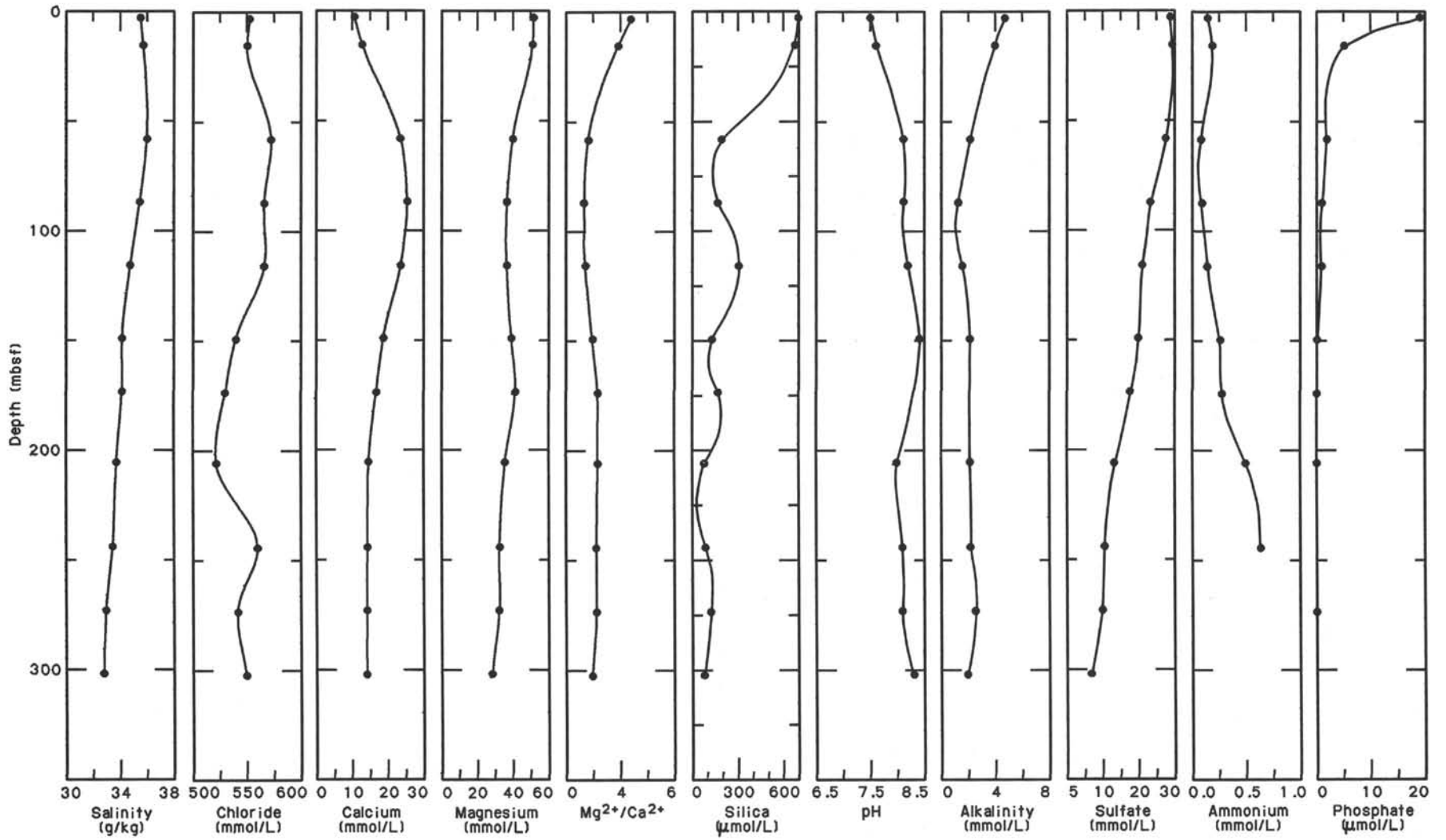


Figure 15. Interstitial-water profiles, Site 742.

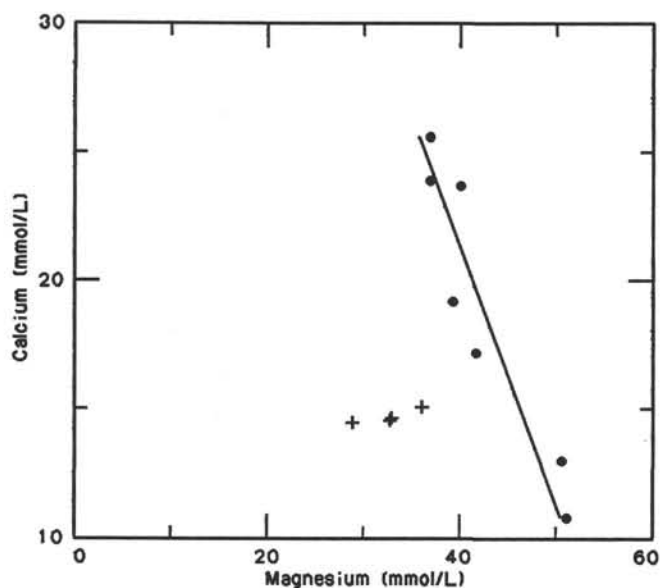


Figure 16. Calcium ion concentration vs. magnesium ion concentration for Site 742 interstitial waters. The regression line passes through data points representing interstitial-water samples in the upper 174 mbsf and has a slope of -0.89 ($r = -0.938$). The samples represented by crosses are deeper than 174 mbsf.

as calcium carbonate. As sulfate reduction is an anaerobic process, the interstitial waters must be devoid of dissolved oxygen and nitrate below 87 mbsf at Site 742.

Ammonium and Phosphate

Ammonium and phosphate concentrations exhibit opposing trends with increasing depth at Site 742 (Fig. 15). Ammonium concentrations are less than 0.2 mmol/L in all of the samples from the uppermost 150 mbsf and gradually increase with increasing depth below this level. The highest phosphate concentration measured occurs at 3 mbsf ($19 \text{ } \mu\text{mol/L}$). Phosphate concentrations decrease with increasing depth, and all of the samples below 15 mbsf are near or below the detection limit (about $2 \text{ } \mu\text{mol/L}$) of the spectrophotometer. As phosphate and ammonium are both supplied to interstitial waters by the oxidation of organic matter, the ammonium concentrations in the upper 150 mbsf are surprisingly low. Ammonium and sulfate concentrations are inversely correlated ($r = -0.875$) in this data set, which indicates that most of the ammonium is produced during sulfate reduction. The opposing trends in phosphate and ammonium concentrations indicate that these species are primarily produced by different processes. Most of the phosphate is probably released during oxidative microbial catabolism using dissolved oxygen and nitrate. The rather low concentrations of ammonium and phosphate in all of the samples indicate that the total supply of reactable organic matter to the sediments is limiting at Site 742 and/or that sedimentation rates are not sufficiently high to incorporate large quantities of organic matter into the sediments.

ORGANIC GEOCHEMISTRY

Site 742 was drilled to 316.0 mbsf before the site was abandoned because of hydrocarbon gas compositions indicative of a petrogenic source, although the concentrations of gases were very low. Organic geochemistry was studied on squeeze cakes of interstitial-water samples and on some samples from physical-properties analyses as outlined in the "Explanatory Notes" chapter.

Hydrocarbon Gases

Initially, hydrocarbon gases were routinely monitored every 30 m and later, from every core by head space (except where recovery was low). Tables 5 and 6 are compilations of the headspace and vacutainer data obtained for Site 742. Figures 17-20 are graphs of the data vs. depth.

Head Space

Head space was generally monitored using the small vial headspace technique. The canned 5-cm whole-round method was used for three cores to determine any problems like those that appeared with the small-vial headspace technique on very hard sediments, such as the diamictite in Prydz Bay. Methane levels were all 35 ppm or less at Site 742. Propane was detected in Samples 119-742A-18R-3, 0-1 cm, and 119-742A-19R-4, 0-1 cm. The levels were very low, and, because ethane was not detected above the limit of quantitation ($\sim 1 \text{ ppm}$), the real existence of propane is questionable. Sample 119-742A-22R-7, 33-34 cm, also had a show of ethane (7 ppm) and propane (on the Hewlett Packard only, $C_3 = 13 \text{ ppm}$). Hydrocarbon gases were not present again until 215 mbsf. Methane was approximately constant downhole. Ethane and propane were measured at 2-6 and 5-12 ppm, respectively, until 260 mbsf, where they dropped below the limit of quantitation.

Table 5. Headspace analysis, Site 742.

Core, section, interval (cm)	Depth (mbsf)	C_1 ($\mu\text{L/L}$)	C_2 ($\mu\text{L/L}$)	C_3 ($\mu\text{L/L}$)	C_1/C_2
119-742A-					
1R-3, 0-1	3.00	3	BD	BD	
3R-1, 128-129	15.38	5	BD	BD	
4R-1, 80-81	24.50	9	BD	BD	
7R-CC, 0-1	45.90	6	BD	BD	
8R-3, 0-1	58.50	6	BD	BD	
9R-1, 0-1	65.10	6	BD	BD	
10R-2, 149-150	77.69	6	BD	BD	
11R-3, 0-1	87.40	5	BD	BD	
14R-3, 0-1	116.30	7	BD	BD	
17R-6, 0-1	149.80	8	BD	BD	a
17R-6, 0-1	149.80	30	BD	BD	
18R-3, 0-1	155.00	35	BD	BD	
18R-3, 0-1	155.00	22	BD	1	a
19R-4, 0-1	166.20	12	BD	BD	
19R-4, 0-1	166.20	8	BD	3	a
20R-3, 0-1	174.30	5	BD	BD	
20R-3, 0-1	174.30	5	BD	BD	a
21R-3, 0-1	184.00	5	BD	BD	
21R-3, 0-1	184.00	BD	BD	BD	a
22R-7, 33-34	200.03	7	3	BD	2.3
22R-7, 33-34	200.03	6	8	13	^a 0.7
23R-6, 0-1	207.83	BD	BD	BD	a
23R-6, 0-1	207.83	BD	BD	BD	
24R-4, 0-1	214.40	BD	BD	BD	a
24R-4, 0-1	214.40	5	TR	TR	
26R-2, 149-150	232.19	8	3	TR	2.7
27R-5, 0-1	244.80	10	5	5	2.0
27R-5, 0-1	244.80	6	4	12	^a 1.5
28R-7, 74-74	258.24	6	2	BD	3.0
28R-7, 75-80	258.25	10	6	6	^b 1.7
28R-7, 75-80	258.25	7	4	11	^{a,b} 1.7
29R-1, 149-150	259.59	5	TR	TR	
30R-4, 145-150	273.75	7	TR	TR	b
30R-5, 0-1	273.80	6	TR	TR	
31R-3, 145-150	281.85	BD	BD	BD	b
31R-4, 0-1	281.90	4	TR	BD	
32R-4, 149-150	293.09	TR	BD	BD	
33R-5, 0-1	302.70	3	BD	BD	

Note: BD = below limit of detection; TR = trace levels detected below limit of quantitation.

^a Analysis with Hewlett Packard 5890 (all others with Carle gas chromatograph).

^b Headspace analysis by canned 5-cm whole-round method.

Table 6. Vacutainer analysis, Site 742.

Core, section, interval (cm)	Depth (mbsf)	C ₁ (μL/L)	C ₂ (μL/L)	C ₃ (μL/L)	C ₁ /C ₂
119-742A-					
16R-1, 97-98	133.67	8	BD	BD	a
16R-2, 19-20	134.39	25	TR	BD	a
17R-2, 67-68	144.47	196	5	TR	a ³⁹
17R-5, 34-35	148.64	178	5	TR	36
17R-6, 82-83	150.62	10	BD	BD	a,b
18R-2, 88-89	154.38	21	BD	BD	a,b
18R-3, 44-45	155.44	166	5	TR	33
18R-4, 34-35	156.84	BD	BD	BD	a,b
18R-6, 60-61	160.10	BD	BD	BD	a,b
18R-6, 61-62	160.11	88	4	4	a,c ²²
19R-4, 130-131	167.50	TR	TR	BD	
20R-1, 80-81	172.10	BD	BD	BD	
20R-2, 74-75	173.54	BD	BD	BD	a
21R-2, 112-113	183.62	6	BD	BD	
22R-3, 112-113	194.82	BD	BD	BD	
23R-4, 69-70	205.49	BD	BD	BD	
23R-4, 70-71	205.50	BD	BD	BD	c
24R-3, 8-9	212.98	BD	BD	BD	c
24R-3, 9-10	212.99	BD	BD	BD	c
26R-2, 83-84	231.53	3	BD	BD	
26R-2, 84-85	231.54	4	BD	BD	c
27R-3, 10-11	241.90	BD	BD	BD	
27R-5, 100-101	245.80	7	TR	BD	a
28R-7, 0-1	257.50	4	BD	BD	
29R-3, 100-101	262.10	6	TR	BD	
29R-3, 101-102	262.11	6	4	12	c
30R-1, 149-150	269.29	TR	TR	BD	
30R-2, 54-55	269.84	BD	BD	BD	a
31R-3, 47-48	280.87	3	BD	BD	
32R-4, 70-71	292.30	BD	BD	BD	
32R-4, 140-141	293.00	TR	BD	BD	
32R-4, 141-142	293.01	BD	BD	BD	c
33R-3, 55-56	300.25	BD	BD	BD	
34R-4, 1-2	310.81	BD	BD	BD	a

Note: BD = below limit of detection; TR = trace levels detected below limit of quantitation.

^a Vacutainer taken after core cut into sections with ends sealed.

^b Vacutainer sampling needle possibly plugged.

^c Analysis with Hewlett Packard 5890 (all others with Carle gas chromatograph).

Vacutainers

The first vacutainer sample was taken on Sample 119-742A-17R-5, 34-35 cm, to supplement the headspace information. It contained 196 ppm methane and 5 ppm ethane. Vacutainers were then taken on previous cores that had been sectioned and sealed with acetone. Gas levels in the vacutainers dropped off after 160 mbsf until Sample 119-742A-29R-3, 101-102 cm (262 mbsf), where low amounts of gas were found (C₁ = 6 ppm, C₂ = 4 ppm, and C₃ = 12 ppm). No significant levels of gas were found downhole.

Problems

Headspace analysis was difficult because of the hardness of the diamictite material ("Lithostratigraphy and Sedimentology" section). Small-vial headspace involves taking a plug of sediment from a freshly cut section of the core (see "Explanatory Notes" chapter for details). The material was so hard that small pieces had to be broken off and put into the headspace vial. This increases the chances that gases can escape, as more surface area is exposed during sampling. Because the can-headspace method yielded similar gas levels and ratios to the small-vial headspace method, gas escape was minimized. Vacutainer analysis was used to help supplement the headspace data. This technique is also suspect, as the core was smaller in diameter than the internal diameter of the core liner. The core liner was capped on both ends upon retrieval from the core barrel, but

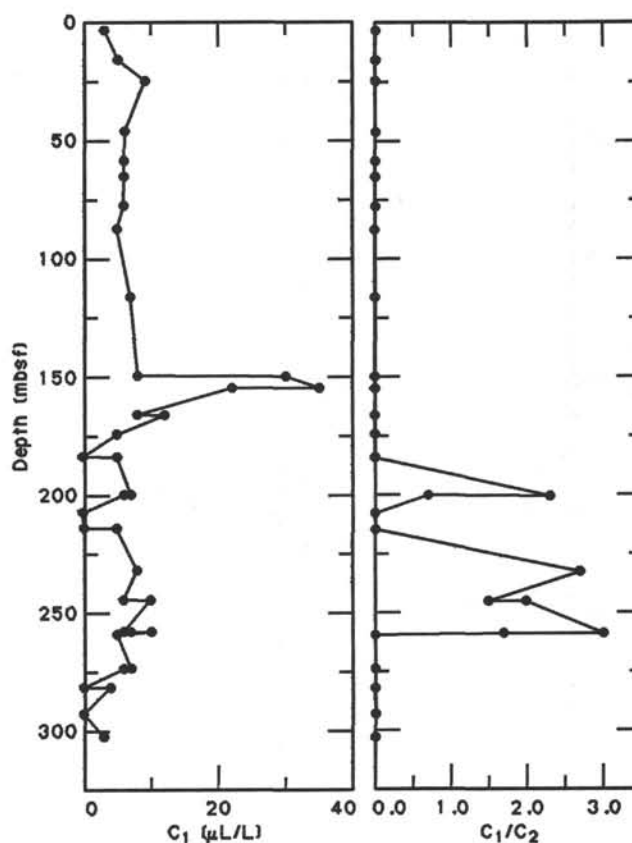


Figure 17. Methane (C₁) and methane/ethane ratios (C₁/C₂) in headspace samples at Site 742.

gas could easily escape in the time that the core barrel sat before extraction of the core liner. Neither method gives a reliable estimate of the *in-situ* gas concentration.

The headspace and vacutainer techniques also gave very different results. Near Cores 119-742A-17R and 119-742A-18R, the vacutainers gave high levels of methane and ethane, while the headspace showed only low levels of methane. In Cores 119-742A-27R and 119-742A-28R, the headspace technique had low levels of both methane and ethane, while vacutainers showed only methane.

The most reliable method of determining *in-situ* levels of gases is to use a pressure core barrel. This is more time consuming, but for sediments of the type encountered at Site 742, it could eliminate the question of how much gas is present. Without the capabilities to quantify total hydrocarbon gas levels, the only criterion for safety monitoring is the composition of gases present. Perhaps abandonment of Hole 742A could have been avoided if the total amount of gas present was known to be as low as the measured levels.

Conclusion

The gas found was real. Similar gases were found in two types of headspace analyses and in vacutainers that were analyzed on two different gas chromatographs. Because the composition of the gas was indicative of a petroleum or bituminous coal source (Claypool and Kvenvolden, 1983) and because of the proximity of the site to seismic structures (see "Site Geophysics" section, this chapter), abandonment of the site was the safest course of action. The determination of gas quantity in the original sediment would have been helpful and could have justified continuation of the hole.

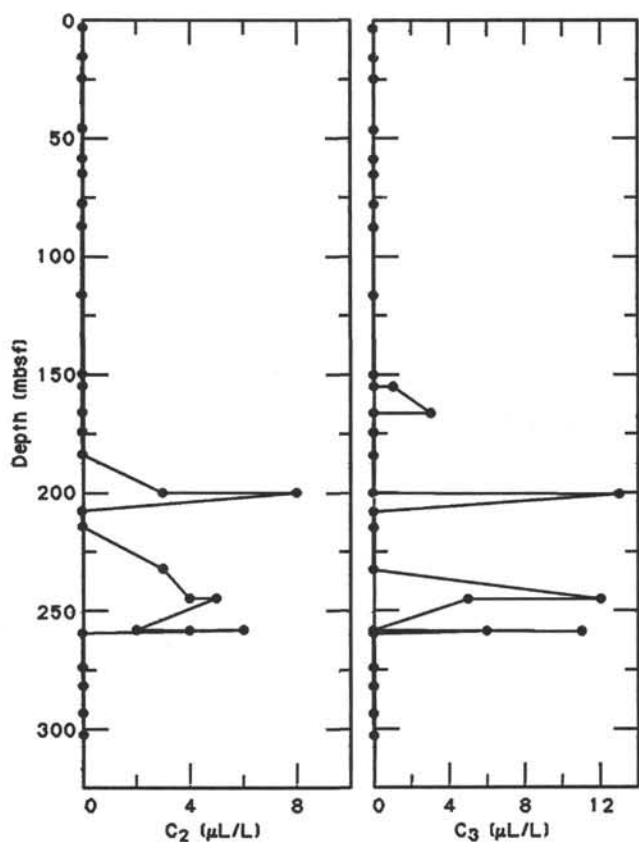


Figure 18. Ethane (C_2) and propane (C_3) in headspace samples at Site 742.

Carbon Analysis

Inorganic carbon was measured on the physical-properties samples and the interstitial-water squeeze cakes. Total carbon was measured on all of the interstitial-water squeeze cakes and most of the physical-properties samples. The difference between total carbon and inorganic carbon is total organic carbon (TOC) (see Table 7 and Fig. 21 for data).

Carbonate values are low (1.5% or less) except for Sample 119-742A-18R-2, 62–64 cm, which is 9.1% carbonate (see "Lithostratigraphy and Sedimentology" section for details on sediment types).

The TOC levels are moderate to high at Site 742. TOC gradually increases from 0.2% at the mud line to 0.4% at 125 mbsf. At 135 mbsf, TOC jumps to 1.5%. The level steadily decreases to 200 mbsf, where values remain constant at 0.5%–0.6% to the bottom of the hole.

Rock-Eval Pyrolysis

Rock-Eval pyrolysis was run on samples used for TOC determination. Table 8 is a summary of the data and important calculations. Figures 22–24 are plots of these parameters. Figure 25 is a modified van Krevelen plot of hydrogen and oxygen indices.

As at Site 741, the T_{max} values are extremely variable, indicative of significant reworking of organic carbon of various compositions and sources (Tissot and Welte, 1984). Most of the reworking appears to be above 125 mbsf (see T_{max} , Fig. 22), although this could be due to sampling bias. The youngest material is immature, as the lowest T_{max} values for this site are below 435°C.

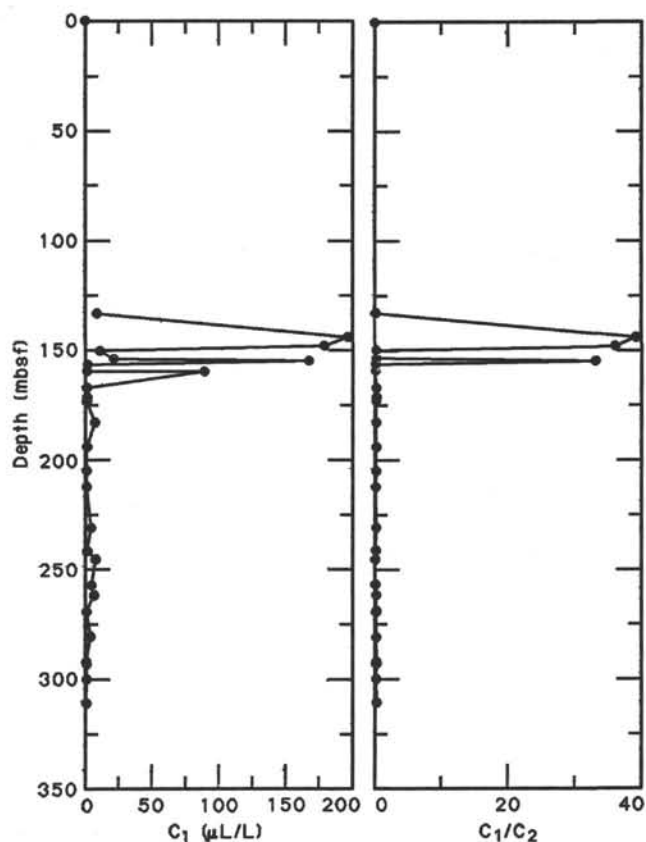


Figure 19. Methane (C_1) and methane/ethane ratios (C_1/C_2) in vacuum samples at Site 742.

As kerogen increases in maturity, it loses hydrogen and oxygen relative to carbon. On the modified van Krevelen plot (Fig. 25), samples would travel toward the origin (Waples, 1985). Generally, all of the samples from Site 742 have low hydrogen and oxygen indices with no preference for maturity near the origin. Samples with low T_{max} and hydrogen and oxygen indices were probably an admixture of several kerogens deposited in an oxygenated environment (Deroo et al., 1984).

The kerogen for Site 742 is type III and is therefore unlikely to have much petroleum-producing potential, as shown by the van Krevelen diagram. Because the samples are near the convergence of types I, II, and III, pyrolyzed carbon (PC) is needed to verify the insignificant contributions of types I and II. Type III kerogens have PC values that are less than 17% of the TOC, whereas types I and II have much higher PC values relative to TOC (Kvenvolden and McDonald, 1986). The PC values for Site 742 are all less than 18% of their respective TOC values. This confirms that the kerogen is type III.

BIOLOGY AND OCEANOGRAPHY

Physical Characteristics of the Marine Ecosystem

Brisk winds shifted between east-northeast and east-southeast from 30 January to the early morning of 2 February 1988 during the occupation of Site 742 (Table 9). The seawater temperature at the drill ship ranged from +0.7° to +1.0°C. The sky was overcast and the Secchi disc disappeared at a water depth of 7.5 m (31 January and 1 February), somewhat deeper than it had previously at Site 741. On this basis, the euphotic zone was estimated to include the upper 20.3 m. Stormy condi-

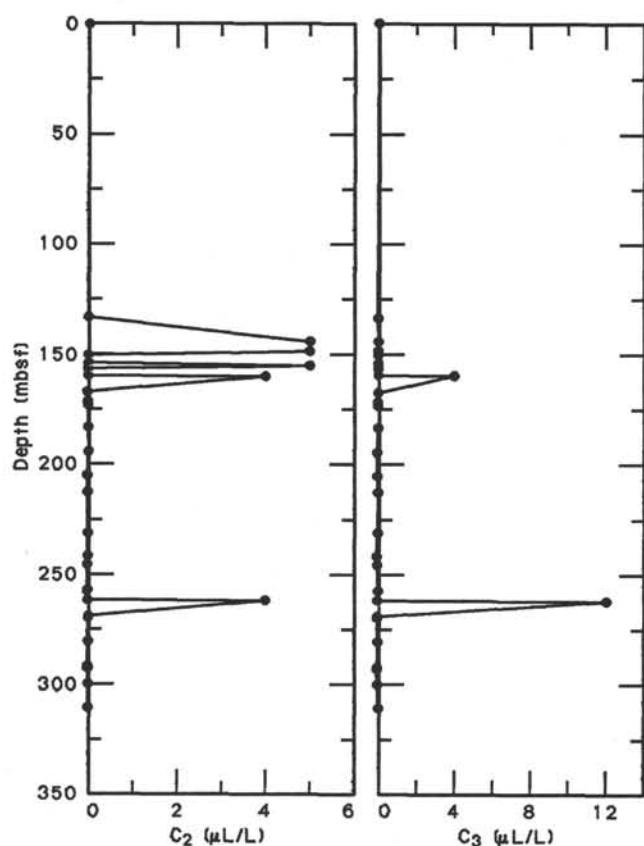


Figure 20. Ethane (C_2) and propane (C_3) in vacuolite samples at Site 742.

tions prior to site occupation resulted in a relatively deep mixed layer (down to 38 m) with a sharp pycnocline at its base well below the euphotic zone (Fig. 26).

Phytoplankton

The phytoplankton was sampled in a time series by net hauls and tows as well as discrete water samples from hydrocasts that were filtered for quantitative microscopic mounts and chemical analyses. Preliminary chlorophyll *a* analysis used as an index of biomass indicated that the pigment had dropped almost an order of magnitude from that recorded at Site 741; the maximum appeared to be at 76 m, well below the pycnocline. The triple-layered set of sediment traps (50, 100, and 200 m) was deployed and recovered twice after approximately 24 and 20 hr (31 January–1 February, 1–2 February, respectively).

Corethron criophilum and *Corethron inerme* again totally dominate the phytoplankton, but many empty cells were seen, especially in the deeper net tows (Table 10). Auxospores were present at all depths, but they were not numerous and did not come into the count in the top 50 m. Only a small fraction fluoresced; most auxospores were empty, a clear indication that this is a most vulnerable stage in diatom life history.

In the top 50 m, *Rhizosolenia alata* was in long (more than 2 mm), straight chains of cells with a diameter of only 5 μm . Cells were characterized by blunt, overlapping processes, each fitting into the envelope built into its sibling valve. Below 50 m, however, *R. alata* was stouter, with diameters of 10 μm . Each cell was about half the length (about 250 μm) of the slender forms above and had small, rounded processes. Below 100 m, several cells were seen with the elongate processes on one valve, which is associated with a winter form.

Table 7. Total carbon, inorganic carbon, organic carbon, and carbonate carbon at Site 742.

Core, section, interval (cm)	Depth (mbsf)	Total carbon (%)	Inorganic carbon (%)	Organic carbon (%)	CaCO ₃ (%)
119-742A-					
1R-1, 120-121	1.20	0.28	0.01	0.27	0.1
1R-2, 145-150	2.95	0.32	0.01	0.31	0.1
1R-3, 120-121	4.20	0.29	0.01	0.28	0.1
2R-1, 89-90	5.39	0.23	0.01	0.22	0.1
3R-1, 110-111	15.20	0.28	0.01	0.27	0.1
3R-1, 129-134	15.39	0.29	0.00	0.29	0.0
6R-1, 7-10	37.97	0.36	0.05	0.31	0.4
8R-1, 53-54	56.03	0.44	0.05	0.39	0.4
8R-2, 140-150	58.40	1.08	0.05	1.03	0.4
8R-C, 12-13	59.74	0.41	0.01	0.40	0.1
9R-1, 24-25	65.34	0.47	0.08	0.39	0.7
10R-1, 34-35	75.04	0.42	0.07	0.35	0.6
10R-2, 89-90	77.09	0.42	0.05	0.37	0.4
11R-1, 121-122	85.61	0.52	0.06	0.46	0.5
11R-2, 140-150	87.30	0.46	0.06	0.40	0.5
13R-1, 50-53	104.20	0.47	0.06	0.41	0.5
14R-1, 113-116	114.43	0.38	0.05	0.33	0.4
14R-2, 140-150	116.20	0.43	0.02	0.41	0.2
14R-3, 64-70	116.94	0.36	0.01	0.35	0.1
15R-1, 104-106	124.04	0.38	0.01	0.37	0.1
15R-3, 22-24	126.22	0.01	0.01	0.01	0.1
16R-1, 60-63	133.30	0.01	0.01	0.01	0.1
16R-3, 1-3	135.71	1.49	0.06	1.43	0.5
17R-2, 91-94	144.71	1.63	0.06	1.57	0.5
17R-4, 43-47	147.23	0.06	0.06	0.06	0.5
17R-5, 140-150	149.70	1.44	0.03	1.41	0.3
17R-6, 1-3	149.81	0.04	0.04	0.04	0.3
18R-2, 26-29	153.76	0.08	0.08	0.08	0.7
18R-2, 40-42	153.90	0.10	0.10	0.10	0.8
18R-2, 62-64	154.12	1.09	1.09	1.09	9.1
18R-4, 48-50	156.98	1.39	0.08	1.31	0.7
18R-6, 32-34	159.82	0.06	0.06	0.06	0.5
19R-1, 13-15	161.83	0.09	0.09	0.09	0.8
19R-3, 88-89	165.58	0.13	0.13	0.13	1.1
19R-6, 69-70	169.89	1.30	0.06	1.24	0.5
20R-1, 56-57	171.86	1.23	0.07	1.16	0.6
20R-2, 140-150	174.20	0.94	0.09	0.85	0.8
20R-3, 40-41	174.70	0.03	0.03	0.03	0.3
21R-2, 63-64	183.13	0.06	0.06	0.06	0.5
22R-1, 72-73	191.42	0.18	0.18	0.18	1.5
22R-3, 87-88	194.57	0.74	0.05	0.69	0.4
22R-5, 82-83	197.52	0.05	0.05	0.05	0.4
23R-1, 70-71	201.00	0.62	0.07	0.55	0.6
23R-3, 73-75	204.03	0.06	0.06	0.06	0.5
23R-4, 140-150	206.20	0.63	0.06	0.57	0.5
23R-5, 73-74	207.03	0.06	0.06	0.06	0.5
24R-4, 69-70	215.09	0.10	0.10	0.10	0.8
24R-4, 81-82	215.21	0.59	0.06	0.53	0.5
26R-1, 71-72	229.91	0.06	0.06	0.06	0.5
26R-3, 70-71	232.90	0.73	0.15	0.58	1.3
27R-1, 73-74	239.53	0.71	0.04	0.67	0.3
27R-3, 77-78	242.57	0.06	0.06	0.06	0.5
27R-4, 140-150	244.70	0.72	0.05	0.67	0.4
28R-1, 1-3	248.51	0.70	0.06	0.64	0.5
28R-3, 110-112	252.60	0.04	0.04	0.04	0.3
29R-1, 60-63	258.70	0.63	0.04	0.59	0.3
29R-3, 80-83	261.90	0.04	0.04	0.04	0.3
29R-6, 77-79	266.37	0.03	0.03	0.03	0.3
30R-1, 50-53	268.30	0.59	0.04	0.55	0.3
30R-3, 30-31	271.10	0.05	0.05	0.05	0.4
30R-4, 135-145	273.65	0.62	0.05	0.57	0.4
30R-6, 10-13	275.40	0.04	0.04	0.04	0.3
31R-2, 63-65	279.53	0.56	0.04	0.52	0.3
31R-4, 73-76	282.63	0.04	0.04	0.04	0.3
32R-1, 30-33	287.40	0.53	0.05	0.48	0.4
32R-3, 53-57	290.63	0.05	0.05	0.05	0.4
33R-1, 29-31	296.99	0.50	0.04	0.46	0.3
33R-3, 24-26	299.94	0.04	0.04	0.04	0.3
33R-4, 140-150	302.60	0.67	0.06	0.61	0.5
33R-6, 9-10	304.29	0.04	0.04	0.04	0.3
34R-3, 77-78	310.07	0.58	0.06	0.52	0.5
34-6, 26-27	314.06	0.04	0.04	0.04	0.3

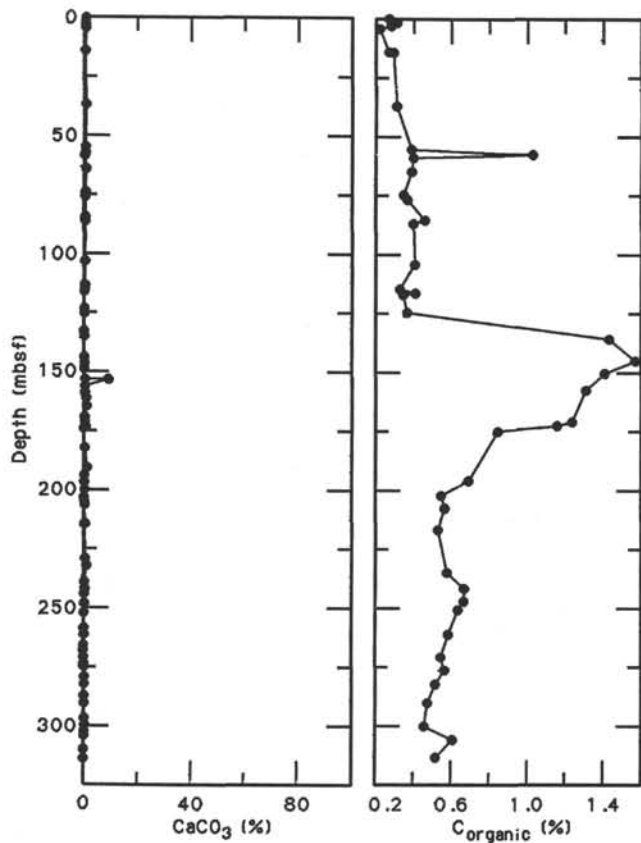


Figure 21. Carbonate and organic carbon at Site 742.

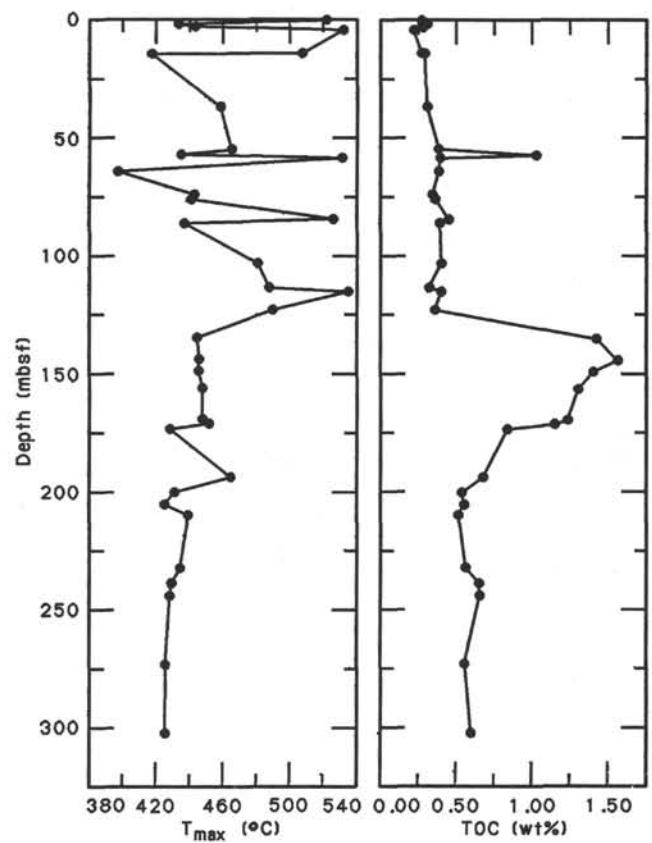


Figure 22. T_{max} and TOC at Site 742.

Table 8. Rock-Eval pyrolysis summary, Site 742.

Core, section, interval (cm)	Depth (mbsf)	Weight (mg)	T_{max} (°C)	S1 (mg HC/g)	S2 (mg HC/g)	S3 (mg CO ₂ /g)	Productivity index	S2/S3	Pyrolyzed carbon (0.08[S1 + S2])	TOC (wt%)	Hydrogen index (mg HC/g C _{org})	Oxygen index (mg CO ₂ /g C _{org})
119-742A-												
1R-1, 120-121	1.20	101.4	521	0.03	0.34	0.32	0.08	1.06	0.03	0.27	125	118
1R-2, 145-150	2.95	104.7	433	0.10	0.15	0.33	0.42	0.45	0.02	0.31	48	106
1R-3, 120-121	4.20	104.8	443	0.11	0.21	0.35	0.34	0.60	0.02	0.28	75	125
2R-1, 89-90	5.39	102.2	531	0.06	0.22	0.27	0.21	0.81	0.02	0.22	100	122
3R-1, 110-111	15.20	99.2	507	0.08	0.36	0.22	0.18	1.63	0.03	0.27	133	81
3R-1, 129-134	15.39	96.4	417	0.14	0.11	0.28	0.58	0.39	0.02	0.29	37	96
6R-1, 7-10	37.97	99.4	458	0.12	0.21	0.29	0.37	0.72	0.02	0.31	67	93
8R-1, 53-54	56.03	99.7	465	0.04	0.12	0.20	0.25	0.60	0.01	0.39	30	51
8R-2, 140-150	58.40	96.9	435	0.52	0.56	0.29	0.48	1.93	0.09	1.03	54	28
8R-CC, 12-13	59.74	98.7	531	0.01	0.28	0.19	0.04	1.47	0.02	0.40	70	47
9R-1, 24-25	65.34	95.8	398	0.01	0.04	0.20	0.25	0.20	0.00	0.39	10	51
10R-1, 34-35	75.04	109.2	443	0.02	0.06	0.19	0.25	0.31	0.00	0.35	17	54
10R-2, 89-90	77.09	96.1	441	0.02	0.05	0.24	0.33	0.20	0.00	0.37	13	64
11R-1, 121-122	85.61	148.4	526	0.03	0.15	0.33	0.17	0.45	0.01	0.46	32	71
11R-2, 140-150	87.30	107.0	437	0.21	0.24	0.23	0.48	1.04	0.03	0.40	60	57
13R-1, 50-53	104.20	119.9	481	0.08	0.30	0.31	0.21	0.96	0.03	0.41	73	75
14R-1, 113-116	114.43	132.5	488	0.05	0.30	0.28	0.15	1.07	0.02	0.33	90	84
14R-2, 140-150	116.20	94.1	535	0.37	0.54	0.22	0.41	2.45	0.07	0.41	131	53
15R-1, 104-106	124.04	128.6	490	0.03	0.39	0.24	0.07	1.62	0.03	0.37	105	64
16R-3, 1-3	135.71	112.2	445	0.18	0.88	0.29	0.17	3.03	0.08	1.43	61	20
17R-2, 91-94	144.71	126.1	446	0.09	0.84	0.32	0.10	2.62	0.07	1.57	53	20
17R-5, 140-150	149.70	111.6	446	0.14	0.93	0.24	0.13	3.87	0.08	1.41	65	17
18R-4, 48-50	156.98	112.8	448	0.04	0.72	0.21	0.05	3.42	0.06	1.31	54	16
19R-6, 69-70	169.89	133.5	448	0.06	0.65	0.27	0.09	2.40	0.05	1.24	52	21
20R-1, 56-57	171.86	132.2	452	0.07	0.77	0.21	0.08	3.66	0.07	1.16	66	18
20R-2, 140-150	174.20	100.2	429	0.37	1.09	0.66	0.25	1.65	0.12	0.85	128	77
22R-3, 87-88	194.57	124.1	465	0.01	0.50	0.48	0.02	1.04	0.04	0.69	72	69
23R-1, 70-71	201.00	129.4	432	0.02	0.38	0.33	0.05	1.15	0.03	0.55	69	60
23R-4, 140-150	206.20	107.8	426	0.14	0.44	0.32	0.24	1.37	0.04	0.57	77	56
24R-1, 81-82	210.71	125.3	440	0.11	0.54	0.39	0.17	1.38	0.05	0.53	101	73
26R-3, 70-71	232.90	124.0	435	0.10	0.62	0.69	0.14	0.89	0.06	0.58	106	118
27R-1, 73-74	239.53	145.4	430	0.10	0.58	0.47	0.15	1.23	0.05	0.67	86	70
27R-4, 140-150	244.70	95.8	429	0.17	0.60	0.41	0.22	1.46	0.06	0.67	89	61
30R-4, 135-145	272.65	102.8	426	0.21	0.61	0.37	0.26	1.64	0.06	0.57	107	64
33R-4, 140-150	302.60	97.5	426	0.27	0.63	0.34	0.30	1.85	0.07	0.61	103	55

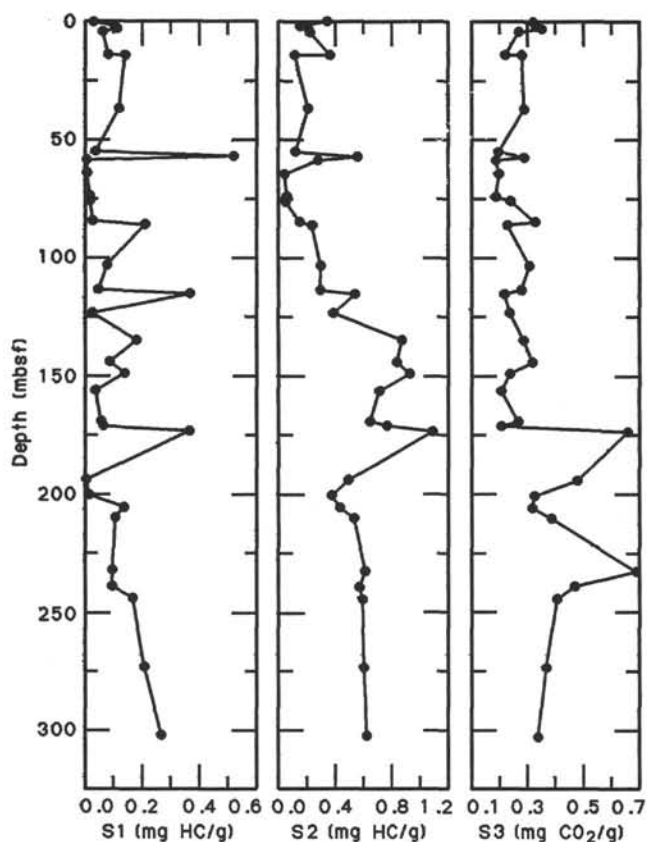


Figure 23. S1, S2, and S3 at Site 742.

In the deepest layer sampled (200–100 m) *Chaetoceros neglectus* resting spores were common within their vegetative chains. In fecal pellets throughout the water column, however, resting spores from *Chaetoceros* sp. cf. *wighamii* were abundant. Many spores retained pigment and had not been digested. Other planktonic species were seen both in a lightly silicified vegetative state and in resting spores. Heavily silicified cold-water forms, such as *Stellarima microtrias*, *Thalassiosira tumida* (southern form), and *Thalassiosira ritscheri* also appeared.

Phaeocystis was still abundant, but the colonies fluoresced only dimly. Grazers, such as tintinnids, were abundant in the 50- to 100-m sample, while many polychaetes were abundant in the deepest layer. Fecal pellets from that layer not only showed intact, pigmented cells, but cells were beginning to protrude from the disintegrating bundles.

Diatoms in Surface Sediments

Although the balance was different, species found at the water/sediment interface (mud-line Sample 119-742A-1H-1, 0 cm) were similar to those found farther inshore in Prydz Bay at Site 740. Species not recorded there include *Azpetia tabularis*, *Nitzschia ritscherii*, *Nitzschia pseudonana*, *R. alata*, and *Synedra reinboldii*. Particularly abundant was *Thalassiosira* sp. cf. *gravid*a, approximately 20 μ m in diameter. In some cases, the heavily silicified frustules were still intact, indicating resting spore structure. This small species will be part of an onshore study and considered in relation to the plankton.

PHYSICAL PROPERTIES

The main objective of drilling at Site 742 was to penetrate a sequence of glacial sediments, inferred from seismic ties to adjacent sites, into preglacial sediments to date the onset of glacia-

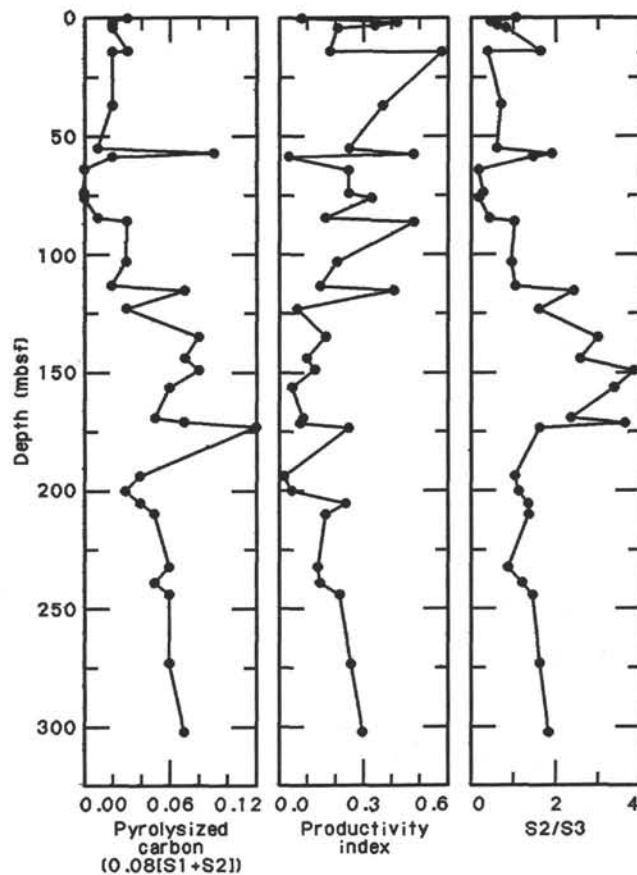


Figure 24. Pyrolyzed carbon, productivity index, and S2/S3 at Site 742.

tion. The physical-properties program was aimed particularly at investigating the glacial sediments with respect to possible effects of variable glacial cover. The sedimentary sequence cored at Site 739 showed changes that may be interpreted in terms of varying proximity to the glacier grounding line, superimposed on trends caused by overconsolidation. The latter could have been caused by direct glacial loading, by sediment loading and subsequent glacial erosion, or by a combination of both. Site 742, 29 km southeast of Site 739, was expected to verify this trend and, hence, give further background data for shorebased consolidation studies of whole-round core samples (see "Physical Properties" section, "Site 739" chapter).

Parameters measured were (1) index properties, (2) undrained shear strength, (3) compressional-wave velocity, and (4) thermal conductivity. Wet-bulk density was measured both gravimetrically and using the GRAPE. Velocity was measured both by means of the continuous *P*-wave logger (PWL) on whole-round cores and in discrete intervals with the Hamilton Frame Velocimeter. Because velocity measurements are essential over as large a distance as possible in poorly sorted diamictites, most measurements were carried out parallel to the length axis of the core, that is, normal to the bedding (A direction). In some intervals, velocity was also measured parallel to bedding on the same samples (C direction). PWL and continuous GRAPE runs were only performed in the uppermost, soft part of the cored sequence, where the samples completely filled the core liner. In all other parts of the sequence, discrete samples were measured. Shear strengths were measured with vane shear and fall cone apparatuses in the upper, soft part of the cored section and with a pocket penetrometer below 5.4 mbsf. Techniques and laboratory methods used are discussed in the "Explanatory Notes" chapter.

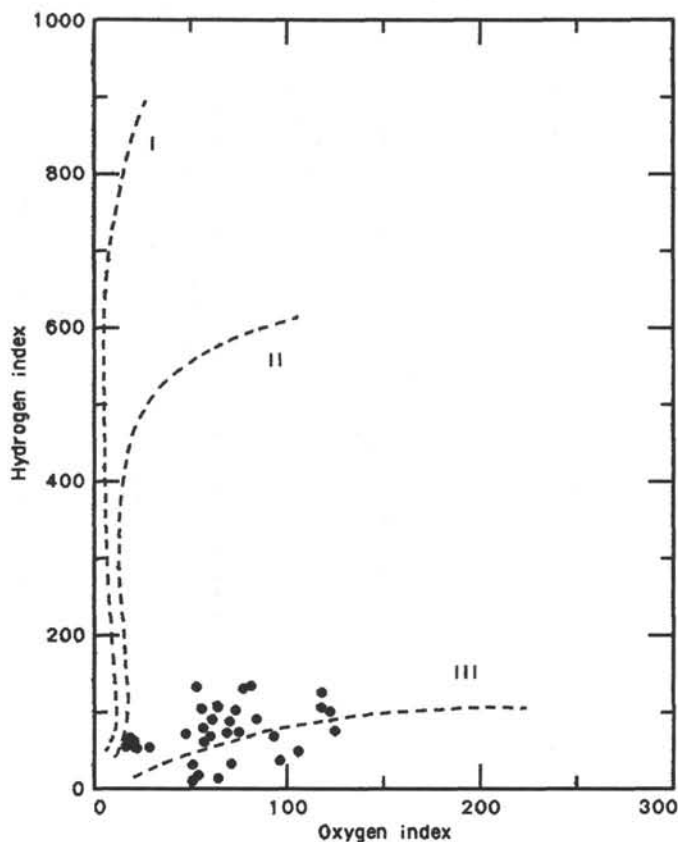


Figure 25. Modified van Krevelen plot of oxygen index vs. hydrogen index at Site 742.

Table 9. Wind and weather summary at Site 742 (67.5°S, 75.4°E) for January–February 1988.

30 Jan., 00–2359Z:	Wind: Northeast-east at 30–40 kt with gusts to 45 kt, decreasing to 22–28 kt by 18Z. Sea-surface temperature: 0.8°–1.0°C. Waves: 5–7 m decreasing to 3–4 m late in period. Sky: Overcast with light snow; pressure rising. Air temperature: Maximum –0.1°C at 18Z, minimum –1.3°C at 00Z.
31 Jan., 00–2359Z:	Wind: East-southeast at 20–25 kt decreasing to northeast 12 kt by 12Z. Sea-surface temperature: 0.7°–0.8°C. Waves: 3 m. Sky: Overcast with snowshowers ending at 10Z; pressure rising slightly then beginning to fall at 06Z. Air temperature: Maximum –1.2°C at 12Z, minimum –2.1°C at 06Z.
1 Feb., 00–2359Z:	Wind: East-southeast at 14–18 kt shifting to the northeast 14–18 kt by 18Z. Sea-surface temperature: 0.7°–0.8°C. Waves: 2–3 m. Sky: Low overcast with light snow developing by 18Z; pressure falling then steady by 18Z. Air temperature: Maximum –0.7°C at 18Z, minimum –2.3°C at 00Z.
2 Feb., 00–04Z:	Wind: Northeast at 18–22 kt. Sea-surface temperature: 0.8°C. Waves: 2–3 m. Sky: Overcast with light snow; pressure rising. Air temperature: –2.2°C at 00Z.

One hole, 742A, was drilled at this site, to a total depth of 316 mbsf, with RCB coring. The drilling was stopped because of the presence of gas. Drilling disturbance is mainly seen as biscuiting of the core and cone-shaped shear planes between biscuits.

Results

The drilled sequence was divided into six main lithologic units, some of which were further divided (see “Lithostratigraphy and Sedimentology” section). Lithologic Unit I (0–5.4 mbsf) is a soft diamicton with a thin cover of diatom ooze and is of late Quaternary age. Units II, III and IV, down to 172.5 mbsf, are diamictites, with various degrees of banding and variable clast contents, interrupted by a thin layer (127.7–128.3 mbsf) of diatomite. The age range for these units is Pliocene to Quaternary. Unit V (172.5–304.3 mbsf) was classified as a calcareous diamictite. The lowermost lithologic Unit VI consists of diamictites; laminated silt, sand, and claystones; and carbonaceous sandstones and shales. Units V and VI were deposited sometime between the middle Eocene and Oligocene (see “Biostratigraphy” section).

Core recovery at Site 742 was variable, averaging 53.4%. However, approximately the upper 100 mbsf had significantly less recovery than farther downhole, precluding a detailed interpretation of the upper part.

Within the constraints set by the core recovery, six geotechnical units have been defined. Geotechnical unit boundaries were placed midway between the two nearest data points in nonrecovery intervals if a match with lithologic unit boundaries was not found. The division is based on a combination of all measured physical properties and may not show up equally well on each individual parameter. All measured properties are presented in Tables 11 and 12 and displayed in Figure 27. Minimum, maximum, and average values of different parameters for the geotechnical units are presented in Table 13.

The scatter in the thermal-conductivity values, as well as for the shear-strength values, is most likely due to the unsorted and rather sandy character of the cored diamictites, which caused highly variable resistance to penetrometers and variable contact between the sediment and the needle probes of the thermal-conductivity apparatus. Although smaller, a variable degree of scatter also occurs in the other physical-properties profiles. This is also ascribed to the unsorted sediment character. All measurements of index properties, GRAPE density, and velocity were carried out on small sample volumes, and gravel may cause severe deviation from values representative for the sediment as a whole. GRAPE samples are not the same as those used for index properties, although they were taken immediately adjacent to each other, and are larger. Therefore, a slight difference is seen between the two bulk density measurements, although they usually compare well. Velocities measured parallel and normal to the bedding show apparently unsystematic variations and, hence, no significant trend in anisotropy. As the measurements were carried out over small distances, occasional clasts may have a great effect, and clast shape and orientation may likewise cause varying measurements in different directions.

Geotechnical Unit G1

With the exception of the upper 0.1 m of diatom ooze, geotechnical unit G1 (0–5.45 mbsf) consists of normally consolidated diamicton. The water content and porosity average approximately 17% and 33%, respectively, whereas bulk density averages 2.14 g/cm³ and velocity 1800 m/s. Shear strength, measured both with the Wykeham-Farrance motorized vane and fall cone apparatus, shows an average of 28.1 kPa. Geotechnical unit G1 corresponds to lithologic Unit I (see “Lithostratigraphy and Sedimentology” section).

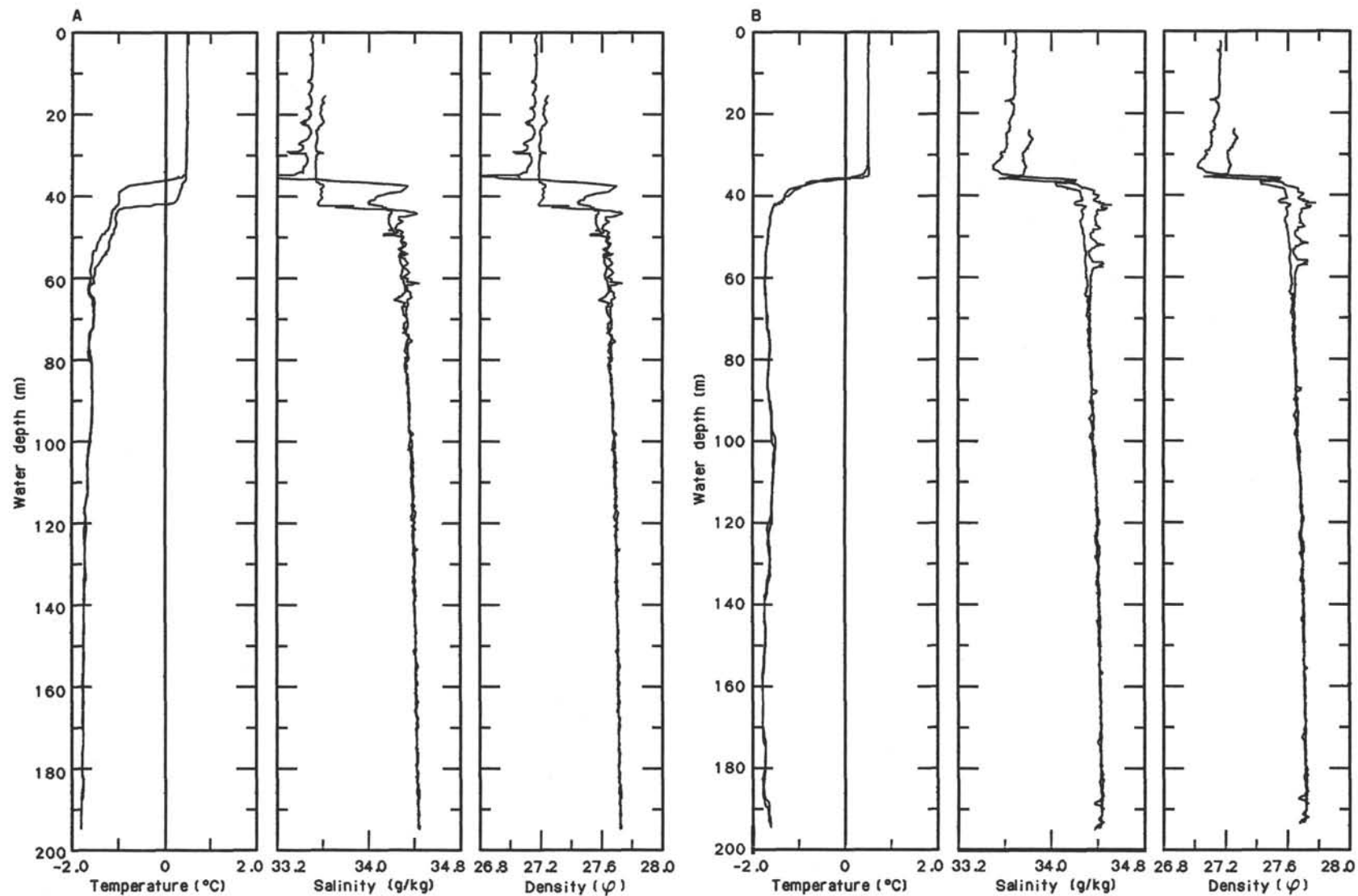


Figure 26. Conductivity, temperature, and depth (CTD) in the top 200 m of the water column, as measured by the self-contained unit. Both the downtrace and uptrace are included over most of the depth to show the reliability of the unit and the variation in the water column. The surface 12–15 m was erased from the downtrace because of noise in the system as the unit became equilibrated to the seawater. **A.** CTD-14, 31 January 1988, 1235–1305 hr (local time); 67°32.5'S, 75°30'E. **B.** CTD-15, 1 February 1988, 0902–0914 hr (local time); 68°34'S, 75°29.5'E. The surface 38 m appears well-mixed, and internal waves possibly were operating at the pycnocline/mixed layer interface from the offset of the downtrace and uptrace in Figure 26A.

Table 10. Life stage and condition of *Corethron*, *Maersk Master* operations 335 and 341, 31 January 1988.

Condition	0–50 m	50–100 m	100–200 m
Vegetative cells			
Empty (%)	21.4	39.7	80.0
Autofluorescing (%)	78.6	50.3	15.0
Auxospores			
Empty (%)	0	9.3	3.5
Autofluorescing (%)	0	0.7	1.5

Geotechnical Unit G2

The boundary between geotechnical units G1 and G2 (95.45–114.0 mbsf) is clearly seen at 95–97 cm in Section 119-742A-2R-1. It is an abrupt transition into significantly stiffer and more sandy material and, furthermore, marks a change from predominantly whole to predominantly broken diatoms (see “Biostratigraphy” section). All physical-properties parameters show a dramatic gradient at this level, which is probably best evidenced in bulk density, shear strength, and velocity. Average values for the unit are water content, 12.15%; porosity, 26.54%; bulk density, 2.31 g/cm³; GRAPE density, 2.33 g/cm³; compressional-wave velocity, 2140 m/s; and shear strength, 585 kPa. The geotechnical unit approximates lithologic Unit II, a homogeneous diamicite with pebbles and boulders (see “Lithostratigraphy and Sedimentology” section).

Geotechnical Unit G3

Geotechnical unit G3 (114.0–135.4 mbsf) approximates lithologic Unit III, which is further divided into four subunits, based on various degrees of stratification and pebble content in the diamicites and also includes a thin layer of diatomite (see “Lithostratigraphy and Sedimentology” section). Unit G3 is easily distinguishable in all the measured geotechnical properties and is characterized by an increase in water content and porosity and a decrease in bulk density, undrained shear strength, and compressional-wave velocity. Average values are water content, 20.52%; porosity, 39.53%; bulk density, 2.12 g/cm³; GRAPE density, 2.01 g/cm³; undrained shear strength, 385 kPa; and velocity, 1793 m/s.

Geotechnical Unit G4

Geotechnical unit G4 (135.4–172.6 mbsf) roughly corresponds to lithologic Unit IV, a homogeneous diamicite (see “Lithostratigraphy and Sedimentology” section). Geotechnically, this unit is not significantly distinguishable from unit G2, with average values of water content, 11.94%; porosity, 25.39%; bulk density, 2.31 g/cm³; GRAPE density, 2.29 g/cm³; and velocity, 2150 m/s. Undrained shear strength is, on the other hand, mostly higher than 900 kPa, which is the upper limit of the pocket penetrometer. Only one shear-strength value was obtained, and this is not representative for the unit.

Geotechnical Unit G5

Geotechnical unit G5 (172.6–195.4 mbsf) lies within lithologic Unit V, which is classified as a calcareous diamicite (see “Lithostratigraphy and Sedimentology” section). The carbonate is probably concentrated in layers, as the carbonate analyses performed on 2–3 samples per core show a general carbonate content of <1% (see “Organic Geochemistry” section). It represents similar trends as unit G3, although not as distinct. Average physical properties values are water content, 15.35%; porosity, 31.88%; bulk density, 2.19 g/cm³; GRAPE density, 2.24 g/cm³; shear strength, 668 kPa; and velocity, 1991 m/s. The sediment appears slightly more clayey in this interval, and grain-size dis-

tribution may be a cause of the difference in the geotechnical units above and below. The drilling disturbance, in the form of shear planes and drilling biscuits, became more obvious in this part of the cored sequence.

Geotechnical Unit G6

Geotechnical unit G6 (195.4–316.0 mbsf, total depth) covers the rest of lithologic Unit V and Unit VI, which are interbedded diamicites, claystones, siltstones, and sandstones that become more carbonaceous in the lowermost part (see “Lithostratigraphy and Sedimentology” section). Average values are close to those of geotechnical units G2 and G4: water content, 12.60%; porosity, 27.43%; bulk density, 2.30 g/cm³; GRAPE density, 2.26 g/cm³; and velocity, 2051 m/s. The undrained shear strength again is generally too high to be measured by shipboard instruments; however, in the lowermost core (Core 119-742A-34R), the shear strength again dropped to measurable values. This occurs in lithologic Subunit VIC, which consists of carbonaceous, well-sorted sands and siltstones with interbedded diamicites. Layers in this core are distorted, but this does not resemble drilling disturbance. Other physical properties also show a slight change in the lowermost part of the hole, in particular water content, porosity, and GRAPE density. However, the changes are small and may not be significant considering the background scatter level. Cemented diamicites were observed within unit G6, starting in Core 119-742A-23R. The high GRAPE density and velocity values measured at 205.64 mbsf represent one cemented layer.

Thermal Conductivity

Thermal-conductivity data were measured on up to four sections per core, where permitted by core recovery. Only values with a temperature drift rate of >0.1°C/min were used. The values average 1.589 W/m/°C and are scattered between 0.145 and 3.177 W/m/°C. The conductivity values show no significant trend that justifies any subdivision into units such as for the other geotechnical parameters. However, the values and scatter recorded may be representative of glacial diamicites. Toward the lower part of the drilled sequence, below approximately 250 mbsf, is a slight tendency of generally higher conductivity values, which could reflect grain-size variations or be an effect of increased cementation.

Summary and Discussion

The cored section at Site 742 is divided into six geotechnical units, G1–G6. The upper geotechnical unit G1 represents young (late Quaternary; see “Biostratigraphy” section), normally consolidated diamicton covered by a thin veneer of diatom ooze. The most distinct physical-properties boundary is the G1/G2 boundary that grades into compacted diamicites. Geotechnical units G2, G4, and G5 show essentially the same physical-properties characteristics, although smaller-scale variations are superimposed on the general trends. Units G3 and G5 show distinctly different characteristics of higher water content and porosity and lower bulk density, compressional-wave velocity, and shear strength than the sediments above and below. The geotechnical boundaries show a generally good correspondence with lithologic boundaries (see “Lithostratigraphy and Sedimentology” section). An exception to this is the G5/G6 boundary, which is within lithologic Unit V, a calcareous diamicite.

A comparison with downhole logging measurements of velocity, porosity, and bulk density is included in Figure 28. All geotechnical units are well defined in the logging results. Deviation between the curves may partly result from pressure differences between the *in-situ* and laboratory environment and partly from problems with cavities in the hole (see “Logging” section). This is particularly well shown in the lower half of the downhole

Table 11. Physical properties measured at Site 742.

Core, section, interval (cm)	Depth (mbsf)	Water content (% wet wt)	Porosity (%)	Wet-bulk density (g/cm ³)	Dry-bulk density (g/cm ³)	Grain density (g/cm ³)	GRAPE density (g/cm ³)	Undrained shear strength		Compressional- wave velocity ^b (m/s)	
								(kPa)	Instrument ^a	A	C
119-742A-											
1R-1, 59	0.59	17.48	35.09	2.11	1.74	2.59		15	W	1774.2	
1R-1, 62	0.62							44	F		
1R-1, 120	1.20	20.10	38.66	2.00	1.60	2.54		11	F	1748.2	
1R-1, 123	1.23							13	W		
1R-2, 80	2.30							17	W		
1R-2, 86	2.36	16.57	33.84	2.16	1.80	2.61		30	F	1811.4	
1R-3, 26	3.26	17.28	35.71	2.16	1.79	2.70		10	W		
1R-3, 27	3.27							34	F	1768.6	
1R-3, 120	4.20	17.55	36.54	2.17	1.79	2.75		27	W		
1R-3, 121	4.21							31	F	1768.6	
1R-3, 122	4.22							30	W		
2R-1, 80	5.30	15.00	31.50	2.19	1.86	2.64		40	W	1913.4	
2R-1, 80	5.30							64	F		
2R-1, 89	5.39	14.20	20.40	2.22	1.91						
2R-1, 98	5.48	10.40	21.30	2.45	2.19	2.35		123	F	1979.2	
3R-1, 56	14.66	12.20	28.90	2.30	2.02	2.97	2.35	650	P	2099.1	
3R-1, 110	15.20	11.70	25.80	2.30	2.03	2.68	2.37	770	P	2165.0	
3R-1, 110	15.20	370	F								
4R-1, 7	23.77	13.86	29.73	2.32	2.00	2.67	2.27			2119.6	
4R-1, 23	23.93							447	P		
4R-1, 75	24.45							817	P		
6R-1, 7	37.97	13.60	29.84	2.30	1.98	2.74		497	P	2169.3	
6R-1, 24	38.14						2.52			5130.0	
8R-1, 53	56.03	10.93	24.38	2.33	2.08	2.67	2.40			2523.3	
8R-1, 66	56.16							530	P		
8R-1, 123	56.73	11.53	24.85	2.28	2.01	2.58	2.29			2084.5	
8R-1, 136	56.86							540	P		
8R-2, 41	57.41	11.00	24.44	2.33	2.07	2.66	2.32			2159.2	
8R-2, 55	57.55							626	P		
8R-3, 45	58.95	10.75	23.66	2.34	2.08	2.62	2.33			2208.7	
8R-3, 107	59.57							705	P		
8R-CC, 12	59.74	14.10	30.31	2.27	1.95	2.69	2.24	500	P	1923.1	
9R-1, 6	65.16							382	F		
9R-1, 20	65.30	11.38	25.17	2.32	2.06	2.66	2.31			2147.2	
9R-1, 36	65.46							740	P		
10R-1, 34	75.04	11.05	24.17	2.31	2.06	2.61	2.33	460	P	2440.7	
10R-1, 125	75.95							643	P		
10R-1, 144	76.14	11.19	24.68	2.31	2.05	2.64	2.39			2029.4	2484.0
10R-2, 45	76.65						2.32			2125.0	2066.0
10R-2, 65	76.85							585	P		
10R-2, 89	77.09	13.16	28.94	2.32	2.01	2.73					
10R-3, 38	78.08	12.13	26.27	2.33	2.05	2.62	2.34	447	P	2179.6	2152.7
11R-1, 42	84.82	10.70	23.94	2.35	2.10	2.67	2.33	730	P	2164.0	2345.8
11R-1, 12	85.61	12.43	27.23	2.35	2.06	2.68	2.30	753	P	2130.0	2165.3
11R-2, 65	86.55	12.37	26.79	2.28	2.00	2.63	2.32			2036.0	2007.5
11R-2, 78	86.68							383	P		
13R-1, 50	104.20	15.31	32.53	2.15	1.82	2.71	2.30			2012.2	1986.8
14R-1, 26	113.56	13.28	27.94	2.26	1.96	2.57	2.31	500	P	2107.8	2285.7
14R-1, 113	114.43	16.98	32.84	2.21	1.83	2.43	2.28			1846.8	2047.6
14R-2, 57	115.37	17.30	33.62	2.22	1.84	2.46	1.78			1916.3	2055.6
14R-3, 64	116.94	17.06	35.60	2.11	2.58	2.73	1.86			1700.7	
15R-1, 24	123.24	26.20	46.91	2.00	1.48	2.52	2.07			1716.7	1697.8
15R-1, 40	123.40							447	P		
15R-1, 104	124.04	19.48	38.62	2.12	1.71	2.64	2.00			1810.5	1773.7
15R-2, 64	125.14							307	P		
15R-2, 112	125.62	27.20	47.10	1.98	1.44	2.42	1.91			1726.9	1709.7
15R-3, 22	126.22	19.03	38.84	2.15	1.74	2.74	2.21			1891.2	1957.6
15R-3, 130	127.30							350	P		
15R-4, 30	127.80							400	P		
15R-4, 55	128.05	25.99	47.53	1.98	1.47	2.62	2.04			1756.9	1821.7
16R-1, 60	133.30	17.25	35.40	2.19	1.81	2.67	2.11	420	P	1780.9	1750.0
16R-2, 90	135.10	18.65	38.79	2.28	1.86	2.81	2.14			2059.9	
16R-3, 1	135.71	13.14	27.71	2.39	2.07	2.57	2.30			2123.3	2289.9
17R-1, 55	142.85	12.77	26.74	2.32	2.03	2.53	2.29	370	F	2163.9	1948.9
17R-2, 91	144.71	8.43	18.86	2.32	2.13	2.56	2.30			2133.6	
17R-3, 28	145.58						2.23			1886.6	
17R-4, 43	147.23	10.57	22.14	2.26	2.02	2.44	2.23			2153.3	
17R-5, 67	148.97	10.09	22.09	2.47	2.22	2.57	2.35			2050.4	
17R-6, 1	149.81	14.03	29.26	2.28	1.96	2.57	2.33			2016.9	
18R-1, 52	152.52	11.39	25.17	2.34	2.07	2.66	2.30			2251.3	2348.6
18R-2, 26	153.76	14.73	29.75	2.18	1.86	2.49	2.29			2185.5	
18R-3, 46	155.46	13.11	27.18	2.27	1.97	2.51	2.30			2107.3	
18R-4, 48	156.98	12.20	26.79	2.32	2.04	2.67	2.26			2141.1	
18R-5, 50	158.50	13.99	27.94	2.22	1.91	2.42	2.29			2276.9	
18R-6, 32	159.82	13.27	25.99	2.21	1.92	2.33	2.31			2235.7	

Table 11 (continued).

Core, section, interval (cm)	Depth (mbsf)	Water content (% wet wt)	Porosity (%)	Wet-bulk density (g/cm ³)	Dry-bulk density (g/cm ³)	Grain density (g/cm ³)	GRAPE density (g/cm ³)	Undrained shear strength		Compressional-wave velocity ^b (m/s)	
								(kPa)	Instrument ^a	A	C
119-742A-											
19R-1, 60	162.30	11.62	24.33	2.36	2.08	2.48	2.31			2266.1	2333.3
19R-2, 41	163.61	13.17	28.45	2.32	2.02	2.66	2.30			2247.4	
19R-3, 88	165.58	11.20	24.78	2.44	2.17	2.65	2.33			2177.8	
19R-4, 63	166.83	10.26	22.77	2.33	2.09	2.62	2.26			2145.4	
19R-5, 44	168.14	10.46	22.99	2.30	2.06	2.60	2.30			2114.5	
19R-6, 69	169.89	10.84	24.11	2.31	2.06	2.66	2.32			2222.2	2157.4
20R-1, 17	171.47							600	P		
20R-1, 56	171.86	11.58	25.42	2.31	2.04	2.64	2.29			2190.5	
20R-2, 63	173.43	13.42	28.57	2.23	1.93	2.62	2.34	583	P	1936.7	
20R-3, 28	174.58							437	P	1892.9	
20R-3, 40	174.70	16.21	32.72	2.12	1.77	2.55	2.18				
21R-1, 11	181.11	14.18	29.21	2.20	1.89	2.54	2.28	800	P	2000.0	2048.4
21R-1, 135	182.35							778	P		
21R-2, 40	182.90							740	P		
21R-2, 63	183.13	14.64	31.05	2.21	1.89	2.67	2.28			2014.0	2028.4
21R-3, 29	184.29	17.44	35.95	2.14	1.76	2.70	2.19			1957.8	2311.9
22R-1, 72	191.42	14.42	30.14	2.20	1.88	2.60	2.25			1894.7	
22R-2, 41	192.61						2.18			1886.4	
22R-2, 52	192.72	16.30	34.05	2.27	1.90	2.69					
22R-3, 87	194.57	16.21	33.33	2.17	1.82	2.62	2.18			1931.4	
22R-4, 104	196.24	12.25	26.86	2.38	2.09	2.67	2.29			2080.2	
22R-5, 61	197.31						2.27			2052.6	
22R-5, 82	197.52	12.32	26.34	2.27	1.99	2.59					
23R-1, 70	201.00	12.44	26.47	2.26	1.98	2.58	2.27			2038.8	
23R-2, 83	202.63	13.09	27.47	2.23	1.94	2.55	2.22			2079.5	
23R-3, 73	204.03	12.57	26.99	2.26	1.98	2.61	2.29			2062.5	
23R-4, 71	205.51	12.03	26.18	2.37	2.08	2.64	2.26			2071.8	
23R-4, 92	205.72	2.05	5.10	2.66	2.60	2.61	2.60			4188.9	
23R-5, 73	207.03	11.66	25.67	2.36	2.08	2.66	2.32			2085.0	
23R-6, 73	208.56	11.76	25.39	2.29	2.02	2.59	2.30			2106.3	
24R-1, 81	210.71	11.40	24.39	2.26	2.00	2.55	2.31			2120.2	
24R-2, 65	212.15							708	P		
24R-2, 82	212.22	11.67	25.54	2.32	2.05	2.64	2.27				
24R-3, 94	213.84	11.38	25.11	2.28	2.02	2.65	2.31			2071.4	
24R-4, 69	215.09	11.14	24.33	2.35	2.09	2.60	2.30			2107.3	
26R-1, 71	229.91	15.00	30.68	2.19	1.86	2.55	2.20			2009.3	
26R-2, 76	231.46	12.53	25.97	2.22	1.94	2.49	2.23			2101.5	
26R-3, 70	232.90	11.92	26.01	2.27	2.00	2.64	2.24			2195.1	
26R-4, 70	234.40	12.39	26.90	2.32	2.03	2.64	2.29			2155.7	
27R-1, 73	239.53	13.73	28.65	2.24	1.94	2.56					
27R-2, 78	241.08	11.84	25.43	2.26	1.99	2.58	2.28			2109.7	
27R-3, 77	242.57	12.13	25.99	2.25	1.97	2.58	2.27			2053.7	
27R-4, 76	244.06	13.96	29.52	2.27	1.95	2.62	2.27			2029.7	
27R-6, 65	246.95						2.28			2078.3	
27R-6, 88	247.18	11.91	25.68	2.26	1.99	2.60					
28R-1, 1	248.51	13.19	28.84	2.29	1.99	2.71	2.20			1916.1	
28R-2, 110	251.10	11.84	26.71	2.31	2.03	2.76	2.25			1974.7	
28R-3, 110	252.60	13.39	28.38	2.16	1.87	2.60	2.03			2154.8	
28R-4, 103	254.03	14.37	30.49	2.24	1.92	2.66	2.23			2068.8	
28R-6, 115	257.15	12.01	26.06	2.37	2.08	2.62	2.23			2137.7	
29R-1, 60	258.70	12.89	28.23	2.22	1.93	2.70					
29R-2, 40	260.00	10.99	26.22	2.45	2.18	2.92	2.11			1795.3	
29R-3, 80	261.90	12.16	27.28	2.30	2.02	2.75	2.30			2118.8	
29R-4, 24	262.84	12.52	27.54	2.34	2.05	2.70	2.31			2117.3	
29R-5, 98	265.08	11.94	26.60	2.50	2.20	2.72	2.00			1808.4	
29R-6, 77	266.37	12.17	27.15	2.35	2.06	2.73	2.34			2055.0	
30R-1, 50	268.30	11.62	26.64	2.41	2.13	2.81	2.33			1673.5	
30R-2, 40	269.70	15.16	31.20	2.21	1.87	2.58	2.26			1910.1	
30R-3, 30	271.10	17.39	35.56	2.16	1.78	2.66	2.15			1757.4	
30R-4, 30	272.60	11.70	27.21	2.41	2.13	2.87	2.28			2009.4	
30R-5, 48	274.28	13.66	29.40	2.23	1.93	2.67	2.26			1977.9	
30R-6, 10	275.40	13.84	29.37	2.24	1.93	2.63	2.22			2000.0	
31R-1, 44	277.84	11.65	25.91	2.29	2.03	2.70				2060.8	
31R-2, 62	279.52	13.61	30.80	2.28	1.97	2.87	2.26			2101.6	
31R-3, 100	281.40	10.63	24.10	2.34	2.10	2.71				2045.5	
31R-4, 73	282.63	10.64	24.09	2.43	2.18	2.71	2.33			2206.3	
32R-1, 30	287.40	12.09	26.32	2.33	2.05	2.64	2.25			2167.7	
32R-2, 97	289.57	11.84	27.16	2.39	2.11	2.82	2.38			2111.1	
32R-3, 53	290.63	11.78	25.48	2.24	1.98	2.60	2.40			2046.9	
33R-1, 29	296.99	14.07	30.35	2.28	1.96	2.70	2.27			2202.9	
33R-2, 75	298.95	11.40	25.52	2.35	2.08	2.71	2.32			2178.7	
33R-3, 24	299.94	15.22	33.71	2.29	1.94	2.88	2.32			2156.5	
33R-4, 90	302.10	14.08	30.07	2.18	1.87	2.67	2.30			2087.3	
33R-5, 86	303.56	11.91	26.10	2.31	2.03	2.65	2.23			2152.1	
33R-6, 9	304.29	14.76	32.46	2.36	2.01	2.82	2.19				

Table 11 (continued).

Core, section, interval (cm)	Depth (mbsf)	Water content (% wet wt)	Porosity (%)	Wet-bulk density (g/cm ³)	Dry-bulk density (g/cm ³)	Grain density (g/cm ³)	GRAPE density (g/cm ³)	Undrained shear strength		Compressional-wave velocity ^b (m/s)	
								(kPa)	Instrument ^a	A	C
119-742A-											
34R-1, 45	306.75							800	P		
34R-1, 83	307.13	15.44	32.66	2.19	1.85	2.70	2.16			1929.3	
34R-3, 77	310.07	12.34	27.28	2.26	1.98	2.71	2.28			1964.3	
34R-5, 8	312.38						2.24			2087.0	
34R-5, 24	312.54	11.11	24.68	2.24	1.99	2.66	2.15				
34R-5, 85	313.15							588	P		
34R-5, 110	313.40							527	P		
34R-6, 26	314.06	10.25	23.49	2.38	2.14	2.73	2053.7				
34R-6, 70	314.50							630	P		
34R-6, 90	314.70							863	P		

^a Measurement by W = Wykeham-Farrance motorized vane, F = fall cone apparatus; P = pocket penetrometer.

^b A = measured normal to bedding; C = measured parallel to bedding.

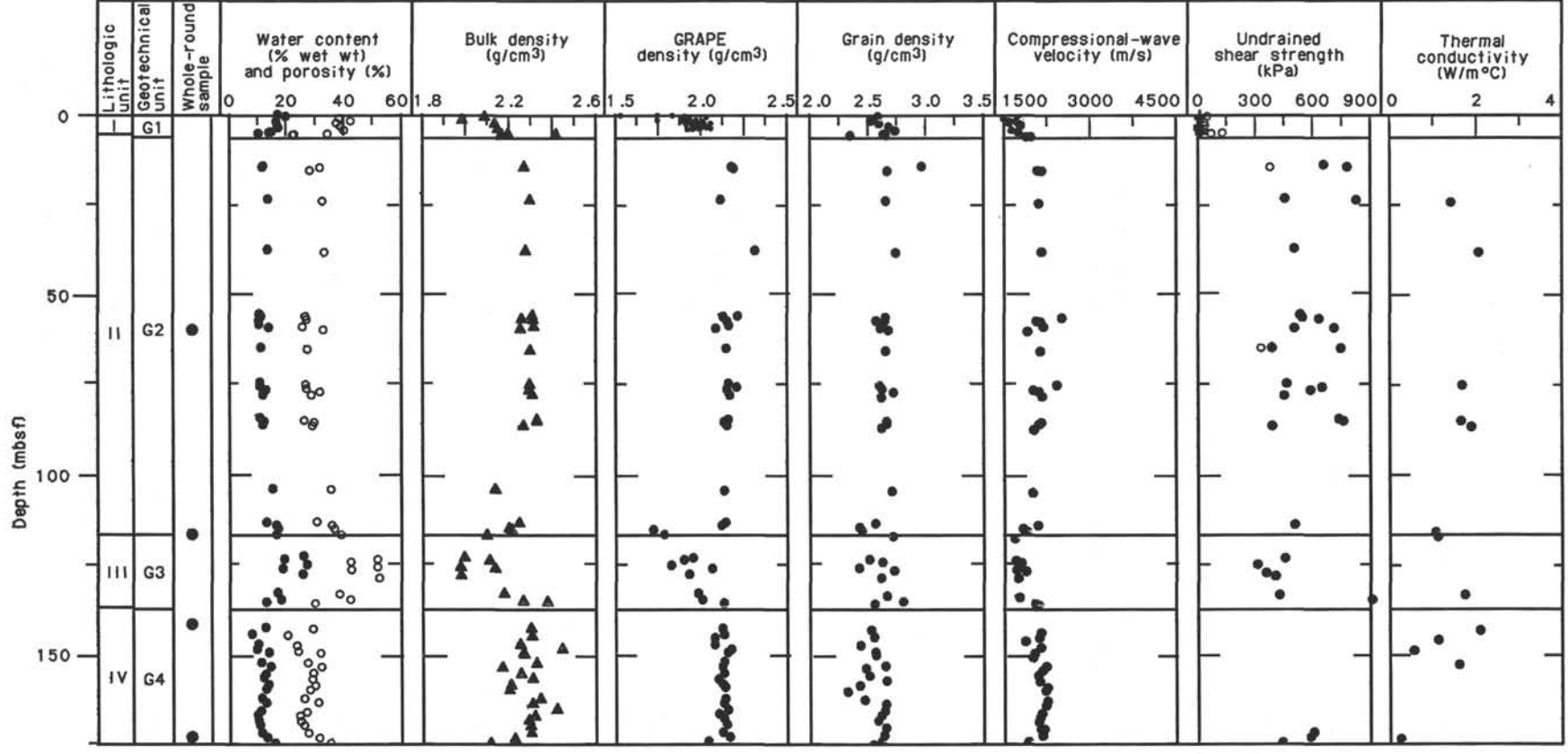
Table 12. Thermal conductivities measured at Site 742.

Core, section, interval (cm)	Depth (mbsf)	Thermal conductivity (W/m/°C)	Temperature drift rate (°C/min)
119-742A-			
4R-1, 60	24.30	1.414	-0.013
10R-1, 63	75.33	1.687	0.059
11R-1, 52	84.92	1.658	0.040
11R-2, 76	86.66	1.888	0.077
14R-2, 50	115.30	1.080	0.049
14R-3, 50	116.80	1.118	0.014
16R-1, 50	133.20	1.759	0.050
17R-1, 50	142.80	2.114	0.030
17R-3, 50	145.80	1.137	0.042
18R-1, 50	152.50	1.637	0.039
20R-2, 50	173.30	0.250	-0.039
21R-1, 50	181.50	2.548	0.057
21R-2, 50	183.00	0.514	-0.043
21R-3, 50	184.50	1.646	0.046
22R-1, 77	191.47	2.020	0.039
22R-5, 66	197.36	0.943	-0.017
23R-1, 70	201.00	1.601	0.018
23R-3, 70	204.00	1.017	0.058
23R-5, 70	207.00	2.143	0.039
23R-6, 70	208.53	0.703	-0.008
24R-1, 65	210.55	0.690	-0.058
24R-2, 65	212.05	1.360	0.037
24R-3, 65	213.55	2.639	0.047
24R-4, 65	215.05	1.959	0.032
26R-2, 48	231.18	0.145	-0.099
26R-3, 48	232.68	1.849	0.029
26R-5, 48	235.68	1.754	0.018
27R-3, 50	242.30	0.930	0.048
27R-5, 50	245.30	1.739	0.021
27R-7, 50	248.30	2.398	0.033
28R-1, 50	249.00	1.530	-0.013
28R-3, 54	252.04	0.538	-0.086
28R-5, 52	255.02	2.430	0.038
28R-7, 45	257.95	1.388	0.016
29R-3, 70	261.80	1.981	0.043
29R-5, 70	264.80	0.513	0.082
29R-6, 70	266.30	1.485	0.029
30R-3, 56	271.36	2.781	0.058
30R-5, 50	274.30	1.543	0.063
30R-6, 43	275.73	2.045	0.049
31R-1, 60	278.00	2.490	0.013
31R-2, 60	279.50	2.788	0.022
32R-1, 50	287.60	1.225	-0.013
32R-2, 50	289.10	3.177	0.040
33R-3, 50	300.20	0.231	-0.053
34R-6, 50	314.30	2.143	0.089

density curve (Fig. 28). Porosity discrepancies also may be due in part to applying values in the downhole calculations (porosity is calculated from resistivity) that are not adequate to the present sediments. Geotechnical unit G1 shows physical-properties values that are typical for glacial diamictos found at previous Leg 119 sites, other areas of the Antarctic continental shelf (Edwards et al., 1987; Lien et al., in press), and in the Arctic (Solheim et al., 1988; Solheim, in press.) The unit most likely represents a glacial marine sediment deposited during and after withdrawal of grounded glacier ice from the site.

The transition into geotechnical unit G2 clearly represents a transition into an overconsolidated sediment. Testing of the consolidation state of the sediment is part of a shorebased study of the whole-round core samples taken at this site (Fig. 27), but the abrupt change in all of the physical properties indicates that the unit G2 sediment has experienced a considerably higher load than its present overburden. Grounded glacier ice is a likely cause for the overconsolidation, considering the physiographic setting and the sediment type, either through direct glacial loading or by glacial erosion of a sediment load, or a combination of both. Other sources of overconsolidation could be effects of permafrost or diagenesis. The latter is excluded, as the sediment did not have any indication of diagenetic effects at this level. Permafrost may pull water out of adjacent sediments and, hence, can cause overconsolidation. Permafrost would, at these water depths, have had to have formed under a grounded, cold-based glacier and cannot be excluded. However, this would again imply grounded ice over the site. The different effects of grounded ice cannot be evaluated at this stage, but we propose glacial loading as the main overconsolidating mechanism.

Geotechnical unit G3 is the most distinct of the geotechnical units, with its sharply raised water content and porosity values and reduced bulk density and velocity. The most likely causes for such an abrupt change are unconformities, variations in compaction, effects of varying grain-size distribution, or combinations of these causes. Unconformities in this kind of relatively ice-proximal environment are likely to be erosional and, hence, are caused by grounded ice. Unless distinct grain-size distribution differences appear, a glacial event would be expected to cause a reverse trend of that observed in unit G3. As the sedimentology of this unit is essentially that of stratified diamictites (see "Lithostratigraphy and Sedimentology" section), grain-size variations seem most likely as the main cause. Possibly this represents a more distal facies than the homogeneous diamictites above and below, with a higher proportion of silt and clay. Preliminary results of postcruise grain-size analyses of index-properties samples seem to support grain-size effects as the main



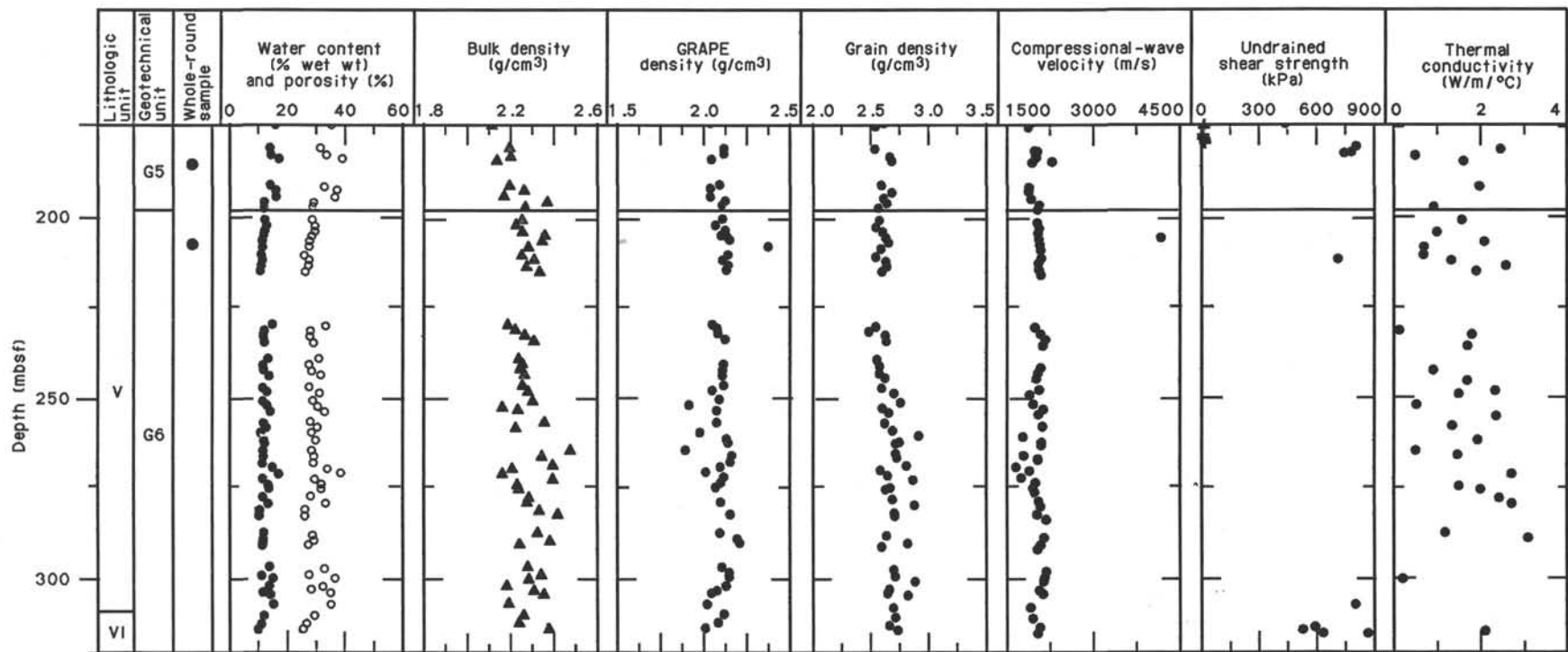


Figure 27. Physical-properties profiles, Site 427. Water content solid circles, porosity open circles. GRAPE values in geotechnical unit G1 mark continuous GRAPE measurements, blocked into 0.1-m averages, whereas the rest of values represent 2-min counts on discrete samples. Compressional-wave velocity values in unit G1 are measurements made parallel to bedding (C direction); the rest of the points are values measured normal to bedding (A direction). Small dots in unit G1 mark continuous PWL results, measured in the C direction and blocked into 0.1-m averages; the rest of the points represent measurements on discrete samples). Undrained shear strength was measured by vane shear (crosses), fall cone apparatus (circles), and pocket penetrometer (dots). In geotechnical units G4 and G6 shear strength was generally beyond the range of the shipboard measurement possibilities.

Table 13. Physical-properties minimum, mean, and maximum values for the different geotechnical units at Site 742.

Unit		Water content (% wet wt)	Porosity (%)	Wet-bulk density (g/cm ³)	GRAPE density (g/cm ³)	Compressional-wave velocity ^a (m/s)	Undrained shear strength ^b (kPa)
G1	min	14.20	20.40	2.00	1.47	1748	10.3
	mean	16.88	33.11	2.14	2.04	1803	28.1
	max	20.10	38.66	2.22	2.20	1913	64.0
G2	min	10.40	21.30	2.15	2.24	1923	382.0
	mean	12.15	26.54	2.31	2.33	2140	585.0
	max	15.31	32.53	2.45	2.52	2523	817.0
G3	min	16.98	32.84	1.98	1.78	1701	307.0
	mean	20.51	39.53	2.12	2.01	1793	385.0
	max	27.20	47.53	2.28	2.21	1916	447.0
G4	min	8.43	18.56	2.18	2.23	1887	Too stiff
	mean	11.94	25.39	2.31	2.29	2150	
	max	14.73	29.75	2.47	2.35	2266	
G5	min	13.42	28.57	2.12	2.18	1886	437.0
	mean	15.35	31.88	2.19	2.24	1991	668.0
	max	17.44	35.95	2.27	2.34	2319	800.0
G6	min	2.05	5.10	2.16	2.11	1674	Too stiff
	mean	12.60	27.43	2.30	2.26	2051	
	max	17.39	35.56	2.66	2.40	2206	

^a Measured normal to bedding. One value of 4189 m/s, measured in a discrete interval of well-cemented diamictite in geotechnical unit G6, is not included.

^b Measurements from all three types of instruments.

cause for the observed variations. This could cause permeability differences that again would result in different degrees of compaction during a subsequent loading event. If such an interpretation is correct, the upper boundary of unit G3 is likely to represent an erosional event during the advance of a subsequent grounded glacier. An unconformity is a likely cause for an abrupt change in recorded facies.

The lower boundary of unit G3 may, correspondingly, also represent an erosional unconformity. Possibly a glacier advance, eroding ice distal sediments and exposing proximal diamictons, overconsolidated the sediments. During withdrawal, unit G3 could have been deposited. Unit G3 causes a distinct velocity reversal that is likely to give rise to a strong seismic reflector. The geotechnical unit is also clearly distinguishable in the downhole logging results (Fig. 28; see "Logging" section).

The next major boundary, between geotechnical units G4 and G5, also involves an increase in water content and porosity and corresponding decreases in bulk density and velocity. A distinct change occurs in sedimentology across the boundary, going from a homogeneous diamictite to a calcareous diamictite with fewer clasts (see "Lithostratigraphy and Sedimentology" section). Furthermore, although datable horizons are sparse at this site, the boundary could also correspond to a major hiatus, with the Miocene missing (see "Biostratigraphy" and "Seismic Stratigraphy" sections). The previous discussion of unit G3 also applies to this boundary, and the trends seen are most likely caused by varying grain-size distribution.

The lower boundary of geotechnical unit G5 has no corresponding lithostratigraphic boundary. However, it is clearly indicated in all geotechnical properties, as well as in the downhole logging results (Fig. 28; see "Logging" section). As lithologic Unit V is a calcareous diamictite with cementation evident at various levels within the unit, an increase in the degree of cementation is a possible cause for the decrease in porosity and

water content across the boundary. Cementation effects may also cause the relatively constant levels of all measured physical properties throughout geotechnical unit G6.

The degree and vertical extent of overconsolidation are difficult to evaluate at this stage. Most published empirical relations between measured parameters and the degree of overconsolidation are from well-sorted clays, particularly from the deep-sea environment, and may be inadequate here. For a brief discussion of this, see the "Physical Properties" section of the "Site 739" chapter. Comparison with data from other glaciated continental shelf areas will be done to the extent possible within the relatively restricted amount of available (nonconfidential) data. At present, however, a few assumptions may be justified: geotechnical unit G1 is normally consolidated, while geotechnical unit G2 is clearly overconsolidated. Unit G3 may be near normal consolidation. The same assumptions may apply to units G4 and G5, respectively, but unit G6 is too much affected by cementation to be incorporated in the present discussion on overconsolidation. From the nature and definition of consolidation through compaction, a decreasing degree of overconsolidation downcore is likely. The differentiation between effects of varying compaction and grain-size distribution is impossible at this stage. However, they may both represent fluctuations in the glacier grounding line with time, and, hence, the physical properties hold important information concerning the glacial history of eastern Antarctica.

A detailed correlation with Site 739 is difficult at present, but it seems clear that the anomalous sequence of geotechnical units G3–G5 at Site 739 (see "Physical Properties" section, "Site 739" chapter) roughly corresponds to the sequence of units G3–G5 at the Site 742, with the sequence being thinner at Site 742, the more landward of the two sites. This laterally persistent sequence of varying physical properties most likely represents a complex combination of effects from erosional unconformities,

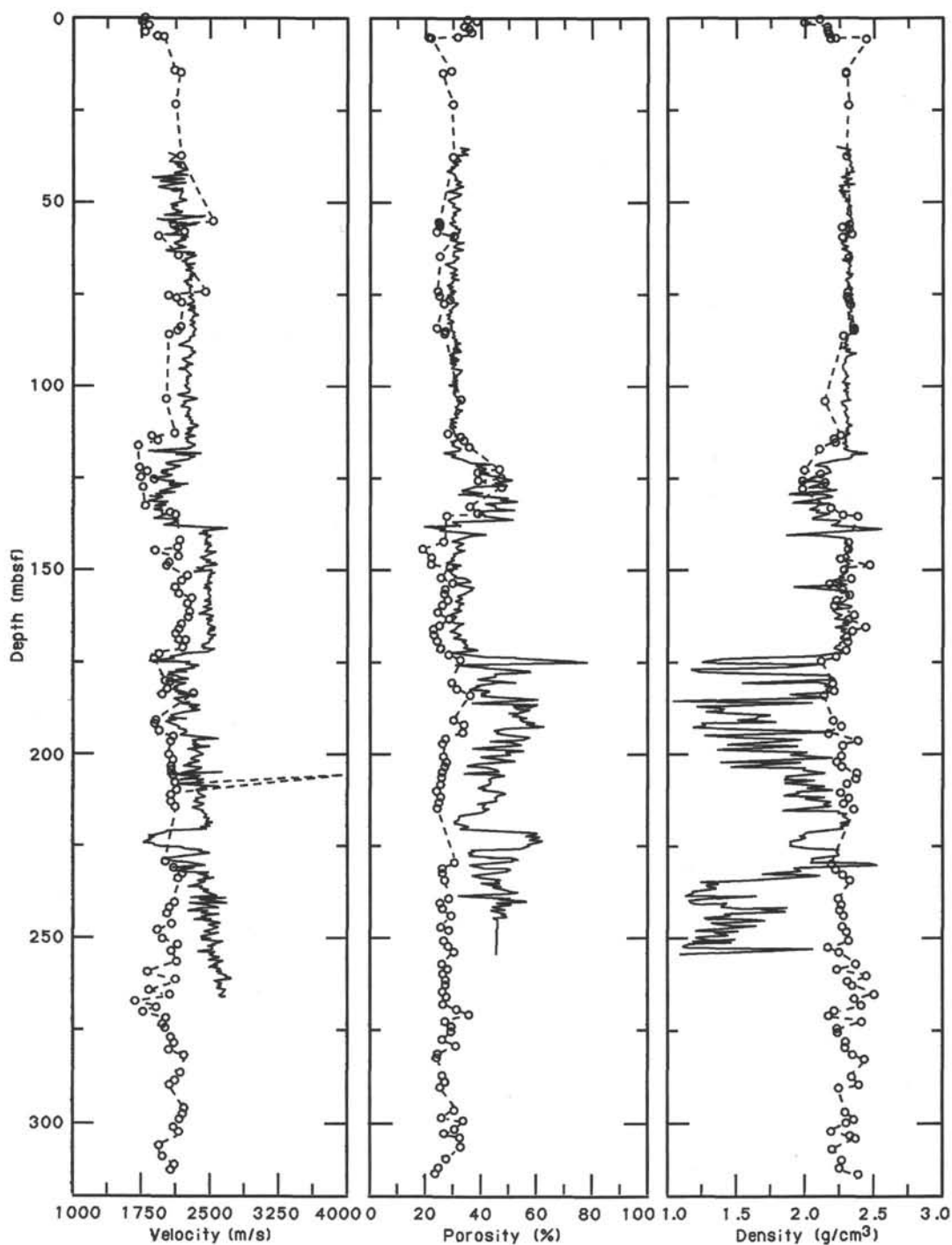


Figure 28. A comparison of downhole logging (solid lines) and laboratory measurements (broken lines with circles) of velocity, porosity, and bulk density for Site 742.

grain-size distribution variations, and varying degrees of loading by sediment and grounded glacier ice.

LOGGING

Operations

Two logging runs were completed at Site 742. The hole was filled with seawater, and conditions were good because of the presence of consolidated pebbly mudstones (diamictites) within

the entire logged section. The pipe was left at 61.8 mbsf and then pulled up to 30.8 mbsf when the tools reached the bottom of the pipe.

The first tool combination, rigged at 1630 hr on 1 February 1988, consisted of dual induction (DIL), caliper (CAL), gamma-ray (GR), and long-spacing sonic (LSS) tools ("Explanatory Notes" chapter). A bridge was encountered at 283.8 mbsf, preventing descent to the bottom of the hole (316 mbsf). Logging was done from 283.8 mbsf (32 m above the bottom). The first logging run ended at 1915 hr on 1 February.

The second tool combination was rigged at 0015 hr on 2 February. The combination consisted of neutron (CNL), lithodensity (LDT), natural gamma spectrometry (NGT), and temperature (AMS) tools (see "Explanatory Notes" chapter). Because of degrading hole conditions, another bridge was encountered at 253 mbsf. The lithoporosity combination was run upward from this level. The second logging run was finished at 0300 hr on 2 February. The water temperatures measured with the AMS tool were -0.3°C at the top of the logged section at 30.8 mbsf and 3.7°C at the bottom of the logged section at 253.8 mbsf. These temperature measurements are probably correct, because the last circulation in the hole was done 9 hr before the second logging run (between 1400 and 1500 hr on 1 February).

At Site 742 the quality of the logs is variable and some logs need additional reprocessing. The logs are presented in Figures 29–33.

Sonic Log

At numerous depths, cycle skipping (see "Logging" section, "Site 737," "Site 738," and "Site 739" chapters, this volume) affects the sonic record. The sonic log was reprocessed using an algorithm described by the Shipboard Scientific Party (1987, p. 124–131). Minimum velocity of 1745 m/s and maximum velocity of 3810 m/s were used as input to the program to filter the sonic record. The reprocessed sonic log is presented on Figure 29. The variations of velocity of the formations read by the sonic log are in good agreement with those measured on cores (see Fig. 28). The log velocities are systematically 250 m/s higher than the velocities from cores.

Density Log

As shown by the wide deflections ($>0.05\text{ g/cm}^3$) of the density quality curve on Figure 30, the density values read by the lithodensity tool are incorrect in the depth intervals 168.8–204.8 and 233.8–253.8 mbsf. The unreliable density intervals correspond to zones where no contact was made between the density tool and the formation. The measured density values are close to those for water and, thus, are underestimated. The comparison between densities measured on cores and log densities confirms the bad log density values below 168.8 mbsf (Fig. 28). The density curve will be processed post-cruise in order to eliminate the peaks occurring at the caved zones.

Logging Units

The description of the cores at Site 742 (see "Lithostratigraphy and Sedimentology" section) indicates that a relatively uniform glacial sequence like that at Site 739 is present and consists mainly of diamictites. The logging parameters are not uniform, however, and show several significant variations. Three distinct logging units were identified (Fig. 32), and the first is divided into subunits 1A and 1B for correlation with Site 739.

Logging Unit 1

The logging parameters are fairly constant within logging unit 1 (35–138.8 mbsf) and correspond to the following values: resistivity of 5 ohm-m, velocity of 2235 m/s, neutron porosity of 30%, bulk density of 2.34 g/cm^3 , and natural radioactivity of 120 API units. The porosity calculated from the logging density (20%) is less than the porosity read by the neutron tool (30%). The high value of the neutron porosity probably is due to the presence of minerals with hydrogen in the formation, such as clays (see "Logging" section, "Site 737" chapter). Logging unit 1 corresponds to an interval of very bad recovery. The few core sections recovered (Cores 119-742A-8R, 119-742A-10R, and 119-742A-11R) and the flat curves of the logging records suggest a

lithology consisting of homogeneous diamictites with pebbles and boulders.

Logging Subunit 1A

The grain density calculated for Subunit 1A (35–120 mbsf) and the other logging units from the porosity log and from the density log has an average value of 2.8 g/cm^3 (Fig. 33). The grain densities obtained from logging are higher than those measured on the cores ($2.6\text{--}2.7\text{ g/cm}^3$). The grain density measured from the cores is based on a small volume (a few cubic centimeters) of fine sediment. The density log and the porosity log measurement from which the grain density is calculated are based on a large volume (few meters) of sediment. The different scale of sampling probably explains the difference in grain density between laboratory measurements and downhole measurements. The laboratory measurements in particular cannot take account of the numerous high density granitic or gneissic cobbles present in the diamictites. This high grain density is higher than expected for a detrital formation in which quartz and feldspar are commonly found. The high grain density of the diamictites may be related to a significant amount of magnetite (grain density of 5 g/cm^3) and other heavy minerals, as observed in thin-section analysis (C. Alibert, pers. comm., 1988).

Logging Subunit 1B

The neutron porosity increases abruptly to 50% at the boundary between logging subunits 1A and 1B (120–138.8 mbsf). Large changes are also seen in the other parameters between subunits 1A and 1B (decrease in resistivity, decrease in velocity, and decrease in density), in good agreement with the porosity decrease. By comparison with subunit 1A, subunit 1B is highly variable, and several peaks occur on the logging curves, indicating an alternating lithology. Stratification within the diamictites, as described in the "Lithostratigraphy and Sedimentology" section, could explain the variations on the logging records.

Logging Unit 2

The boundary between logging subunit 1B and unit 2 (138.8–172.8 mbsf) corresponds to an abrupt change in the characteristics of the resistivity and velocity logs. The resistivity and the velocity values increase, respectively, from 2 to 7 ohm-m and from 1990 to 2480 m/s. The logs that are usually strongly influenced by the lithology (e.g., the photoelectric log, the radioactivity log, and the density log) do not indicate any major lithologic change at the boundary between subunit 1B and unit 2. The only difference observed in the cores between the two is a difference in the texture, of the diamictites—subunit 1B is stratified, whereas unit 2 is massive. As cementation was not observed in unit 2 (see "Lithostratigraphy and Sedimentology" section), the increase in velocity and resistivity at the top of unit strongly indicates that unit 2 could be an overcompacted zone. The boundary between subunit 1B and unit 2 probably is a disconformity caused by glacial erosion beneath a grounded ice sheet.

Logging Unit 3

The boundary between logging units 2 and 3 (172.8–283.8 mbsf) is marked by an increase in neutron porosity from 35% to 45%. The neutron porosity change corresponds to a decrease in resistivity and velocity from 7 to 4 ohm-m and from 2480 to 1867 m/s, respectively. Natural radioactivity decreases from unit 2 to unit 3. The decrease results from a lowering in potassium and thorium content of the diamictites from 4% to 2.5% and from 14.8 to 13.12 ppm, respectively (Fig. 31). Logging unit 3 is described in the "Lithostratigraphy and Sedimentology" section

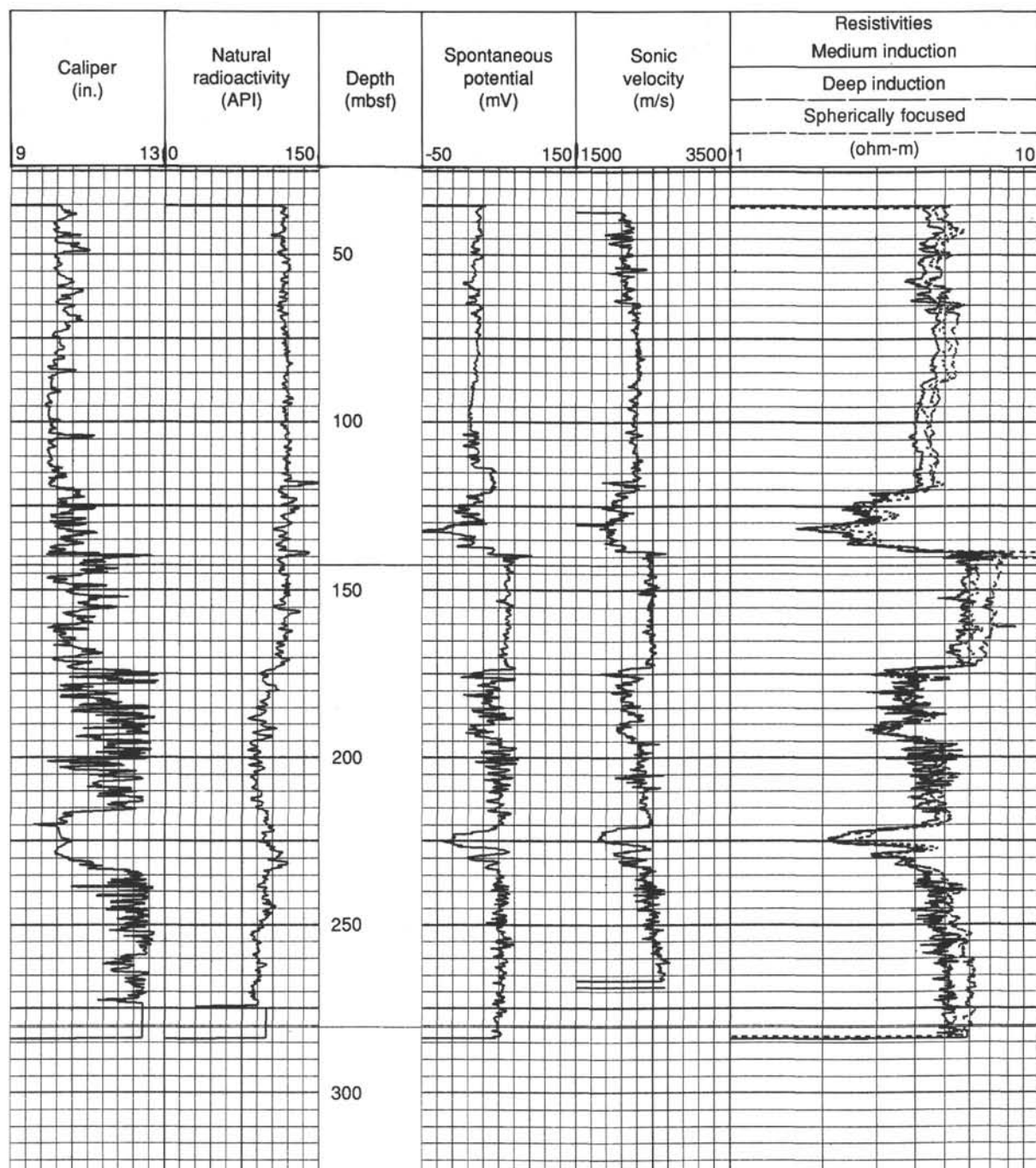


Figure 29. Downhole logs at Site 742 for the seismic stratigraphic combination: caliper, natural radioactivity, spontaneous potential, sonic velocity, and resistivity (deep, medium, spherically focused) from 35 to 280 mbsf.

as diamicrites that tend to be calcareous due to the presence of detrital micrite. Numerous caved zones occur within unit 3, as shown by the caliper measurements, making the density log unusable. The caved zones are probably caused by compaction or cementation heterogeneities in the diamicrites.

A 15-m-thick layer corresponding to low-resistivity (2 ohm-m) and low-velocity (1755 m/s) values occurs in logging unit 3 between 215 and 230 mbsf. The bulk-density (Fig. 32) decrease from 2.3 to 1.9 g/cm³ and the neutron porosity increase from 30% to 60% are in good agreement with the velocity and the

resistivity logs. No core was recovered in this same depth interval. A sand layer is probably the best explanation for the nonrecovered and highly porous interval between 215 and 230 mbsf. The presence of sand is suggested by the increase in sand in the diamicrites overlying the nonrecovered interval.

Synthetic Seismogram

A synthetic seismogram was computed for Site 742 to accurately tie the drilled sequence in the hole to seismic-reflection data over the site (Fig. 34). The seismogram covers the logged

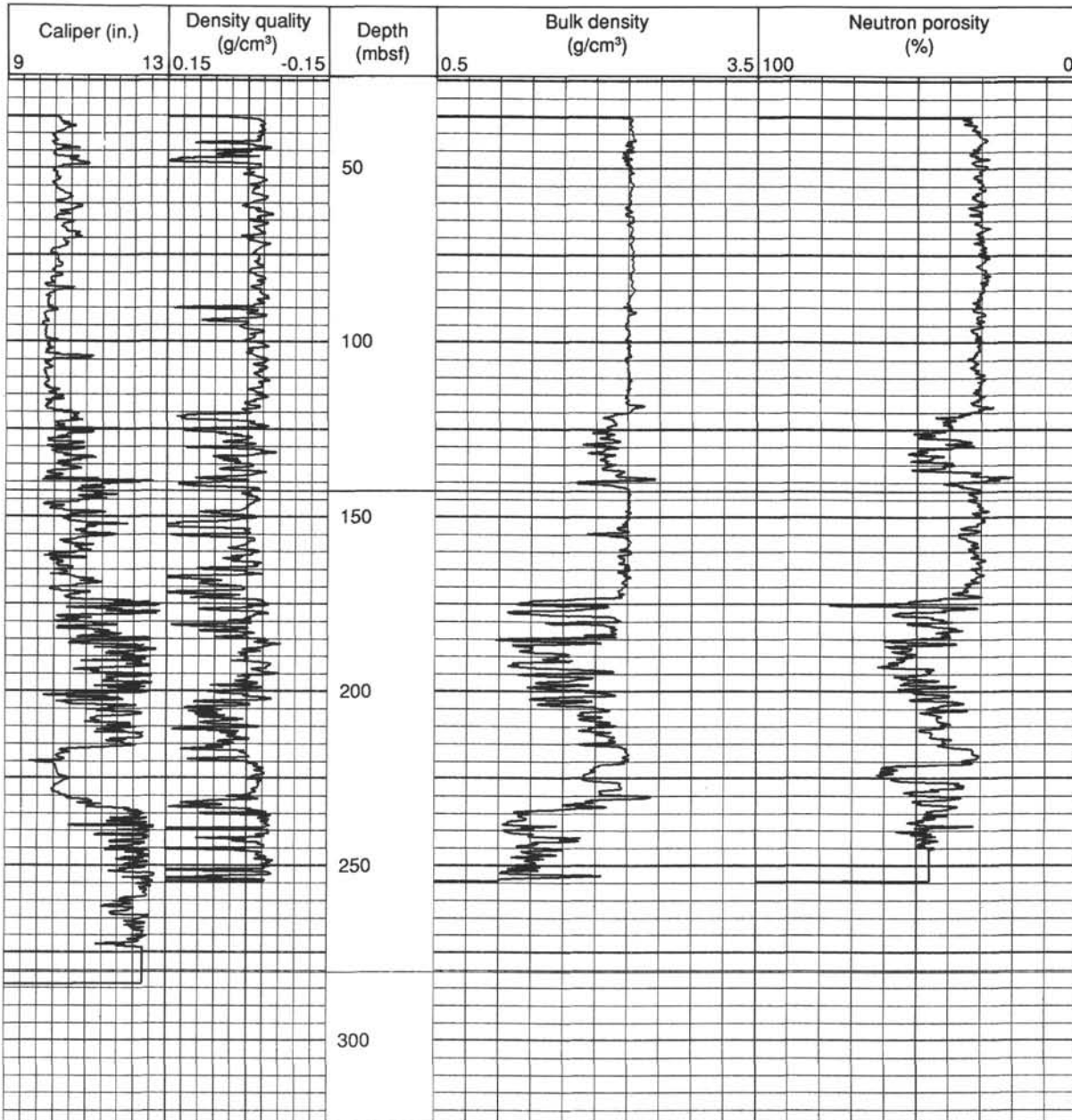


Figure 30. Downhole logs at Site 742 for the lithoporosity combination: caliper, density quality, bulk density, and neutron porosity from 35 to 255 mbsf.

interval from 30 to 268 mbsf. The LSS velocity log (log-spacing transit time = 3.5 m) values only were used to compute the acoustic impedance for the synthetic seismogram because downhole density values were significantly degraded by poor hole conditions (e.g., washouts). An arbitrary density of 1 g/cm³ was assumed for the entire section; thus, impedance values can be read directly from Figure 34 as velocity. Densities measured aboard ship were not used because the sampling interval was too sparse to give a reliable synthetic seismogram (e.g., a sparse sample interval commonly gives spurious reflections). The use of velocity log data only usually gives a good approximation of the synthetic seismic trace (see "Logging" section, "Site 738" chapter). A velocity of 2.2 km/s was assumed for the interval from 0 to 30 mbsf to place the synthetic seismogram at the proper initial depth on the seismic profile.

Site 742 was drilled into a glaciomarine sequence composed of flat (0–170 mbsf) and gently seaward-prograding (below 170 mbsf) strata. Convoluted fluvial beds lie at the bottom of the hole. The velocities (and other logged parameters) are highly variable throughout the section, causing a complex synthetic seismogram and seismic-reflection profile (Figs. 35 and 36).

Analysis of the synthetic trace indicates

1. The complex waveforms and high amplitudes of the seismic trace are caused by abrupt and large (up to 0.8 km/s) variations in the *in-situ* velocity (e.g., lithology and compaction) throughout the sedimentary section.
2. The reflection amplitudes vary in proportion to the size of the velocity contrast and thickness of the zone. Where small (0.1 km/s) velocity variations exist (e.g., 30–80 mbsf), reflec-

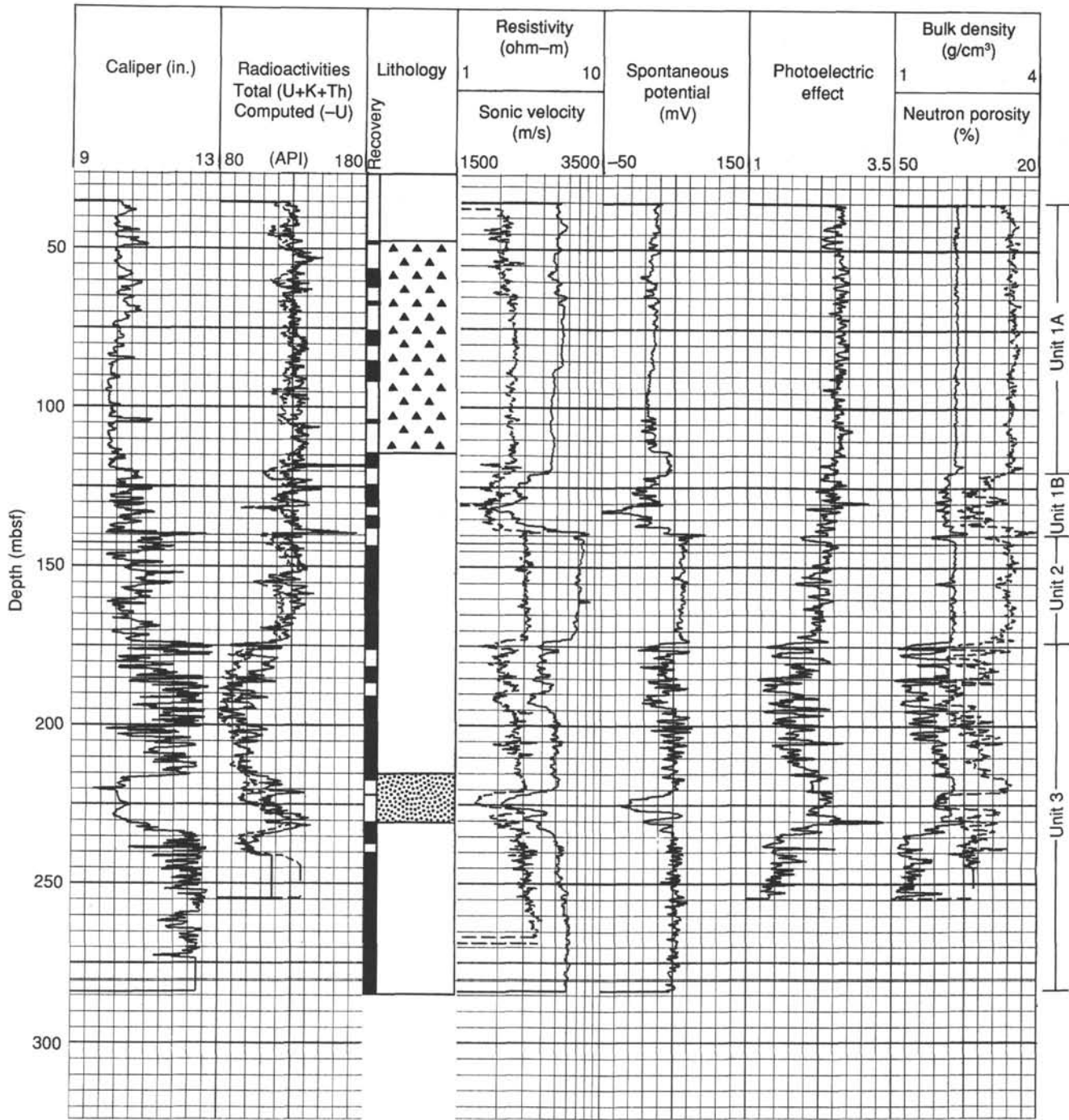


Figure 32. Summary Site 742 core recovery, inferred lithology (diamictite and sand), logging units, and major logs: caliper, natural radioactivity, resistivity, velocity, spontaneous potential, photoelectric effect, density, and neutron porosity from 35 to 280 mbsf.

and the other (southeast side) is possibly from truncation of a buried layer or channel. The seafloor diffraction does not occur on the initial Site 742 crossline and the buried diffraction is greatly attenuated. Possible reasons for the preferential appearance of these diffractions on one, but not the other, seismic line are the “correct” orientation of seafloor features and subsurface velocity anisotropy. Alternatively, the two reciprocal seismic-lines may have been offset slightly, even with GPS navigation. The shotpoint selected for the correlation (SP 3619) is the

best estimate of the drill-site location, given the uncertainties of beacon location and seismic-system geometry (see “Underway Geophysics” chapter). The selected location is probably within 100 m (four shotpoints) of SP 3619 on the seismic record.

The correlation of the synthetic trace with the seismic profile (Fig. 36) is surprisingly good, considering the complexity of the downhole logs and the observed seismic data. The good assessment is based on correlations between observed and synthetic seismic data for (1) most high-amplitude positive reflections from

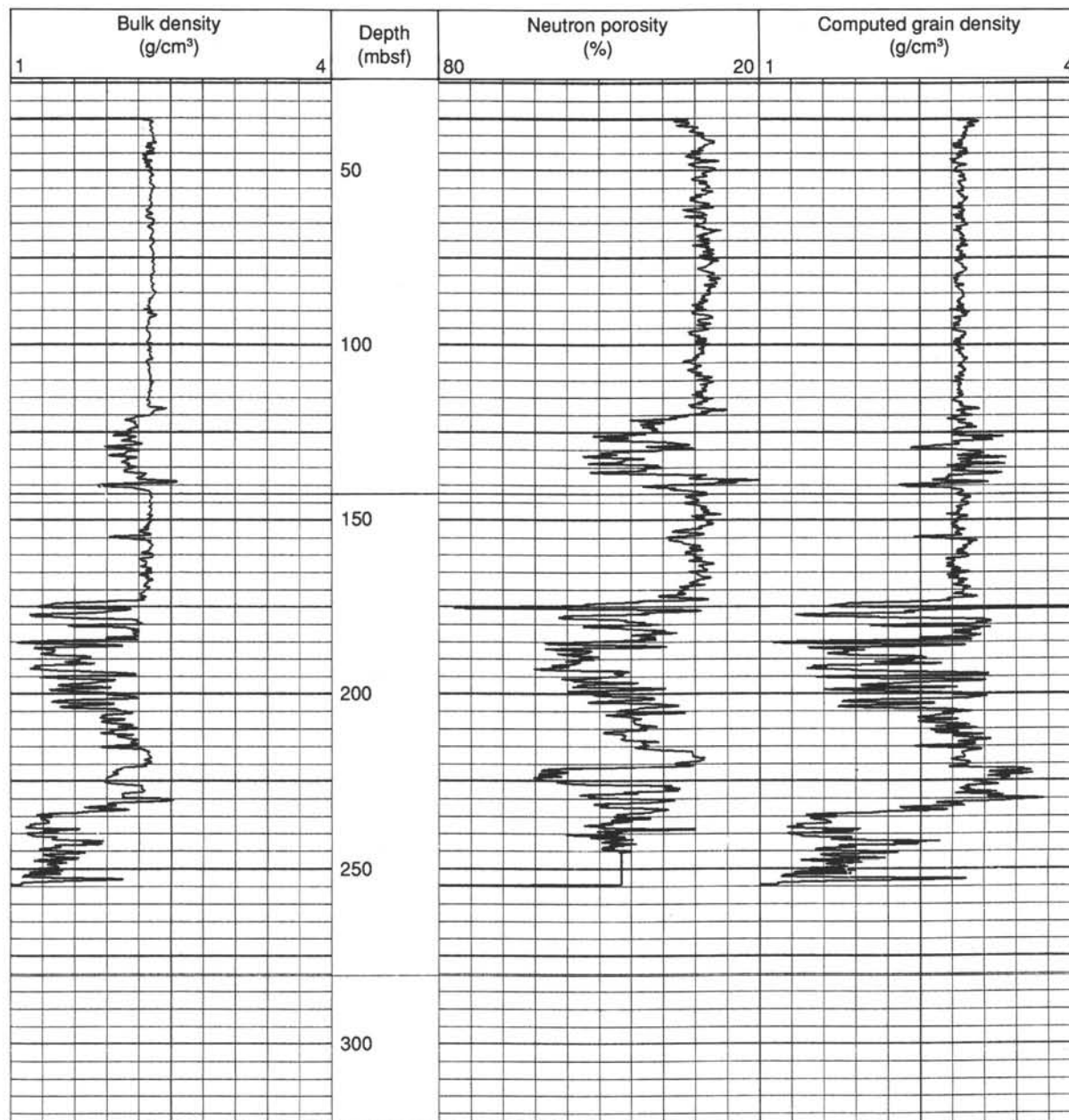


Figure 33. Computed grain density for 35–235 mbsf at Site 742.

100 to 225 mbsf; (2) the narrow, large-amplitude negative reflections at 215 mbsf; and (3) the wide positive and negative peaks at 135 and 190 mbsf.

A few general interpretations of the rocks comprising the sedimentary section beneath Site 742 can be made by extrapolating the downhole velocity results onto the seismic-reflection profile (Fig. 37).

1. 0–100 mbsf: High-frequency, discontinuous reflections characterize this interval. The lack of coherent reflections in the seismic profile is due to the superposition of the water gun bubble pulse, the high- and low-frequency diffractions from sea-floor irregularities, and the sparse primary reflections in the uniform-velocity rocks. The lack of reflection continuity indicates that the small velocity variations observed in the downhole

logs probably do not continue laterally over distances of more than 2550 m, or otherwise traceable or segmented reflections would be expected.

2. 100–140 mbsf: Low-velocity rocks compose this interval. A broad negative reflection, with great lateral variability, can be seen in the seismic profile northwest of shotpoint 3611 (Fig. 36). The poor coherency of this reflection suggests that the low-velocity rocks are of variable thickness and lithology.

3. 140–170 mbsf: This interval, like one at similar depth at Site 739, is composed of uniform diamictite with a nearly constant velocity of 2.5 km/s. Strong reflection peaks were observed at the top and bottom of the interval and are excellent markers for this acoustic unit. In the seismic profile over Site 742, the bottom of the layer is characterized by a dual-peak reflection in some traces. The two peaks in the synthetic trace

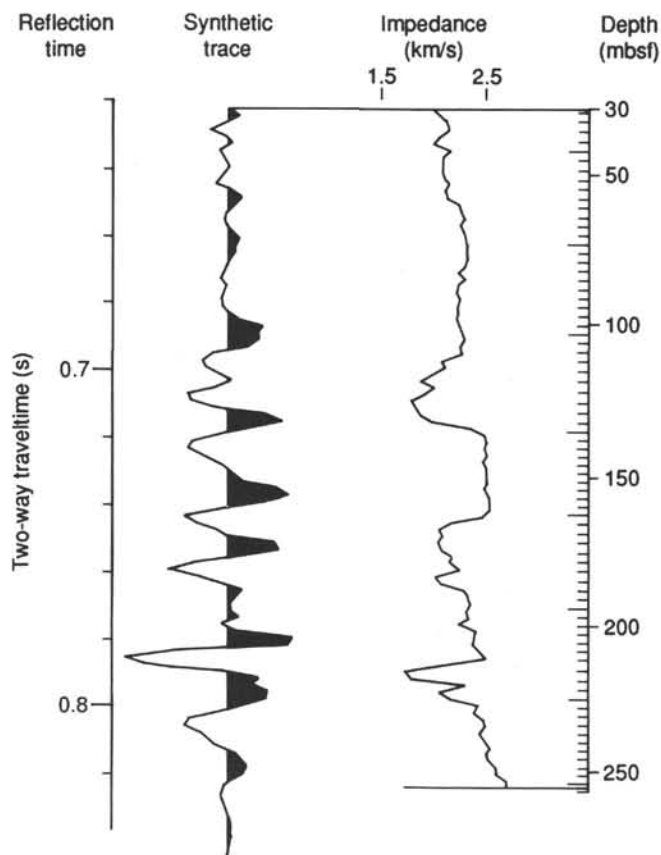


Figure 34. Synthetic seismic trace computed from the downhole velocity log. The impedance is velocity in km/s (assumed density of 1 g/cm^3). Reflection time is from sea level.

(155 and 170 mbsf) may explain the observed dual-peak reflection. The two peaks are a superposition of reflections from different lithologic units.

4. 170–250 mbsf: This interval has the most complex waveforms of the synthetic trace, and the complexity arises from the “sawtooth” shape of the velocity profile. Two intervals of downward-increasing velocity topped by a low-velocity zone occur at 170–210 and 210–255 mbsf. The variable velocities, possibly caused by cyclic rock sequences, produce the complex and high amplitudes seen in both the synthetic and observed seismic traces. The seismic profile between Sites 742 and 739 (Fig. 38) shows several high-amplitude and continuous (5- to 10-km-long) reflections that probably correlate with rocks from the lower part of this interval. The strong reflections are probably caused by 5- to 10-m-thick, low-velocity layers that may be unconsolidated sands or gravel. An example is the low-velocity (1.7 km/s) layer at 220–227 mbsf that can be traced laterally for at least 1100 m (Fig. 39). Core recovery was poor in this layer.

5. Below 250 mbsf: A subtle change occurs in the acoustic character of the seismic records below 300 mbsf. Reflections are commonly segmented or disrupted. Where continuous, the reflections are wavy. Near Site 742, the change in acoustic character occurs beneath a nearly flat reflector (about 330 mbsf) that has a similar acoustic character (e.g., strong negative peak) to that observed for the low-velocity zone at 220–227 mbsf. The reflector at 330 mbsf is also likely to be a low-velocity layer, possibly consisting of well-sorted sands similar to those near the bottom of Hole 742. Lateral changes in the thickness of this layer are one explanation for the wavy appearance of flat-lying layers (e.g., waviness caused by velocity pull-downs and pull-ups). Al-

ternatively, the waviness may represent a once-irregular surface that has since been filled in by well-sorted sands(?). Disrupted reflections directly beneath this and other low-velocity layers indicate that seismic dispersion is responsible, in part, for the unit's acoustically disrupted character.

Correlation of Sites 739 and 742

The correlation of the downhole logs between Sites 739 and 742 is tentative because the sites are separated by 29 km and the glacial rocks found at both sites are diverse in their lithology and paleodepositional environment. The two sites are located on glacial deposits of a formerly prograding continental shelf. The seismic-reflection data between the two sites (Figs. 38A and 38B) illustrate the upper prograding glacial units sampled at both sites and the lower fluvial(?) and lacustrine(?) deposits sampled only in the bottom of Hole 742.

The glacial diamictites in the upper 175 m of the sedimentary section are the only rocks that can be reliably correlated between Sites 739 and 742 (Fig. 39). These rocks are part of logging units 1 and 2 at Site 739 and logging units 1 and 2 at Site 742. Logging units 1 and 2 exhibit similar characteristics in velocity, resistivity, gamma ray, and porosity at both sites (Fig. 39), and the correlation is predicated on these similarities. For example, the subsurface velocity values show equivalent fluctuations at Sites 739 and 742. High-amplitude reflections occur at the top and bottom of logging unit 2 (uniform velocity of 2.5 km/s), and they can be traced as nearly flat reflectors between Sites 739 and 742.

Unconformities occur between logging units 1 and 2. Downhole logs below the deeper unconformity at 175 mbsf are not similar and cannot be correlated between Sites 739 and 742. The seismic-reflection data indicate that the diamictites in the lower part of Hole 742 may be equivalent to rocks below the level reached at Site 739 (Fig. 38). The downhole logs in the lower part of the two holes are of inadequate length and of such different appearance that no correlation is possible. The only similarity is that reflections in the lower parts of both holes are caused by low-velocity rocks (less consolidated sands and gravels?) lying within a high-velocity matrix. Isolated high-velocity layers are uncommon. Low-velocity layers at both sites may have been deposited in a similar glaciomarine environment but at different times.

Summary

In summary, 15 downhole logs were successfully recorded on two logging runs at Site 742, leading to identification of three major logging units and one subunit (Fig. 32). In these units, large fluctuations occur in porosity, velocity, and resistivity values at depth. The large variations in log values probably result from different degrees of compaction and dewatering caused by intermittent periods of loading by grounded ice sheets on glacially-derived sediments. These sediments probably were deposited on a shallow, slowly subsiding and prograding continental shelf.

Comparison of the synthetic seismogram derived from downhole logs with seismic-reflection profiles across Site 742 (Figs. 36 and 37) indicates that the large velocity variations (up to 0.7 km/s) occur at unconformities and low-velocity layers and are the principal cause of observed reflections. The acoustic character of the seismic-reflection data changes below about 275 mbsf; although below the level of logging, the change may be due to a major shift from highly variable glacial deposition (fluctuating logging values) to more uniform depositional environments (smoothly changing logging values). At Site 742, as at Site 739, the greater continuity of reflections at depth could be due to laterally extensive low-velocity horizons, commonly 2-5 m thick, that are probably unconsolidated sands.

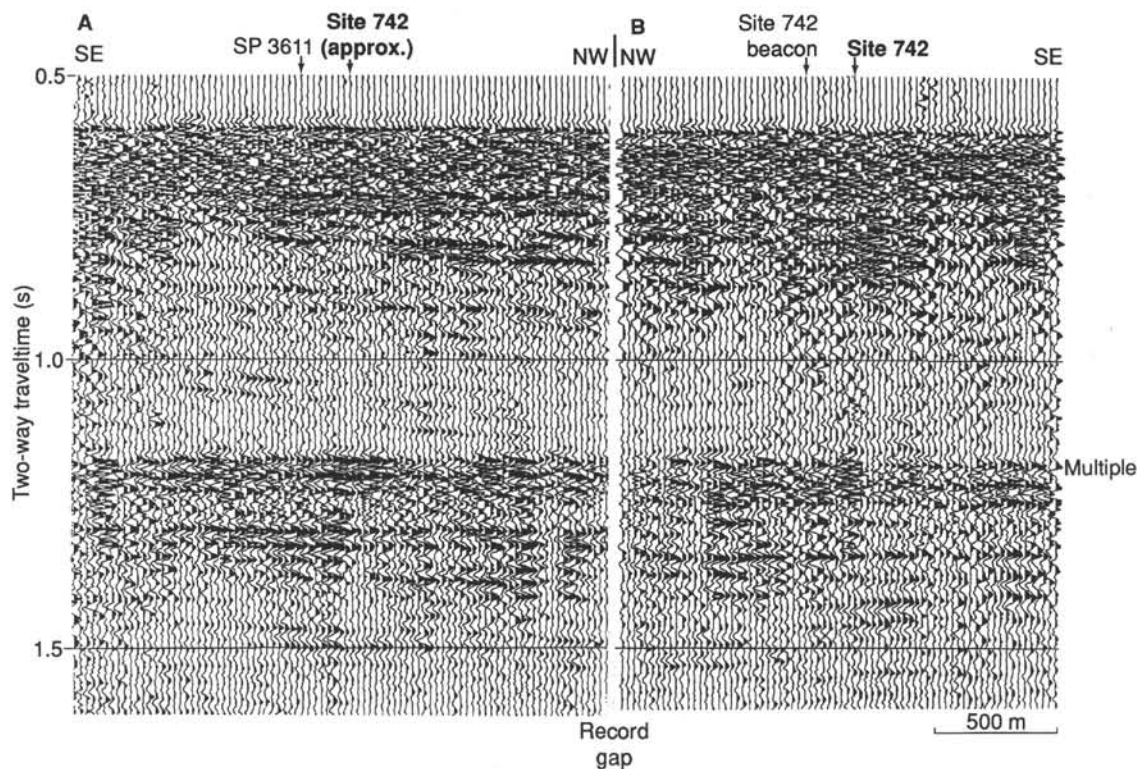


Figure 35. Segments of seismic-reflection profiles across Site 742. A. Initial approach line shows approximate location of Site 742. B. Reciprocal seismic line along which the beacon for Site 742 was dropped.

Correlation of downhole logs at Sites 739 and 742 is only possible for depths less than 170 mbsf. At both sites, similarities exist in velocity, resistivity, gamma ray, and porosity values above 170 mbsf, but below 170 mbsf, the logs differ. The seismic profile from Sites 742 to 739 shows that reflections above 170 mbsf are flat, but that below 170 mbsf they prograde seaward. The prograding units below 170 mbsf at Site 742 are probably the same as those below the bottom of Hole 739A.

SEISMIC STRATIGRAPHY

Site 742 is located in the northern part of Prydz Bay about 60 km from the continental shelf edge and 170 km from the Antarctic coast. The site lies 29 km southeast (landward) of Site 739.

Site 742 lies above a sequence of nearly flat to gently seaward-dipping reflections that comprise the proximal parts of the prograded sedimentary units underlying the outer Prydz Bay shelf. The reflectors beneath Site 742 are part of Stagg's (1985) unit PS-2, which he identifies under the entire central and outer Prydz Bay shelf. On ODP line 119-07 (Figs. 40 and 41), the stratigraphy is complex, and five seismic units are recognized within the glacial and nonmarine? strata at Site 742. Four units were sampled in Hole 742A and one seismic unit lies beneath the hole (and above the seafloor multiple). The upper three units (0–304 mbsf) are highly reflective, glacial diamictites; the fourth unit (304–316 mbsf, total depth) comprises weak and wavy reflectors of glacial and nonmarine? sands and siltstone; and the lower unit contains relatively strong and continuous reflections that were not sampled.

Seismic Units

Seismic Unit I (0–175 mbsf) is composed of high-amplitude reflections that are highly disrupted within the upper 120 mbsf, but are more continuous, and of higher amplitude, in the lower

part of the unit. Three high-amplitude, continuous reflections occur between 120 and 175 mbsf, and these reflections correspond to the top, middle, and bottom of an alternating low-high-low-velocity zone, based on downhole logs and a synthetic seismic study (see “Logging” section). Fossils recovered within the low-velocity interval are Quaternary to early Pliocene, and those directly below the high-velocity zone (e.g., top of seismic Unit II) are Eocene–Oligocene. The lowermost reflector of Seismic Unit I traces a likely unconformity.

The disrupted (e.g., discontinuous) reflections in the upper part of the unit occur where rapid, but small, velocity changes are observed in downhole logs. These small changes, in conjunction with diffractions from seafloor and iceberg scour troughs, produce a seismic record without apparent internal stratification (see Fig. 41) that is typical of other Prydz Bay areas.

Seismic Unit II (175–220 mbsf) contains mostly negative polarity reflections with complex waveforms at Site 742. The complexity results from the small thickness of the unit and large variability of subsurface velocities within the unit. Seismic Unit II, which is composed of Eocene–Oligocene diamictite, thickens seaward, as can be seen from broadening waveforms (Fig. 40) and regional seismic data (Fig. 41). The maximum thickness is about 300 m between Sites 742 and 739. A more typical description of seismic Unit II is for areas seaward of Site 742, where the unit consists of weak, continuous, and segmented reflections that dip gently seaward toward Site 739. These reflections correlate with Site 739 seismic Unit III (see “Seismic Stratigraphy” section, “Site 739” chapter).

Downhole velocities for seismic Unit II increase with depth, indicating a burial-compaction gradient different from the overlying diamictites, in which velocities are commonly constant or decrease with depth. The different compaction gradient and reflection character for seismic Unit II, as opposed to seismic Unit I, indicate that seismic Unit II was deposited in a different

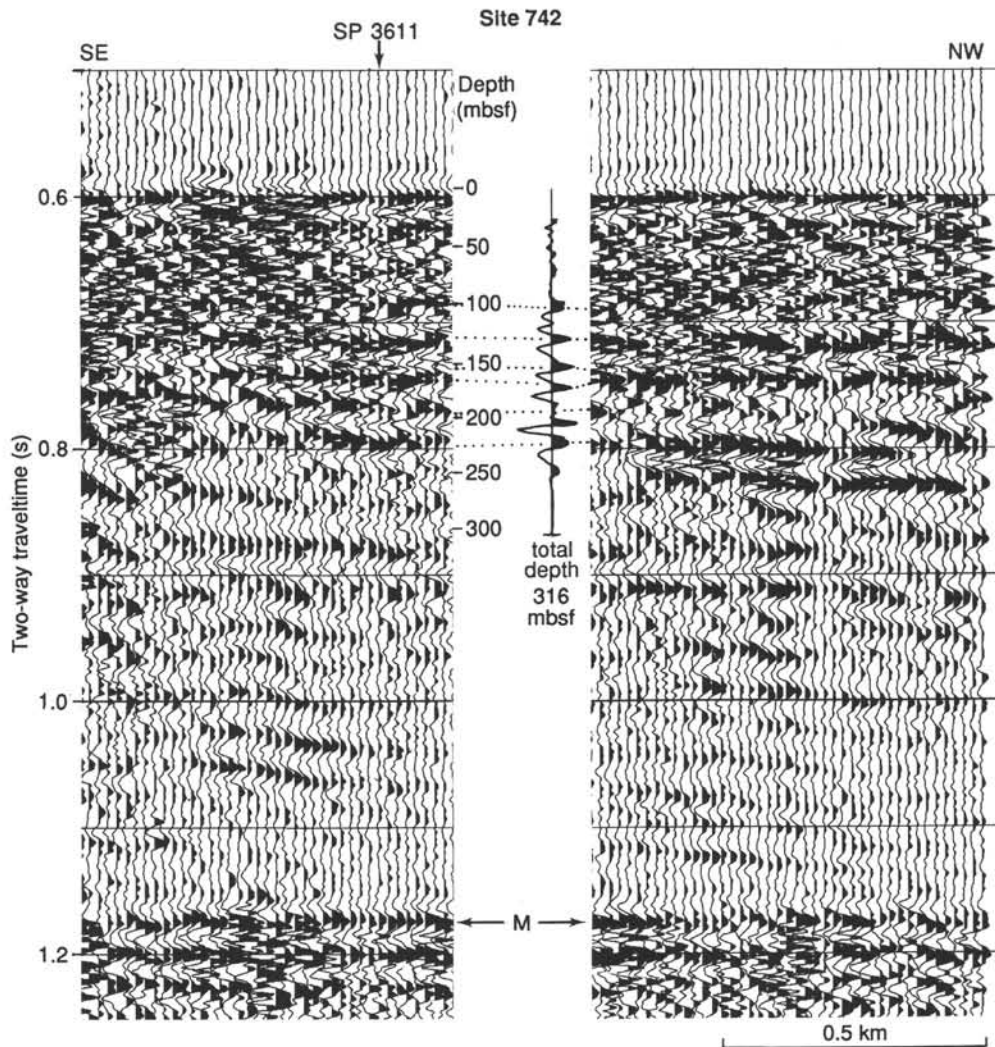


Figure 36. Comparison of vertical-incident seismic-reflection data recorded over Site 742 with synthetic seismic trace computed from downhole velocity measurements.

environment than Unit I. The weak, continuous reflections that dip gently seaward indicate deposition of relatively uniform velocity layers on a slowly subsiding (or gently dipping) surface. As *in-situ* velocities normally increase with depth, deposition was probably not beneath a grounded ice sheet, but in front of one. The uniformity in apparent thickness and seaward-stacking of reflectors indicates a slowly prograding sequence. In this sequence, good reflector continuity implies relative stability (e.g., no major slumping) and widely distributed sediment distribution (e.g., limited channeling). The diamictites of seismic Unit II were probably deposited on the outer part of the continental shelf near, but in front of, the glacial ice front.

Seismic Unit III (220–304 mbsf) is characterized by high-amplitude reflections of variable length, continuity, and waveform complexity. Seismic Unit III differs from seismic Unit II in acoustic character, but drill cores at Site 742 indicate similar diamictite compositions. Near Site 742, reflection wavelets change in amplitude, width, and internal shape commonly over short distances (100–200 m; Fig. 40). These changes imply large, lateral, velocity variations that are probably caused by lithologic, rather than rock-compaction (e.g., glacial loading), changes. Regionally, seismic Unit III can be traced about 25–30 km along ODP lines 119-07 and 119-08 from about 10 km

landward of Site 742 to about 10 km landward of Site 739. Between Sites 742 and 739, the upper surface of seismic Unit III dips gently seaward, but the bottom is irregular because of infilling, to a maximum thickness of 150 m, of an eroded substrate.

The high-amplitude reflections, characteristic of seismic Unit III, are probably due to low-velocity, unlithified sand layers, such as the probable sand layers at 225 mbsf in Hole 742A and between 300–387 mbsf in Hole 739C (see “Logging” sections, this chapter and “Site 739” chapter). Although distinct logging characteristics for sands were recorded, no core was recovered from these depths. The seismic characteristics of large negative and positive amplitudes, variable reflector widths, changing waveforms, terminal diffractions, and wavy underlying reflectors are strong indicators of low-velocity layers of restricted and variable thickness that may compose channel, deltaic, or local meltwater sand bodies. The continuous high-amplitude reflections in seismic Unit III lie farther seaward from Site 742 and may be due to a more distal facies of the sand layers. The *in-situ* velocity-depth profile for seismic Unit III increases with depth, like that for seismic Unit II, indicating that reflections are not caused by velocity inversions due to compaction by glacial loading (as seen in seismic Unit I). Seismic Unit III may thus consist

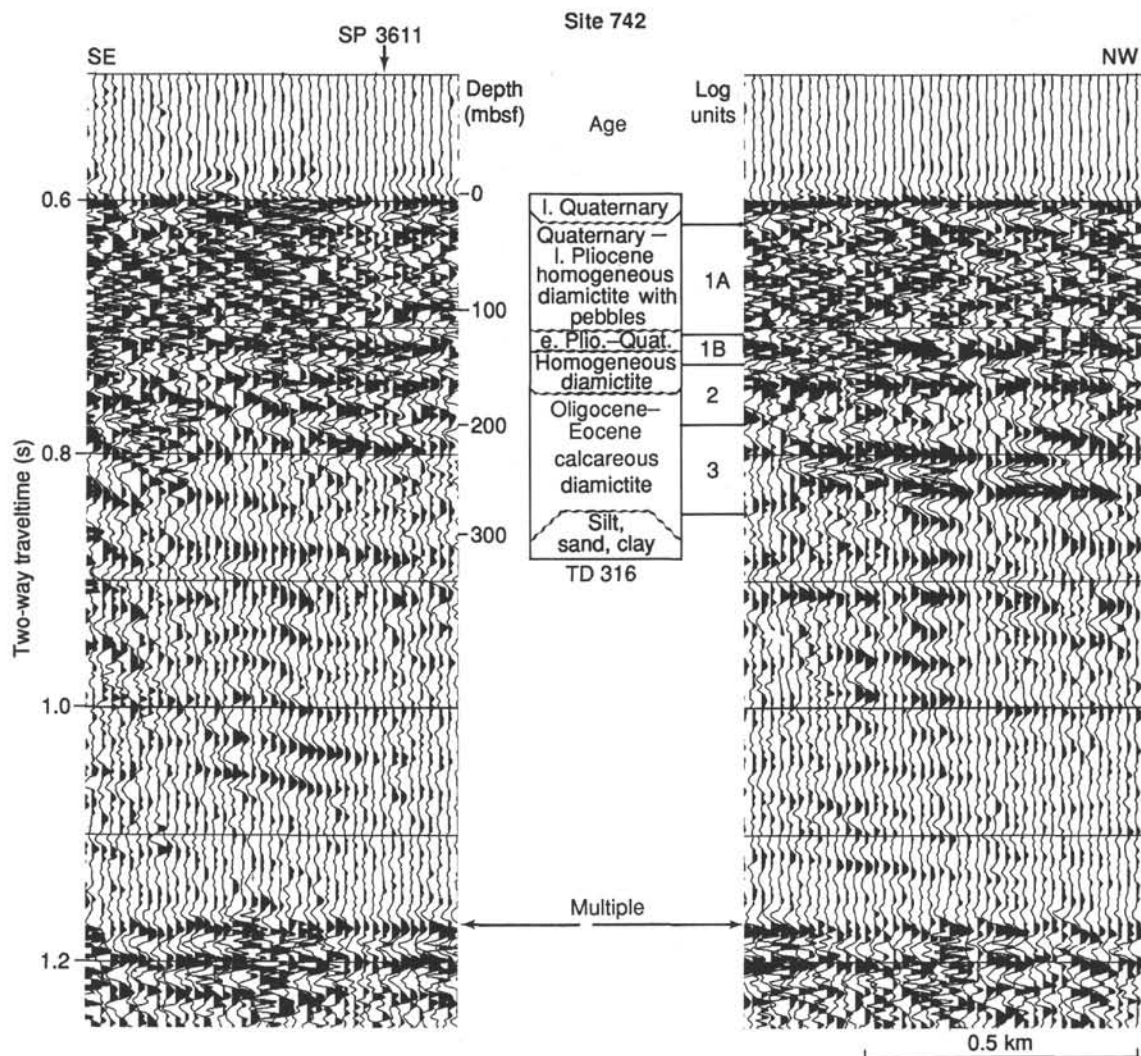


Figure 37. Seismic-reflection data over Site 742 showing depths to logging units, major lithologic boundaries, and unconformities. Depths are from synthetic seismic trace of Figure 34.

principally of glacial diamictites with interbedded sands that were deposited on a shallow continental shelf in front of, rather than beneath, nearby glaciers.

Seismic Unit IV lies at 304–316 mbsf in Hole 742A, but the unit may continue downward to 415 mbsf, as indicated by seismic data (Fig. 40). The unit is characterized by semicontinuous and wavy (e.g. rapid, small undulations) reflections that are commonly weak, discordant with overlying strata, and associated with diffractions. In Hole 742A, seismic Unit IV consists of sand-silt-claystones, interlayered diamictite, and carbonaceous well-sorted sand and siltstone at the bottom of the hole. The unit can be identified regionally over about 75 km in ODP lines 119-07 and 119-08. Near Site 742, the thickness of seismic Unit IV changes quickly, due in part to erosion of the top of the unit, reaching a maximum thickness of about 200 m 2 km seaward of Site 742. Landward, seismic Unit IV thins over a slight rise and then thickens (up to 350 m thick) to infill a 40-km-wide trough beneath the central Prydz Bay shelf.

Downhole logging did not reach seismic Unit IV, but laboratory measurements on cores from the top of this unit indicate that velocities and densities are similar to those of seismic Unit III (see “Physical Properties” section). The wavy appearance of seismic Unit IV is distinctly different from all overlying glacially-derived units at Sites 742 and 739 and seaward, even those that have weak, discontinuous reflections. Seismic Unit IV has

greater similarities to the acoustic character of the nonmarine, carbonaceous seismic Unit II at Site 741 on the inner Prydz Bay shelf. At Site 742, the wavy character could be caused by lateral velocity variations and by changes in thickness of overlying low-velocity layers that cause velocity pull-downs and pull-ups in underlying units. The probable occurrence of sand layers in seismic Unit III would indicate the latter explanation. Alternatively, the wavy appearance may be related to the existence of carbonaceous material that could cause lateral variations in bulk density and velocity, resulting in the apparent waviness and the attenuation of the seismic signal. The similarities in acoustic signatures at Sites 741 and 742, where carbonaceous debris was found (but not elsewhere), indicate that the existence of carbonaceous material is affecting the seismic data.

Seismic Unit IV fills pre-existing or slowly-subsided depressions lying 2 km seaward (Fig. 41) and 30 km landward of Site 742. The areas of severe diffractions in seismic Unit IV occur where the unit has been eroded and once-continuous layers terminate. The wavy and mostly flat-lying reflections that infill depressions and are truncated along the top of the unit indicate that seismic Unit IV is a mostly nonmarine sequence, of possible lacustrine origin, that was eroded during the initial period of glacial advance. The well-sorted sands, carbonaceous debris, and interbedded diamictite at the bottom of Hole 742A lie at the top of this sequence.

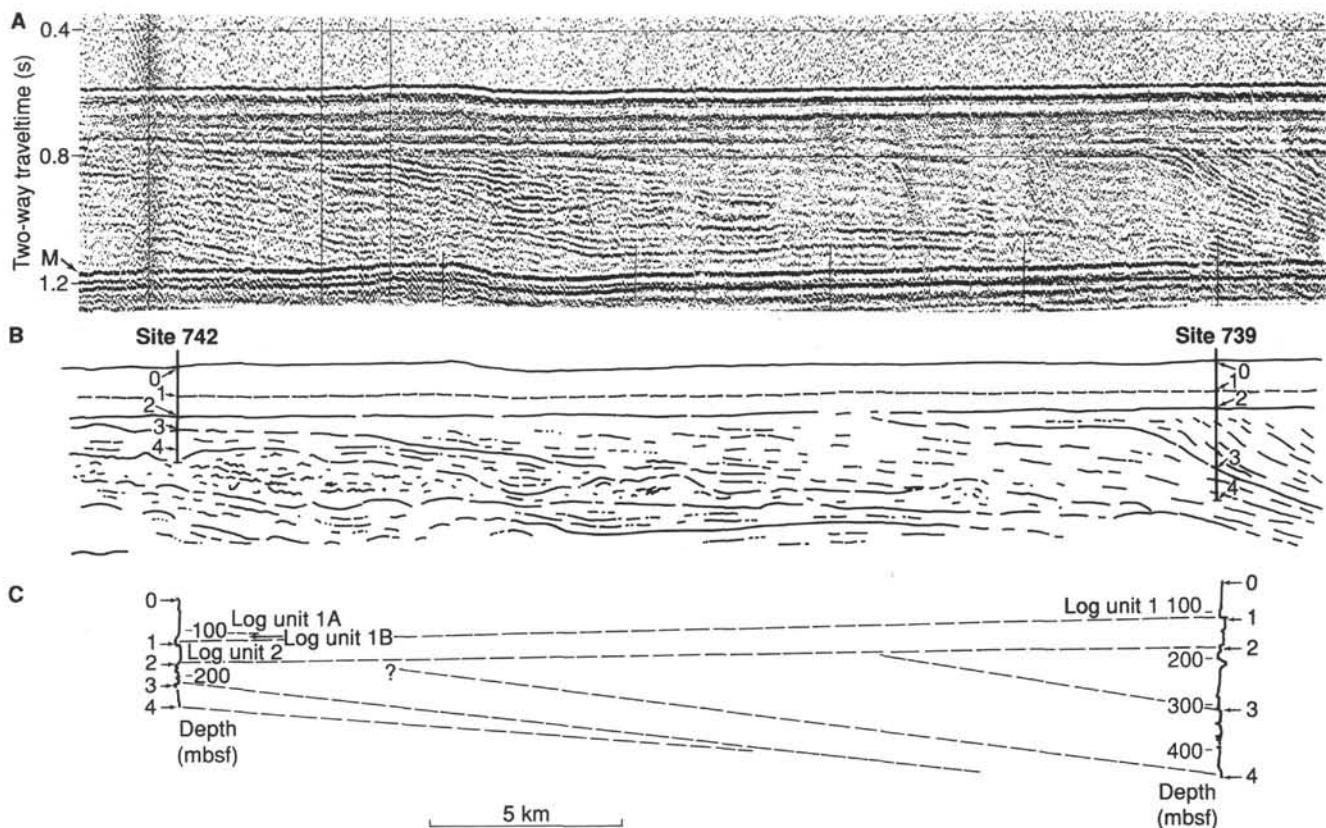


Figure 38. Seismic-reflection data, seismic interpretation, and correlation of downhole logging units between Sites 739 and 742. Seismic sections (A, B) show reflection time below sea level. Log correlations (C) show velocity logs in depth (see Fig. 39 for scale).

Seismic Unit V lies between seismic Unit IV and the seafloor multiple beneath Site 742. The unit, at depths of about 415–675 mbsf, was not sampled by drilling. Near Site 742, seismic Unit V consists of well-layered, continuous, and semicontinuous reflections of variable amplitude in both depth and horizontal extent. The unit is significant because it can be traced in seismic profiles and sonobuoy data for nearly 90 km from Site 739, where it disappears into the seafloor multiple, to a point 35 km seaward of Site 741, where it is eroded near the seafloor. Regionally, the unit changes in reflection character, from weakly reflective and semicontinuous (landward) to more strongly reflective and continuous (seaward). The relatively uniform thickness, continuity, and absence of major deformation indicate that the unit was deposited on a relatively stable platform, possibly as shallow marine (seaward parts) or alluvial plain (landward parts) deposits. For seismic Unit V, the seismic data do not show the highly variable acoustic signature characteristic of glacial deposits sampled at Sites 739 and 742. Thus, the unit is presumed to be nonglacial.

Seismic Structures

Site 742 is located on the seaward flank of a broad (40-km wide) rise that has a vertical relief of 150–200 m and is the outer edge of a mid-shelf trough. The trough lies between Sites 742 and 741 and consists of the downbowed rocks of seismic Unit V (and older) that are infilled with rocks of seismic Unit IV. The rise may be an important paleogeomorphic feature, marking the initial edge of the grounded ice sheet, because the oldest diamicite unit (i.e., Eocene–Oligocene seismic Unit III) thins landward and truncates at the crest of the rise and at the base of seismic Unit I.

Initial interpretation of analog and low-frequency, digital, shipboard seismic profiles indicated that the rise crest might be incised by a few minor faults that displace seismic Unit V and possibly seismic Unit IV. However, further analysis of the suspected faults based on high-frequency, digital seismic data and downhole log information yields greater uncertainty on the fault interpretation. The seismic data over the glacial deposits near Site 742 are marked by features commonly associated with faulting, such as laterally discontinuous large-amplitude variations, one-sided diffractions, and apparent reflection-displacements. The downhole logs (Sites 739 and 742) and high-frequency seismic records indicate that most of these features could result from (1) large lateral and vertical velocity variations caused by nonuniform processes of glacial deposition and compaction and (2) spurious diffractions and sideswipe from seafloor features.

The age of faulting is unknown, but may coincide with initial deposition of seismic Unit III (Eocene–Oligocene diamicite) because the faults appear to displace only seismic Units IV and V. If so, then the faulting, which is highly localized and of small displacement, may be related to sediment loading of the outer continental margin by rapid? glacial deposition.

Seismic Correlations of Sites 739 and 742

Figure 41 illustrates the probable seismic stratigraphic correlations between Sites 739 and 742. The figure is based on the analog seismic data shown and on analysis of full waveform, shipboard-processed digital data. The seismic units for Site 742 are as described here, and those for Site 739 are discussed in the “Seismic Stratigraphy” section of the “Site 739” chapter. Additional comments regarding the detailed velocity structure and downhole logging correlations are given in the “Logging” sec-

tions of this and the "Site 739" chapters. The following seismic unit correlations are proposed, based on Figure 41:

Site 742	Site 739
Unit I	Unit I
Unit II	Unit III (bottom of Hole 739C)
Unit III	Unit III (lower part, below Hole 739C)

No correlations are proposed for seismic Units III and IV at Site 742 and seismic Unit II at Site 739.

Seismic Correlations of Sites 741 and 742

Direct correlations cannot be made between seismic units that were drilled at Sites 741 and 742, about 100 km apart. The total thickness of the sedimentary section is unknown but would be greater than 3 km between Sites 741 and 742, based on simple projection of the dips. A few general observations, however, can be made about regional stratigraphy of the upper part of the sedimentary section between the two sites:

1. Seismic units can be reliably traced between Sites 741 and 742 in high-frequency-filtered seismic data along ODP Line 119-07 because the seismic units are continuous and gently dipping (not lost in the seafloor).

2. The general character of the seismic-reflection units changes from weakly reflective, wavy, and semicontinuous near Site 741 to more highly reflective near Site 742, indicating a probable regional change from nonmarine at Site 741 to glacial and shallow marine or nonmarine at Site 742.

3. Greater diversity occurs in the number and thickness of the seismic units proceeding seaward from Site 741, indicating more varied depositional paleoenvironments (e.g., lacustrine?, glacial, and shallow marine?).

4. Seismic units are mostly undeformed, other than by erosion and slight downwarping in the central part of the shelf, indicating long-term stability in depositional environments seaward to Site 741.

If reflections are traced from the lowermost unit drilled at Site 741 across the central shelf to Site 742, then they would lie about 0.5 s (750 m) below the bottom of Site 742. This projection is valid if the seismic units do not change thickness significantly within 40 km of Site 742, where the traced reflection lies within the seafloor multiple. Shallower reflections, directly above, do not change thickness. Projection of the Site 741 reflection farther seaward to Site 739 is not possible because this reflection lies within the seafloor multiple.

Summary

Five seismic units were identified at Site 742 and illustrate a wide range of reflection characteristics and likely depositional environments ranging from glacial (seismic Units I–III) to likely nonglacial (seismic Units IV and V). Unit I (0–175 mbsf) is nearly flat and contains high-amplitude reflections due to glacially compacted (high-velocity) and normally consolidated (low-velocity) layers of ?early Pliocene to Quaternary age. Seismic Unit II (175–220 mbsf) is characterized by weakly reflective, but continuous, reflections caused by Eocene–?Oligocene diamictites that may have been deposited on the outer continental shelf seaward of the glacial ice front. Seismic Unit III (220–304 mbsf) has high-amplitude, laterally variable reflections from possible unlithified sands, within Eocene–?Oligocene diamictites, that may be nearshore to distal glacial sands.

Seismic Unit IV (304–316 mbsf and 100 m below the total depth of Hole 742A) is composed of wavy and semicontinuous weak reflections that are ?early Eocene–Oligocene age glacial

and carbonaceous rocks in the uppermost part, but deeper, may be nonglacial lacustrine deposits that fill nearby depressions. Seismic Unit V (425–675 mbsf) consists of highly continuous reflections of variable amplitude that can be traced regionally and may be nonglacial rocks of either shallow marine or nonmarine origin.

Regional interpretations of the seismic units around Site 742 indicate that (1) reflections from rocks at the bottom of Hole 741A may correlate with reflections about 750 m beneath the bottom of Hole 742A, (2) only two correlations of seismic units can be made between Holes 742A and 739C (between Unit I at Site 742 and Unit I at Site 739 and between Unit II at Site 742 and Unit III at Site 739), and (3) the wavy character of seismic Unit IV (Site 742) is similar to that of nonmarine units at Site 741 and may be due to lateral velocity variations caused, in part, by the presence of carbonaceous debris.

Site 742 lies on the flanks of a gentle rise that may be the location of the ?early Eocene–Oligocene ice front, as this rise marks the most landward occurrence of ?early Eocene–Oligocene age diamictites based on landward projection of seismic Unit III. The underlying unit is interpreted as consisting of nonglacial, nonmarine, carbonaceous rocks that were heavily eroded during subsequent glaciation.

SUMMARY AND CONCLUSIONS

Site 742 is located 60 km from the shelf break, 170 km from the Antarctic shore, and approximately midway along the Leg 119 Prydz Bay drilling transect. Sites 742 and 739 provide the principal deep penetrations of the Prydz Bay glaciogenic stratigraphy. The main objective was to sample and date the sediment section that lies between the marine Paleogene glacial units recovered further north at Site 739 and the nonmarine ?Paleogene sequence cored at the landward Site 741.

A seismic survey run from Site 741 to determine the geometric structure of the sediment units involved passed over Site 742. The underlying seismic stratigraphic structure is a sequence of nearly flat to gently seaward-dipping reflections, representing parts of the prograding sediment wedge of the Prydz Bay outer shelf. Sonobuoy 8 was deployed during the site survey to study the acoustic velocity structure and actual depths of the strongest reflections. High interval velocities of 2.22–2.35 km/s immediately below the seafloor indicated glacial compaction of the sediments. For depths to about 400 mbsf, only a small general increase in velocity was observed; alternating high- and low-velocity layers are in evidence between 30 and 270 mbsf.

In line with experience at the previous sites drilled in Prydz Bay, the RCB was used throughout the hole. Weather conditions were not good initially, resulting in some delay in setting up the automatic station-keeping system and also in determining whether the ship could hold position with sufficient accuracy for drilling in this shallow water. Hard, coarse glacial sediment was encountered at 24 mbsf, and recovery down to 150 mbsf was poor, usually consisting of only a few cobbles that apparently were rolling under the bit and also jamming the core catchers. The approach of a large iceberg, which was judged to be too large for *Maersk Master* to tow, added delays at this stage, but it eventually changed direction and passed safely away from the ship. As a precaution against having to redrill the hole, a free-fall funnel was deployed during the iceberg approach. At about 150 mbsf, normally compacted glacial units were entered; core recovery and rate of penetration increased dramatically from that point onward.

The site was drilled to 316 mbsf before being abandoned upon the detection of very low levels of gas (methane 35 ppm or less) and detection of higher weight molecules (ethane, 2–6 and 5–12 ppm). In addition, the proximity of the site to seismic fault structures warranted abandonment of the hole.

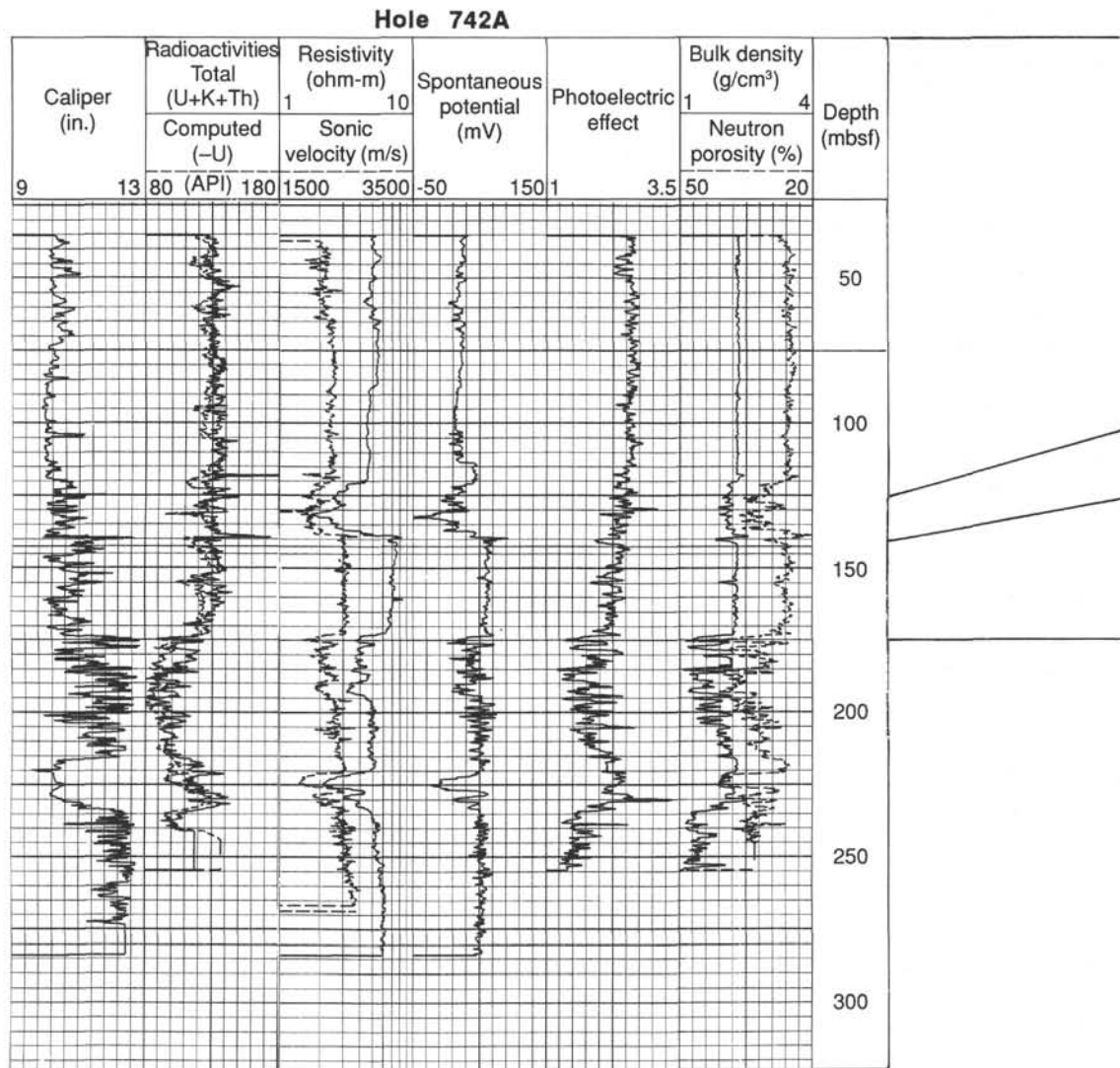


Figure 39. Correlation of principal downhole logs (velocity, resistivity, porosity, and natural radioactivity) between Sites 739 and 742. A reliable correlation is only possible for depths less than 175 mbsf. Deeper units probably do not occur at both sites.

Although diamictite and diamicton composed the bulk of recovery, five lithostratigraphic divisions were recognized, based on some significant minor lithologies (e.g., diatomite and sorted sands) or on differences in the diamictites (e.g., layering and carbonate content).

The surficial lithologic Unit I (0–5.4 mbsf) is a soft, uncompacted, pebbly diamicton and olive diatomaceous silt-clay and is Quaternary in age. Gravel contents are 5%–10%. No oriented grain fabrics were detected, indicating that the diamicton was deposited in water, probably as proximal marine waterlain till. Grounding icebergs appear to have played a role in the disruption of the unit as grounding scars are visible in 3.5-kHz records over the site. Fossil remains include benthic foraminifers, diatoms, and (Pleistocene) radiolarians.

Lithologic Unit II consists of a considerable thickness (5.4–115.2 mbsf) of compacted, massive, dark-gray diamictite. Some intervals of exceptionally low recovery may mark levels with a high content of pebbles and boulders. Gravel contents are high (up to 15% in recovered intervals), but do vary considerably. Depositional conditions were probably diverse, and the nonrecovered intervals may conceal a complex advance-retreat glacial sequence. Preferred orientations are typical of most of the unit,

indicating deposition primarily as a lodgement till. Random grain fabrics and a massive character at the base indicate early waterlain till deposition. Portions of the unit contain rare and preserved upper Pliocene–Quaternary marine diatoms and also specimens of reworked lower Eocene to Quaternary nannofossil and diatoms.

Lithologic Unit III (115.2–134.4 mbsf) is a thin, comparatively well-stratified, lithologically diverse unit. An 80-cm-thick diatomite of late early to early late Pliocene age lies between poorly consolidated diamictites that show evidence for discrete episodes of soft-sediment deformation and intraclast erosion/redeposition. Proximal glaciomarine deposition on an unstable slope is probable.

Crudely layered diamictites making up lithologic Unit IV (134.4–172.5 mbsf) lie below. Gravel contents increase steadily upward in the sequence and reach 10%–15% adjacent to the bouldery interval represented by Subunit IIID (133.7–134.4 mbsf). Grain orientations are random throughout, indicating waterlain till deposition. The content of redeposited organic matter is high compared to that of the surrounding units (1%–2%). A sharp lower boundary defines the underlying lithologic Unit V, and reworking from the lower unit is evident in the basal

Hole 739C

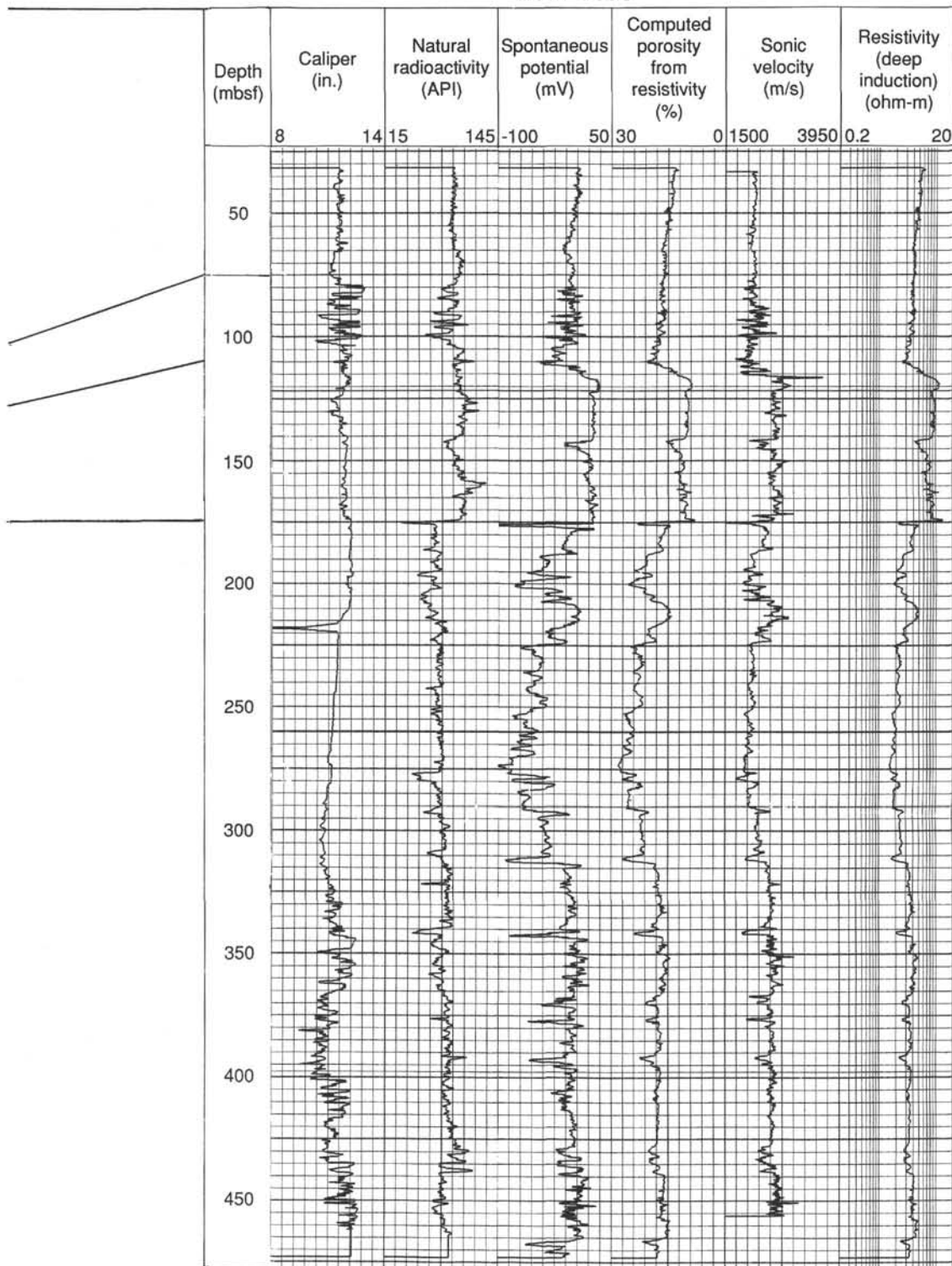


Figure 39 (continued).

few meters. Thus, the lower boundary, which corresponds with important levels in the seismic stratigraphy, physical properties, and downhole logging, is probably erosional. No biostratigraphic control exists for lithologic Unit IV.

Lithologic Unit V (172.5–304.3 mbsf) consists of diamictites, characterized by relatively pale tones, a minor calcareous component, and low percentages (1%–5%) of gravel. The massive,

homogeneous character and random grain orientations indicate that it was deposited as a waterlain till or proximal glaciomarine till. The carbonate content is due to detrital micrite and is comparable to that in the lowest lithologic Subunit IVB at Site 739. A suggested lithologic correlation of those units is supported by the fact that both contain Eocene–Oligocene fossils. In Unit V, the occurrences of rare diatom fragments at 170–174 mbsf and

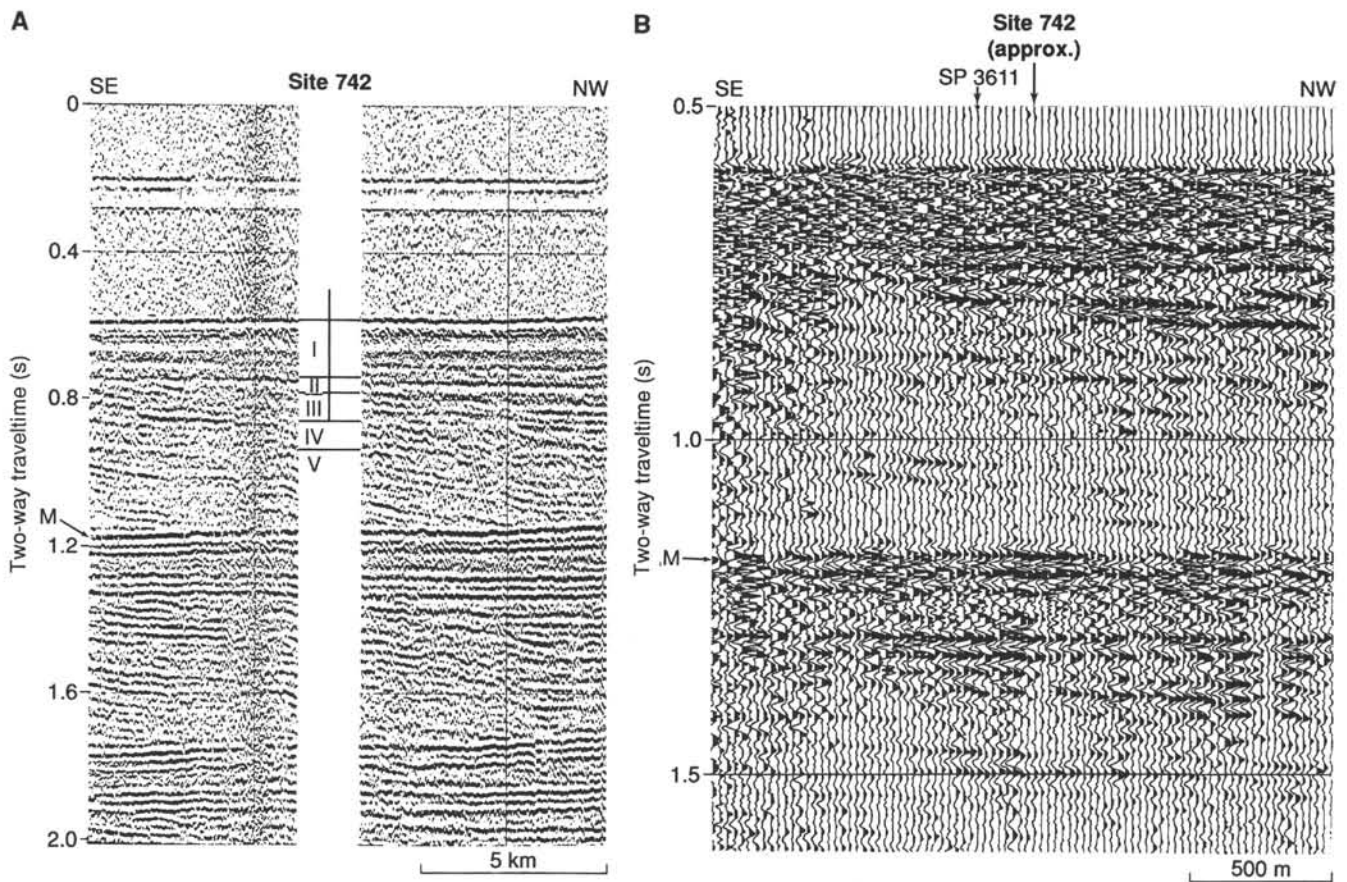


Figure 40. Analog seismic-reflection profiles (ODP line 119-07) across Site 742. **A.** Analog record. **B.** Digital record.

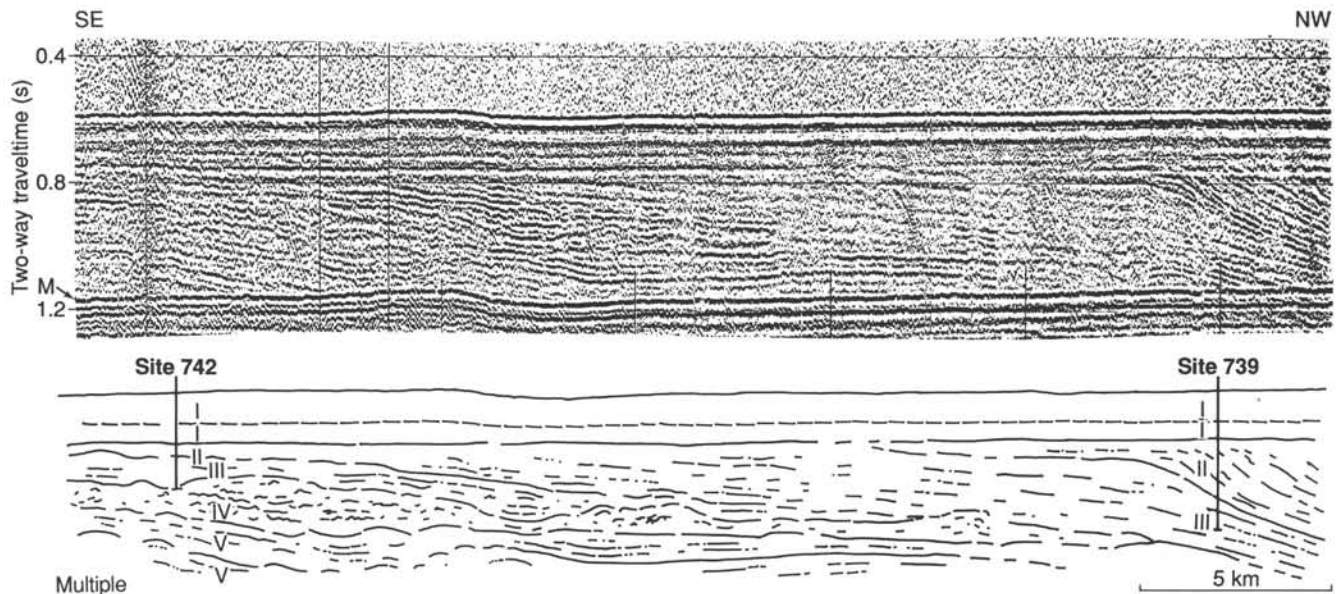


Figure 41. Seismic-reflection profile with interpretation showing acoustic stratigraphy and correlations between Sites 742 and 739.

nannofossils (associated with ?bivalve remains) at 245 mbsf each suggest an Eocene to Oligocene age.

Finally, lithologic Unit VI (304.3–316.0 mbsf) shows diamictite interstratified with laminated claystones and (at the base) texturally sorted sandstones and carbonaceous siltstones. These levels are apparently of fluvial-lacustrine origin and probably

indicate proglacial environments associated with standing and flowing water, perhaps meltwater. The laminated silty claystones show no graded bedding and no evidence of bottom-current scouring, but gravel dropstones and the interbedded sand-silt-clay beds indicate synchronous ice-rafted deposition. The thicker sand-silt-clay and diamictite accumulations of lithologic Unit

VI contain 1%–5% gravel, for which no preferred orientation was found. At the base of the unit lies a thick interval of interbedded sorted sandstones, carbonaceous siltstones, and sand-silt-clays. The entire interval underwent soft-sediment deformation (folding), apparently before deposition of the overlying strata. Two different explanations for the emplacement of these beds are currently held: (1) that they were deposited as part of lithologic Unit VI, but underwent glaciotectionic deformation, or (2) that they were glaciotectionically transported to the site, perhaps from a great distance and probably from another (?lower) unit. In any case, they indicate some period of simultaneous fluvial/lacustrine and glacial nonmarine deposition. The clastic supply was identical to that throughout lithologic Unit VI, but has undergone greatly improved textural sorting without the rounding of grains. The inferred depositional environment tallies with that of the lacustrine silty claystones above. Abundant spore pollen and dinoflagellate remains occur throughout lithologic Unit VI, but most appear to be reworked; most of the coal in the unit occurs as pebbles. A small number of dinoflagellate cysts were observed, indicative of an early Eocene–Oligocene age or younger (if reworked).

No definitive correlation between the paleomagnetic reversal sequence found at this site can be made with reference to paleomagnetic time scales. NRM values for the upper part of the hole were very large, perhaps reflecting relatively high contents of heavy minerals in the sediments. Magnetic inclinations decrease downhole from 180 mbsf, and this is interpreted as a decrease in the paleolatitude with increasing time. Below 172 mbsf, the diamictites of lithologic Unit V display a dominant normal polarity, which is interrupted by six brief reversals. With the middle Eocene to earliest Oligocene age interpretation constrained by the *in-situ* calcareous nannofossils and diatom assemblages overlying this interval in the strata at Site 739, the magnetostratigraphy most closely resembles that of magnetic polarity Chrons 16–18 (late middle to late Eocene).

The interstitial-water program of analyses detected salinity decreases with increasing depth, but these may have been drilling-fluid contamination. The correlation between dissolved magnesium and calcium also deteriorates with depth.

The physical-properties program was aimed particularly at investigating the effects of variable glacial cover in terms of sediment consolidation. Six geotechnical units were distinguished and show a generally good correspondence with the lithostratigraphic divisions. The upper geotechnical unit G1 (0–5.45 mbsf) is a normally consolidated diamicton covered with a thin veneer of diatomaceous silt-clay. The transition into geotechnical unit G2 clearly represents a transition into an overconsolidated sediment. The abrupt change in all physical properties indicates that geotechnical unit G2 sediments have experienced a considerably higher load than their present overburden. Grounded ice is a probable explanation, either through direct loading or glacial removal of a former sediment load. Geotechnical units G2 (5.45–114.0 mbsf), G4 (135.4–172.6 mbsf), and G5 (172.6–195.4 mbsf) have essentially the same physical-properties characteristics—low water contents and porosities and higher bulk densities, compressional-wave velocities, and shear strengths. Geotechnical units G3 (lithologic Unit III) and G5, on the other hand, cause distinct velocity reversals that are likely to give rise to a strong seismic reflector; in particular, this is the case for unit G3. These units are characterized by relatively higher water contents and porosities than those of the surrounding sediments and decreased bulk densities and undrained shear strengths. The cyclic variations probably result from a combination of grain-size distribution variations and variations in the degree of consolidation, both of which reflect fluctuations in the glaciation of the region.

Downhole logging results were accomplished for the depths 30.8–283.8 mbsf, between the base of the drill pipe and an ob-

struction in the drill hole (with another occurring later at 253.8 mbsf). Changes of velocity and porosity correspond well with the boundaries of geotechnical units based on laboratory measurements and appear to outline several units of overcompaction. A synthetic seismogram computed from the downhole log indicated that the largest velocity and density variations occur at unconformities and low-velocity layers in the lithostratigraphy and that these are the principal cause of seismic reflections. The logging indicates that a 15-m-thick unit of sand was not sampled by drilling in an interval of no core recovery at 215–230 mbsf. The interval has low resistivity, low acoustic velocity, decreased bulk density, and high porosity, indicating that the lithology was loose and nonlithified.

On closer inspection, and with the benefit of the lithostratigraphic and downhole logging results after drilling, the seismic stratigraphy yielded information of the larger scale internal structure and broader geometry of facies in the Site 742 area. The seismic units are mostly undeformed, other than by erosion and slight downwarping in the central part of the shelf, indicating long-term tectonic stability in the region. Seismic Unit I (0–175 mbsf) is nearly flat and contains high-amplitude reflections, discontinuous because of glacially compacted (high-velocity) and normally consolidated (low-velocity) layers. It is without apparent internal stratification in the upper 120 mbsf (equaling lithologic Units I and II), but is more continuous below (lithologic Unit III).

The *in-situ* velocity-depth profile for seismic Units II and III increases with depth, indicating that reflections at these deeper levels are not caused by velocity inversions resulting from compaction by glacial loading. Combined, the two represent lithologic Unit V, composed of diamictite. Seismic Unit II (175–220 mbsf) is characterized by weak but continuous reflections that broaden seaward. The entire unit also thickens seaward, reaching maximum thickness between Sites 742 and 739. Seismic Unit III is characterized by high-amplitude and laterally variable reflections of complex shape. It can be traced over a 25- to 30-km distance in the region of Sites 742 and 739. Between the two sites, the upper surface dips gently seaward, but the bottom is irregular because of the infilling of an eroded substrate. The high-amplitude reflections in seismic Unit III are probably due to low-velocity, unlithified sand layers such as those identified by the downhole logging. Their acoustic characteristics, including changing waveform shapes, terminal diffractions, and wavy underlying reflectors, are strong indicators of areally restricted, low-velocity sand bodies with variable thickness that may compose channel, deltaic, or meltwater sand bodies. Continuous high-amplitude reflections farther seaward may represent a more distal facies.

Seismic Unit IV represents 304–316 mbsf in the drilling at Site 742, but continues down to 415 mbsf. It, therefore, seems to be represented by the probably proglacial fluvial/lacustrine facies of lithologic Unit VI. The semicontinuous and wavy reflections are typically weak, discordant with overlying strata, and associated with diffractions. The unit is identifiable over 75 km in the ODP seismic lines, filling pre-existing or slowly subsiding depressions seaward and landward of Site 742. The reflection character and style of truncations indicate that seismic Unit IV is a mostly nonmarine sequence of possible lacustrine/fluvial origin that was eroded in the initial period of glacial advance.

Seismic Unit V, between seismic Unit IV and the seafloor multiple beneath Site 742 (415–675 mbsf), was not sampled by drilling. It consists of well-layered, continuous to semicontinuous reflections with variable amplitudes in both depth and distance. It is traceable over 90 km, from Site 739 (where it disappears into the seafloor multiple) to a point 35 km seaward of Site 741 (eroded near the seafloor). Seaward, it becomes more strongly reflective and continuous. The relatively uniform thick-

ness, continuity, and absence of major deformation indicates that the unit was deposited on a relatively stable platform, possibly as shallow marine and alluvial plain deposits and possibly nonglacial.

Correlations of the seismic units indicate that the thickness between Sites 741 and 742 is about 3 km and that if reflections from the lowermost beds drilled at Site 742 are traced they lie approximately 750 m below the bottom of Site 742.

In brief, Site 742 appears to have been a location of fluvial/lacustrine deposition at those times corresponding with the base of the hole (?early Eocene–Oligocene), although glacial (proglacial) deposition was also clearly already in operation. Distinct erosional surfaces and possible glaciotectionic deformation in the stratigraphy at about this level indicate that bodies of ice moved over the bed, rather than floating, in addition to supplying ice-rafted debris to a lake. Younger diamictites of probable Oligocene age continue the glacial record. Fossil remains in lithologic Unit V (245 mbsf) seem to indicate the level at which glaciomarine conditions began.

The earliest evidence of grounded ice based on oriented grain fabrics is in lithologic Unit IV (between 140 and 150 mbsf), which displays coarsening-upward gravel contents and is overcompacted because of the grounding of ice (i.e., ice loading and/or sediment load removal) at Site 742. This level (173 mbsf) is an especially significant one in the seismic stratigraphy, marking the initiation of the horizontal shelf accumulations at this particular location within the Prydz Bay continental prograding sequence. The underlying units have the form of gently sloping, progradational deposits. This transformation, and the indications of ice grounding, therefore, predate the Pliocene and post-date Oligocene beds. Sediments representing open marine conditions where diatom accumulation was not overwhelmed with glaciomarine clastics may have accumulated on several occasions at Site 742, but are only preserved for the late early to early late Pliocene (lithologic Unit III). However, two different time intervals of similar deposition are preserved at Site 739. Thick accumulations of coarse diamictite followed, but were perhaps a result of more than one depositional phase.

No detailed history of this interval is available because of the exceptionally poor core recovery, but the downhole logging indicates that it underwent overconsolidation as one unit. That event probably coincided in its final stages with the Quaternary surface between lithologic Units I and II at 5.4 mbsf (Unit I/II boundary) because clast orientation fabrics below that level indicate a considerable thickness of lodgement tills. Subsequent deposition has been of proximal glaciomarine clastics and in recent times, diatomaceous silt-clay.

REFERENCES

- Barrett, P. J., Hambrey, M. J., and Robinson, P. H., in press. Cenozoic glacial and tectonic history from the CIROS-1, McMurdo Sound. In Thompson, M.R.A. (Ed.), *5th International Antarctic Earth Science Symposium Volume*: Cambridge (Cambridge Univ. Press).
- Claypool, G. E., and Kvenvolden, K. A., 1983. Methane and other hydrocarbon gases in marine sediments. *Annu. Rev. Earth Planet. Sci.*, 11:299–327.
- Deroo, G., Herbin, J. P., and Huc, A. Y., 1984. Organic geochemistry of Cretaceous black shales from Deep Sea Drilling Site 530, Leg 75, eastern South Atlantic. In Hay, W., Sibuet, J.-C., et al., *Init. Repts. DSDP*, 75: Washington (U.S. Govt. Printing Office), 983–999.
- Edwards, B. D., Lee, H. J., Karl, H. A., Reimnitz, E., and Timothy, L. A., 1987. Geology and physical properties of Ross Sea, Antarctica, continental shelf sediment. In Cooper, A. K., and Davey, F. J. (Eds.), *The Antarctic Continental Margin: Geology and Geophysics of the Western Ross Sea*: CPCMR Earth Sci. Ser., 58:191–216.
- Eyles, N., and Miall, A. D., 1984. Glacial facies. In Walker, R. G. (Ed.), *Facies Models* (2nd ed.): Geol. Assoc. Canada, 15–38.
- Kotova, I. Z., 1983. Palynological study of Upper Jurassic and Lower Cretaceous sediments, Site 511, Deep Sea Drilling Project Leg 71

(Falkland Plateau). In Ludwig, W. J., Krasheninnikov, V. A., et al., *Init. Repts. DSDP*, 71: Washington (U.S. Govt. Printing Office), 879–1006.

- Kvenvolden, K. A., and McDonald, T. J., 1986. Organic geochemistry aboard *JOIDES Resolution*—an assay: *ODP Tech. Note*, 6.
- Lien, R., Solheim, A., Elverhoi, A., and Rokoengen, K., in press. Iceberg scouring and sea bed morphology on the Antarctic continental shelf; a local study in the eastern Weddell Sea. *Polar Res.*
- Lopatin, B. G., and Semenov, V. S., 1982. Amphibolite facies rocks of the southern Prince Charles Mountains, East Antarctica. *Antarct. Geosci. Symp. Antarct. Geol. Geophysics*, 3rd 1977 (1982), 465–471.
- McLachlan, I. R., and Pieterse, E., 1978. Preliminary palynological results: Site 361, Leg 40, Deep Sea Drilling Project. In Bolli, H. M., Ryan, W.B.F., et al., *Init. Repts. DSDP*, 40: Washington (U.S. Govt. Printing Office), 857–882.
- Oliver, R. L., James, P. R., Collerson, K. D., and Ryan, A. B., 1982. Precambrian geologic relationships in the Vestfold Hills, Antarctica. *Antarct. Geosci. Symp. Antarct. Geol. Geophysics*, 3rd 1977 (1982), 435–444.
- Ravich, M. G., and Fedorov, L. V., 1982. Geologic structure of MacRobertson Land and Princess Elizabeth Land, East Antarctica. *Antarct. Geosci. Symp. Antarct. Geol. Geophysics*, 3rd 1977 (1982), 499–504.
- Shipboard Scientific Party, 1987. Site 645. In Srivastava, S. P., Arthur, M. A., et al., *Proc. ODP, Init. Repts.*, 105: College Station, TX (Ocean Drilling Program), 61–418.
- Solheim, A., in press. The depositional environment of surging, sub-polar tidewater glaciers: a case study of the morphology, sedimentation and sediment properties in a surge affected marine basin outside Nordaustlandet, northern Barents Sea. *Skr. Nor. Polarinst.*
- Solheim, A., Milliman, J. D., and Elverhoi, A., 1988. Sediment distribution and sea floor morphology of Storbanken: implications for the glacial history of the northern Barents Sea. *Can. J. Earth Sci.*, 25:547–556.
- Stagg, H.M.J., 1985. The structure and origin of Prydz Bay and MacRobertson Shelf, East Antarctica. *Tectonophysics*, 114:315–340.
- Stumm, W., and Morgan, J. J., 1981. *Aquatic Chemistry* (2nd ed.): New York (Wiley).
- Tingey, R. J., 1982. The geologic evolution of the Prince Charles Mountains—an Antarctic Archean cratonic block. *Antarct. Geosci. Symp. Antarct. Geol. Geophysics*, 3rd 1977 (1982), 455–464.
- Tissot, B. P., and Welte, D. H., 1984. *Petroleum Formation and Occurrence* (2nd ed.): Berlin (Springer-Verlag), 155–158.
- Waples, D. W., 1985. *Geochemistry in Petroleum Exploration*: Boston (International Human Resources Development Corporation).
- Williams, G. L., and Bujak, J. P., 1985. Mesozoic and Cenozoic dinoflagellates. In Bolli, H. M., Saunders, J. B. and Perch-Nielsen, K. (Eds.), *Plankton Stratigraphy*: Cambridge (Cambridge Univ. Press), 847–964.

Ms 119A-110

APPENDIX

Petrography of Gravel Clasts in Diamictites Recovered at Prydz Bay Drilling Sites 739–742

The presence of a thick crystalline Archean basement on the eastern part of Antarctica is largely responsible for the highly detritic nature of the sediment accumulated in the extension toward open sea of the graben structure beneath the Lambert Glacier area.

Detrital grains (mainly quartz and feldspars, with minor biotite, chlorite, white mica, hornblende, clinopyroxene and orthopyroxene, orange to pink garnet, and locally abundant magnetite) make up a major component of the diamictites and siltstones recovered in Holes 739C–742A. In addition, pebbles and boulders are abundant in each core and show metamorphic mineral assemblages reminiscent of the Antarctic Shield. The coverage is likely to depend upon relative mineral resistance to alteration and could explain, in part, the relative scarcity of sediments, schists, and granitoid rocks actually observed. Charnockites, which constitute the most common metamorphic rocks from the Antarctic Archean basement, in particular in the Humboldt Series (Queen Maud Land) and the Reinbolt and Larsemann Series (eastern part of Amery Ice shelf), have not been observed. The most abundant pebbles are garnet and biotite-bearing paragneisses, and to a lesser extent, amphibolites,

mafic gneisses, and impure quartzites. All the schists and gneisses, and also the diamictite and siltstone host sediments, are distinctive by their high magnetite content. This characteristic was previously observed in moraines and pebbles rafted by the Lambert Glacier, near the Vestfold Hills and could account for the magnetic anomaly reported in Prydz Bay (Ravich and Fedorov, 1982).

We have selected 16 samples for thin sections, in order to get an initial view of the variety of compositions and metamorphic grades and to compare them with metamorphic rocks exposed on the continent. In addition to these samples, we have observed augen gneisses, minor sandstones, quartzites, and highly altered granitoid and pegmatitic rocks.

The comparison was based on several research papers, including a geologic map, dealing with the East Antarctica Shield (see Tingey, 1982). We are also grateful to S. Harley (Oxford University), for his short visit, from Davis Station, onboard and valuable improvement of information concerning the Vestfold Hills, Rauer, and Larsemann geology. Descriptions are given in the following of the main compositions arranged in increasing metamorphic grade from the greenschist facies to the granulite facies.

Greenschist to Epidote-Amphibolite Facies

These rocks consist of fine-grained, quartz-rich schists and quartzites, either strongly foliated or with little preferential orientation.

Section 119-739C-38R-1, 3-5 cm: Fuschite Quartzite

Large porphyroblasts of quartz are strongly deformed (undulose extinction and subgrains development). Ribbons are embedded or crosscut by bundles of green mica (fuschite).

Section 119-739C-35R-CC, 45-46 cm: Microfolded Banded Iron Formations (BIF)

Magnetite layers alternate with quartz-green biotite-sericite layers. The crystals lack preferential orientation. The folds are outlined by magnetite layers, have axes making an angle of about 40° with the earlier compositional layering, and involve probably both shortening and shear. Accessory minerals are strikingly abundant and consist chiefly of zircon and tourmaline.

Section 119-739C-34R-4, 63-64 cm: Mica-Schist

Magnetite, green biotite, and muscovite are scattered in a quartz-rich (sericite and calcite) matrix. Accessory minerals are apatite, zircon, and tourmaline.

Section 119-739C-4R-1, 131-133 cm: Mica-Schist

The strong foliation is outlined by needles of muscovite and poikilitic large green biotites. Interstitial quartz is euhedral to elongated. Some muscovite flakes make an acute angle (40°) with the main schistosity layering and could record an earlier crenulation. Magnetite is abundant (10%–20%). Among abundant accessory minerals, such as zircon and apatite, we have also noted dumortierite (50 μm) characterized by its orthorhombic symmetry and pleochroism (pink-lavender-green). These minerals reflect the high content of zirconium, phosphorus, and boron. In a coarse-grained layer, quartz, clinocllore, and minor biotite are associated.

Section 119-739C-48R-1, 140-143 cm: Epidote-Amphibole Mica-Schist

Well-foliated schist with alternating layers of garnet (almandine) + epidote (pistacite), blue-green hornblende, green biotite or alternatively muscovite, and quartz. Quartz is either recrystallized or as ribbons with subgrains.

Banded iron formations, fuschites, quartzites, and epidote-amphibole schists of similar composition and sedimentary origin have been described on land, in the southern Prince Charles Mountains, where they overlie the upper Archean basement. They are either retrogressed in the lower amphibolite facies (Menzi Series) or greenschist facies (Ruker Series). However, the mineralogy differs slightly: alkali amphibole was not observed in the dropstones.

Amphibolite Facies

These rocks are characterized by the assemblage green hornblende + plagioclase + biotite and quartz.

Section 119-739C-16R-1, 69-71 cm: Amphibolite

Layered amphibolite showing bands of green hornblende + green biotite alternating with quartzofeldspathic layers. Feldspars are altered to chlorite + sericite.

The slightly higher pressure (characterized by kyanite and staurolite) that prevailed in some lower amphibolite facies pelites from the southern Prince Charles Mountains have not been observed. Amphibolite facies basic rocks have been described from the Menzi Series and Mawson escarpment, southern Prince Charles Mountains, and are Proterozoic in age (about 1 Ga).

Lower to Upper Granulite Facies

These rocks are abundant as dropstones or large boulders (Core 119-742A-16R). Compositions range from (1) mafic gneisses, characterized by layering and by the coexistence of pyroxenes and green-brown hornblende, to (2) garnet paragneisses, and (3) little foliated, quartzofeldspathic garnet gneisses, the two latter with variable contents of biotite, sillimanite, and cordierite.

Section 119-739C-42R-1, 30-32 cm: Garnet-Biotite-Magnetite Schist

This strongly foliated and microfolded schist is interbedded with coarse-grained relict gneissic layers. The foliation is outlined by bands of very-fine-grained subhedral magnetite, garnet, biotite, or quartz. Medium-grained quartz ribbons or eye-shaped relict porphyroblasts of quartz-feldspars-garnet-biotite record sinistral shear displacement and migmatitic folding parallel to the foliation. The garnet is fractured and partly recrystallized on the margins to small grains. Biotite and quartz are also finely recrystallized around garnets and along shear microfractures. Magnetite is very abundant and accounts for the dark color of the rock. Zircon is the main accessory mineral.

Section 119-740A-4R-CC, 2-5 cm: Orthopyroxene and Clinopyroxene-Amphibole-Garnet Gneiss

Layering is well-developed and outlined by alternating quartz ribbons and green amphibole, orthopyroxene-clinopyroxene-garnet + biotite, magnetite, plagioclase, and minor alkali feldspar and quartz. The layering corresponds to the main cleavage of the pyroxenes, while amphibole develops either as subhedral crystals or at the expense of relict biotite and pyroxenes. Garnet is finely recrystallized and amounts to less than 5%. Polysynthetic twinning in clinopyroxene and clinopyroxene as lamellae in orthopyroxene are common. Accessory minerals: zircon and apatite. This sample is particularly fresh. It could represent a retrograde assemblage from higher granulite facies.

Section 119-742A-13R-1, 20-22 cm: Mafic Gneiss

Both orthopyroxene and clinopyroxene, the latter showing orthopyroxene lamellae, coexist with minor biotite, and with plagioclase and alkali feldspar. Equant grains with triple junctions are common in pyroxene and feldspars. Brown hornblende develops in bands, at the expense of pyroxene and minor biotite. The main cleavage of the amphibole defines a lineation parallel to the light layering. Magnetite is abundant, subhedral, and scattered in both amphibole-rich and amphibole-free layers.

Section 119-740A-5R-CC, 10-12 cm: Biotite-Garnet-Orthopyroxene Gneiss

Alternating layers of biotite + feldspar, or biotite + garnet + orthopyroxene or feldspars (alkali feldspar with perthites and plagioclase with sodic exsolutions). Plagioclase may be poikilitic and includes subhedral crystals of biotite, zircon, magnetite, and orthopyroxene. Garnet occurs as small rounded grains. Magnetite is locally abundant either interstitially or growing at the expense of biotite, around garnets, in association with quartz, sericite, and chlorite. Alteration is characterized by calcite veins crosscutting feldspars and pyroxenes.

Section 119-739C-13R-1, 82-84 cm: Garnet-Bearing Quartzofeldspathic Gneiss

The foliation is outlined by layers of biotite + garnet. Biotite is Ti-rich and some of the flakes make an acute angle with the foliation, suggesting an earlier crenulation. Garnet is a pink pyrope-almandine and occurs as rounded corroded grains. Quartz occurs as large porphyroblasts only partly recrystallized, with undulose extinction and sub-

grains. Large microcline, sometimes perthitic, is abundant compared to orthoclase, plagioclase, and quartz. Accessory mineral: zircon.

Section 119-739C-23R-2, 56–60 cm: Quartzofeldspathic Gneiss

Dark brown, Ti-rich subhedral biotite is scattered as small flakes, without any preferential orientation, in a coarse-grained quartzofeldspathic matrix where quartz coexists with alkali feldspar (antiperthites) and plagioclase. Myrmekites are abundant. Garnet occurs as rounded, poikilitic, and corroded grains.

Section 119-740A-5R-CC, 15–20 cm: Garnet-Biotite-Feldspars Paragneiss

Large poikilitic and rounded garnet porphyroblasts are set in a plagioclase-alkali feldspar-biotite matrix with equant texture. Antiperthites are common both in potassium feldspar and plagioclase. Biotite is found as abundant large crystals or as relicts in a magnetite-chlorite assemblage. It is partly altered to chlorite and quartz ribbons.

Section 119-739C-2H-1, 10–11 cm: Cordierite-Sillimanite Gneiss

Cordierite and magnetite are abundant and coexist with quartz, perthitic microcline, alkali feldspar, and plagioclase. Sillimanite bundles are observed locally. Quartz shows undulose extinction and subgrains. Most of the feldspars and cordierite grains show rounded or interlocked grain structure.

Section 119-741A-4R-1, 15–20 cm: Garnet-Sillimanite-Biotite Paragneiss

This garnet-rich gneiss shows a reactive assemblage, with two stages of biotite. Old, slightly pleochroic and brown biotite (1) has reacted with garnet and quartz to form biotite (2) + sillimanite + K-feldspar + H₂O, in coronas around garnet porphyroblasts. Biotite type 2 is a red, pleochroic Ti-biotite that crystallizes as radial sheafs intergrown with sillimanite. Excess iron is accommodated in magnetite. Sillimanite also crystallizes as large prisms. Plagioclase participates in the reaction, and transforms along its margins into alkali feldspar + apatite or myrmekites. Alkali feldspar is abundant and darkened by fluid inclusions. Several generations of dark fluid inclusion streaks (presumably CO₂-rich) are common, even in garnet and sillimanite. As in most other minerals (plagioclase, sillimanite, and old biotite), quartz records a strong deformation—including sinistral shear—without recrystallization, except in the reactive zones around garnet, and shows undulose extinction and subgrain development. Kink bands and bending are observed in sillimanite and plagioclase, suggesting syn- to post-deformation relative to crystallization. Zircon is common as an accessory mineral in biotite and garnet.

Section 119-742A-16R-1, 131–134 cm: Garnet-Biotite-Sillimanite Paragneiss

Layering is blurred by 1–10-cm-scale folds. Compositional bedding is outlined by layers of hercynite + Fe-Ti magnetite or biotite + sillimanite, or garnet. Quartz and both potassium feldspar (microcline or orthoclase) and plagioclase have interlocked boundaries. Perthites and antiperthites are abundant. Quartz forms curved ribbons with undulose extinction. Garnet is abundant, rounded, and poikilitic (quartz + bio-

tite inclusions). Biotite is Ti-rich and subhedral, except when involved in reaction zones where it turns into sillimanite. Textural relationships suggest the following qualitative reactions: biotite (1) = biotite (2) + sillimanite + Fe-Ti magnetite + quartz hercynite + biotite = sillimanite + Fe-Ti magnetite + K-feldspar hercynite + quartz = sillimanite + magnetite. Hercynite is also found in association with altered relicts of andalusite, at the boundary with a coarse-grained “pegmatitic” layer characterized by large, altered, perthitic K-feldspar porphyroblasts. Sillimanite as thin bunches or needles develops rarely from andalusite or from K-feldspar and as tiny needles in garnet. Zircon is abundant as an accessory mineral.

These high-temperature amphibolite-granulite facies rocks compare fairly well with the upper Archean basement gneisses and schists in the Lambert Series of the northern Prince Charles Mountains (Tingey, 1982) and the synchronous Insel Series in Queen Maud Land. They are typically polymetamorphic rocks, retrograded to a moderate grade of the granulite facies. Similar rocks are actually encountered along the present Lambert Glacier and its tributaries and make up the Mawson Escarpment and Mounts Newton, Twigg, and Crosswell (Lopatin and Semenov, 1982).

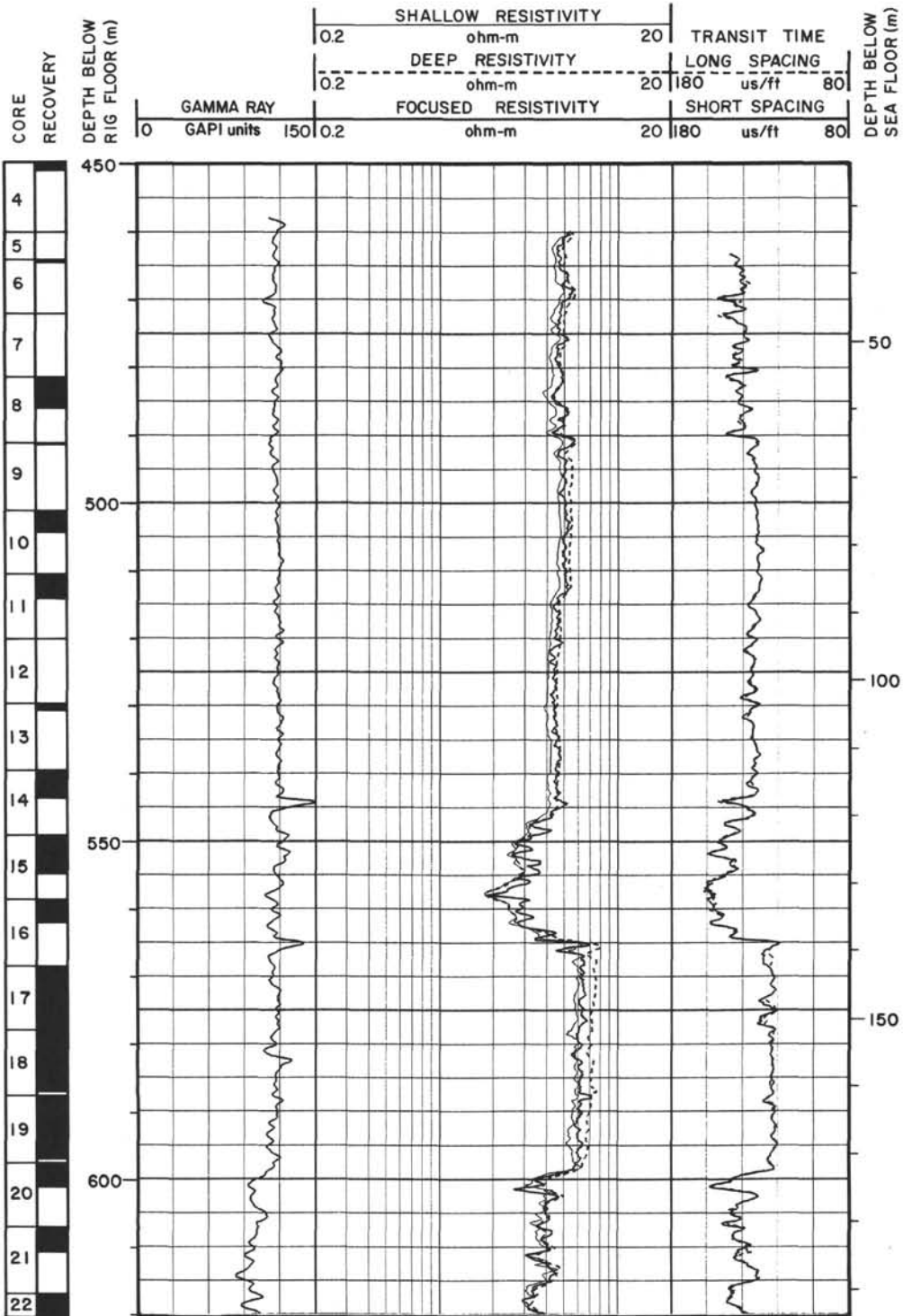
When compared with the upper Archean gneisses from Vestfold Hills, rather similar layered paragneisses, garnet-biotite plagiogneisses, and also quartz-magnetite BIF are found. However, orthopyroxene is described as frequent in the pelitic paragneisses from Vestfold (Oliver et al., 1982) while it is lacking in the present paragneisses. Neither did we observe (1) the acid to intermediate, orthopyroxene-bearing orthogneisses and “gray gneisses” from the Vestfold Hills, (2) orthopyroxene-plagioclase symplectites around garnet, typical of some granulitic rocks from Rauer, nor (3) the charnockites from the Reinbolt and Larsemann Series, which are correlative to the Humboldt Series from Queen Maud Land (Ravich and Fedorov, 1982).

Conclusions

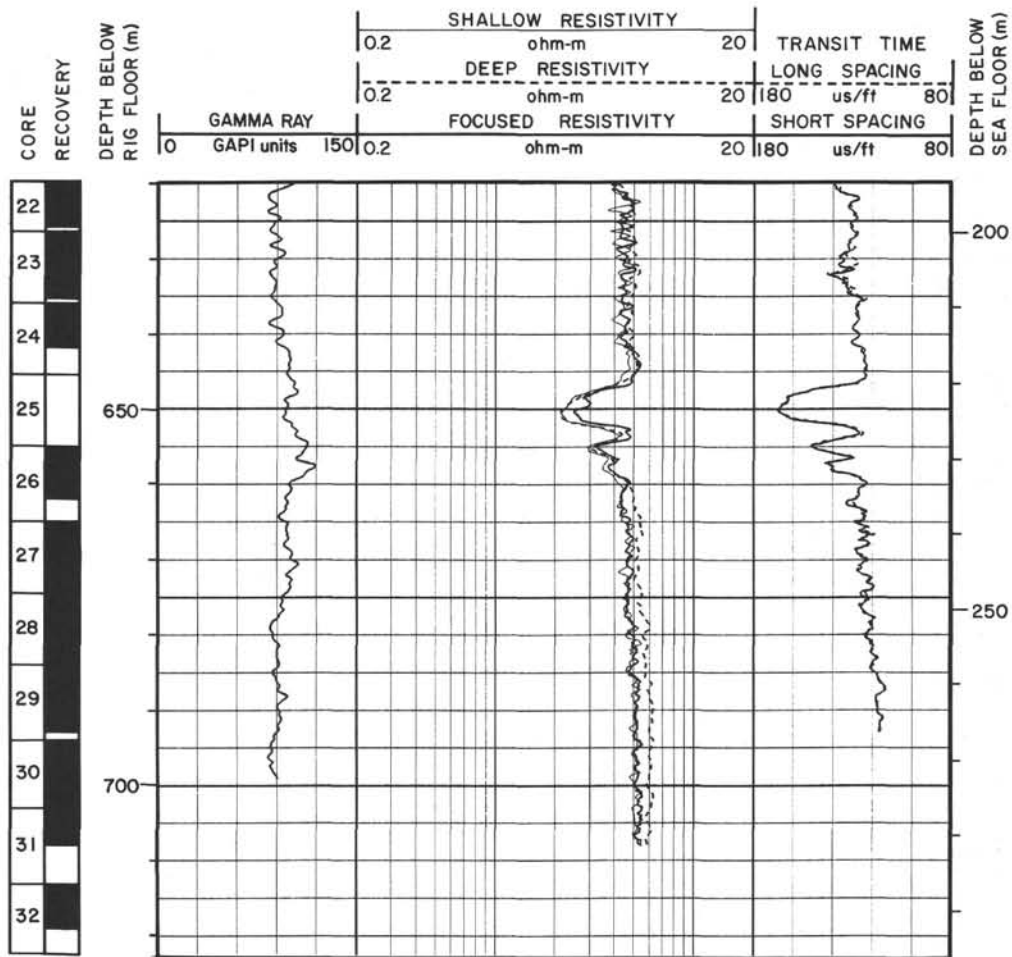
This preliminary description of the metamorphic pebbles from Prydz Bay cores may have implications concerning:

1. The major transport directions from glaciers or icebergs toward Prydz Bay. Even though it is only a conservative choice, the similarity of the rocks recovered in the Holes 739C–742A with those from the nearby Lambert Glacier area do not suggest a more remote origin, for instance from Enderby Land or Queen Maud Land more westward.
2. The relationships between alteration of the pebbles and preglacial periods. For instance, Hole 741A is characterized by continental sandstones and contains more altered rocks compared to other sites dominated by diamictite glacial sediments. A comparison between the gravel clasts recovered at different sites is also necessary.
3. The age(s) of accumulation and metamorphism(s) of the quartz-magnetite schists (BIF) recovered in this cruise. Ages could be determined (i.e., by U-Pb method), owing to the abundance of large zircons. These rocks are in general associated with Archean terranes or Paleozoic ones, such as in Africa. The concentration of heavy minerals and the reducing conditions probably explaining the remarkable development of magnetite reflect the distinctive metamorphic environments.

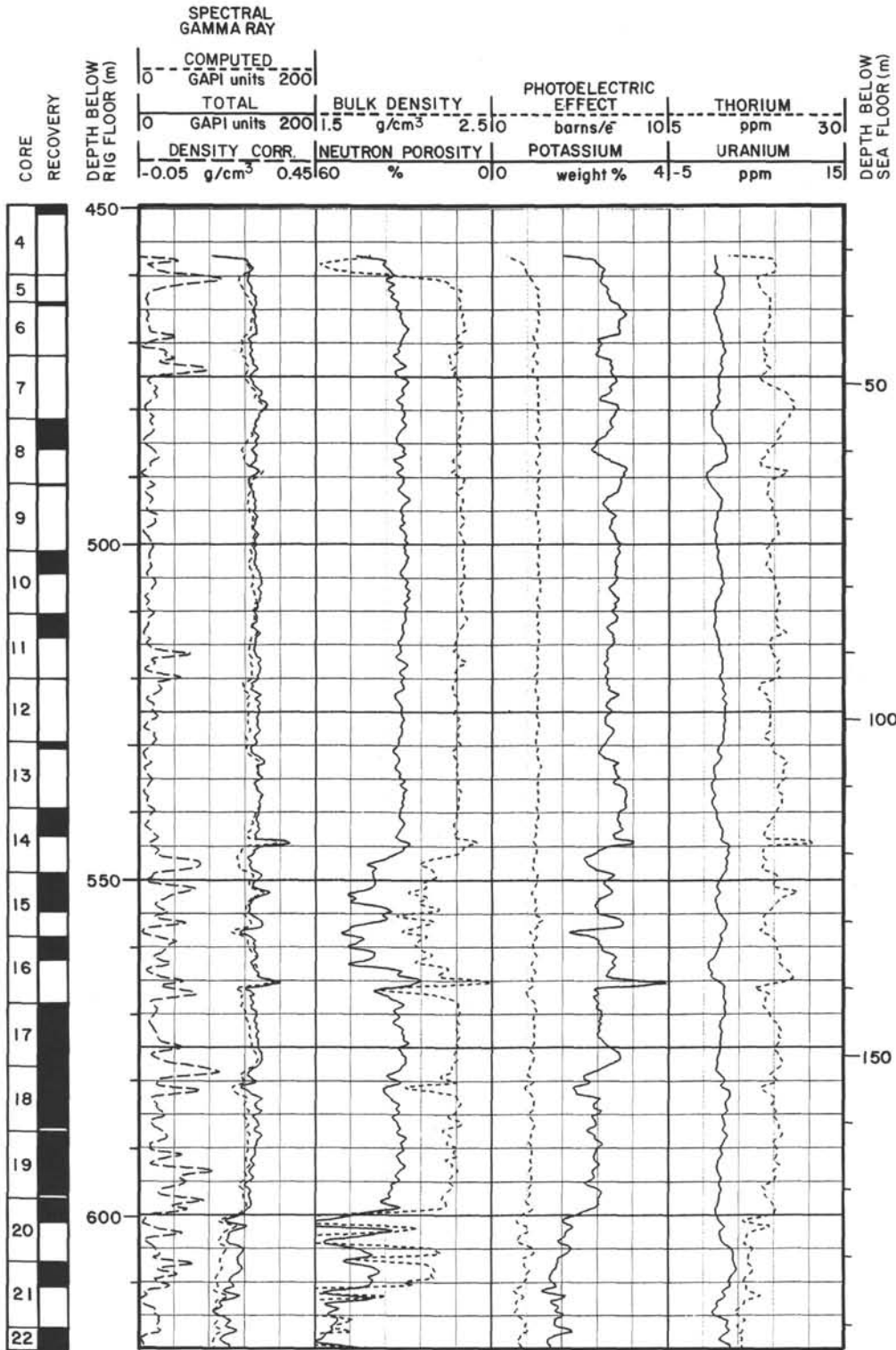
Summary Log for Hole 742A



Summary Log for Hole 742A (continued)



Summary Log for Hole 742A (continued)



Summary Log for Hole 742A (continued)

